THE UNIVERSITY OF CHICAGO

PHASE BEHAVIORS AND COMPOSITION PARTITIONING IN POLYELECTROLYTE COMPLEXATION SYSTEMS

A DISSERTATION SUBMITTED TO
THE FACULTY OF THE PRITZKER SCHOOL OF MOLECULAR ENGINEERING
IN CANDIDACY FOR THE DEGREE OF
DOCTOR OF PHILOSOPHY

BY
LU LI

CHICAGO, ILLINOIS
JUNE 2019

TABLE OF CONTENTS

LIST OF FIGURES

LIST OF TABLES

ABSTRACT

Lu Li: Phase Behaviors and Composition Partitioning in Polyelectrolyte Complexation Systems

Under the Direction of Professor Matthew V. Tirrell

Polyelectrolyte complexation (PEC) is an associative phase separation process initiated by mixing of two kinds of oppositely charged polyelectrolyte solutions. PEC-based materials have been recognized as ideal prototypes to study membraneless organelles, self-assembled into smart delivery vehicles for nucleotides and proteins, and fabricated into functional devices for purification purposes. Continuous studies have been devoted to understanding thermodynamics, kinetics, morphology, and structures of the polyelectrolyte complexation systems, which were summarized in Chapter 1 of this dissertation. However, a lot of the studies remained qualitative, and the fundamental understanding of the polymer physics involved has not kept pace. Specifically, a precise description of the binodal phase diagram capturing detailed phase behaviors and partitioning of different components into the two respective phases is still lacking. Moreover, joint efforts by experiments and theories are needed to provide an overarching framework with the predictive capacity to control the properties of the PEC-based materials.

Accordingly, we have designed a new experimental approach combining salt resistance measurement and thermogravimetric analysis with minimum processing and approximation to produce accurate binodal phase diagrams. Chapter 2 of this dissertation focused on illustrating the phase behaviors of a "clean" polypeptide system, poly(lysine) and poly(glutamic acid) with hydrophilic backbones and matched chain lengths. Essential features of this system were demonstrated, including the screening effect of salt, self-suppression and the change of the volume fraction of the complex phase with addition of salt. Additionally, the salt partitioning

into the supernatant phase was found to initially increase and then decrease on increasing the salt concentrations, manifesting as a distinct minimum in the salt partition coefficients. These trends were shown by simulations to be strongly influenced by the excluded volume interactions in the complex phase, which were not accounted for in their entirety in earlier theories.

Equipped with the knowledge from the polypeptide system, we have further extended our research to an aliphatic pair of poly(acrylic acid) and poly(allylamine hydrochloride) with hydrophobic backbones in Chapter 3 of the dissertation. While we found the phase behaviors were, to some extent, similar under neutral/basic pHs and followed general expectations of PEC materials, remarkably different behaviors were observed under acidic conditions. Unintuitively, polymer content in the complex phase increased as salt was added, due to the hydrophobicity of aliphatic polymer backbones coupled with hydrogen bonding of unionized monomer units. We systematically investigated both of these specific interactions using turbidimetry, microscopy, and FTIR spectroscopy. These binodal phase diagrams detailed the associative secondary phase assembly from electrostatic complexation, precipitation of an individual polymer, and other noncovalent contributions as a function of pH, polymer concentration, and added salt.

Lastly, Chapter 4 of the dissertation has compared the binodal phase behaviors of both polypeptide and aliphatic polyelectrolyte systems to accentuate the effect of solvent quality and chain length. The experimental results could be qualitatively explained by the scaling theory and random phase approximation calculation. The threshold value of Flory-Huggins χ parameter distinguishing complexation disintegration upon salt addition and that remaining stable even at high salt concentrations could be estimated. Additionally, the salt resistance concentration was shown to be proportional to the square root of the polymer chain length.

ACKNOWLEDGEMENT

Working as a Ph.D. student under the supervision of Professor Matthew V. Tirrell in the Institute for Molecular Engineering (IME) at the University of Chicago was a fruitful and challenging experience for me. I am exceptionally glad to be a member of the founding class of IME Ph.D. students and excited to have the opportunity of interacting with researchers from different disciplines of various backgrounds. I am fortunate to receive countless direct and indirect help from people in my home department, sister departments at the university, and collaborative institutions from Northwestern University and National Institute of Standards and Technology (NIST). Without the instructive and patient support and advice from those personalities, the completion of my dissertation would have been impossible.

First and foremost, I would like to thank my dear advisor, Professor Matthew V. Tirrell, for his scientific and profound instruction, inspiration, and criticism throughout the whole time of my doctorate study. He taught me how to investigate an academic research topic rigorously and drove me to understand the importance of the subject from a big picture when I was too absorbed into details. By the example of him, I learned to improve my understanding of concepts and theories as precisely as possible, observe the experimental findings in an objective manner, and present my scientific discoveries and interpretation accurately and professionally. Besides academic research, he has also provided insightful guidance for my personal career path with love and respect. I am greatly indebted to his valuable support throughout my doctorate years and my future career.

Then I would like to thank my committee members, Professor Juan de Pablo and Professor Paul Nealey, for spending their time reviewing my dissertation, giving instructions for my research projects, and providing advice on my defense. They offered important suggestions

and different perspectives for my experimental design and theoretical comprehension. I feel greatly honored to have the opportunity to present my work before those distinguished scientists.

I would like to give my special thanks to my previous labmate, Professor Samanvaya Srivastava at UCLA, for his encouragement and mentorship starting from the time when I first joined the Tirrell lab. He showed me the serious attitude for conducting research and attention on details. I would like to thank Professor Handan Acar, Professor Lorraine Leon, Professor Blair K Brettmann, Professor Dimitrios Priftis, and Professor Amanda Marciel, for the beneficial discussion and collaboration to help me understand phase behaviors of polyelectrolyte complexation in the polypeptide project. I would like to thank Dr. Justin Juller, Dr. Philip Griffin, and Dr. Antoni Jurkiewicz for their help in physical characterization and chemical analysis of my polymer samples. I would like to thank Dr. Jeffrey M. Ting, Dr. Michael Lueckheide, Dr. Angelika Neitzel, Dr. Sean Mao, Dr. Jeffrey Vieregg, Hao Wu, Siqi Meng, Dr. Alexander Marras, and Dr. Dean Mastropietro for their valuable discussions concerning my research, without which it would have taken me much longer to solve some of the problems I encountered during my study. I would like to thank all the current and previous Tirrell group members for their camaraderie, support, and patience through the five years. They helped me overcome a lot of difficulties in everyday life when I first came to the USA.

Additionally, I would like to thank our collaborators from Professor Juan de Pablo's group, Dr. Marat Andreev and Dr. Artem M. Rumyantsev, for providing simulation and theoretical inputs for multiple polyelectrolyte complexation projects. Communications and discussions with them sparkled innovative ideas and promoted further understanding of the physical relationships of the complicated systems. I would like to thank Professor Zhengang

Wang and Professor Pengfei Zhang for their instructive comments on my first manuscript and insights on the salt partitioning predictions. I feel grateful for those feedbacks from theorists.

My sincere thank also goes to my boyfriend, Ruoyu Xu, for his love and understanding in school life as well as inspiration and support for my future career. I would like to thank my long-time friends Yige Gao, Ning Zheng, Xinyu Tang, Qiaomei Wu, Jiayun Lin, and Jiajing Li for their continuous care and patience.

Finally, I would like to thank my parents, Xiaolan Fan and Jiansheng Li, along with all my family members for their unconditional trust and love all the time. They granted me the freedom and confidence to pursue my dream, guided me through ups and downs in life, and raised me up when I have doubts about myself. This work is dedicated to them whole-heartedly.

CHAPTER 1. Introduction of Polyelectrolyte Complexation and Its Application

1.1 General Introduction of Polyelectrolyte Complexation

Polyelectrolyte complexation is an associative phase separation process, initiated by mixing of two kinds of oppositely charged polyelectrolyte solutions in aqueous media. The solution mixture will have a polymer-rich phase, complex phase, and a polymer-deficient phase, supernatant phase. Phase separation driven by polyelectrolyte complexation distinguishes with more commonly seen phenomenon of segregative phase separation in the fact that both of the polyelectrolytes partition into the complex phase instead of separating into different phases. This phenomenon was first recognized by Bungenberg et al by mixing gelatin and gum arabic together.[1,2] The complex phases are mostly amorphous, and the complex morphology could either be water-rich liquid coacervates or solid precipitates as dictated by the chemical structures, architectures, charge densities and lengths of the polyelectrolytes as well as the environment ionic strength and pH.[3–6] In special cases, the polyelectrolytes can adopt specialized secondary structures (β-sheets) under the influence of secondary intermolecular interactions.[7,8] Complexation between oppositely charged polyelectrolytes generally leads to macroscopic phase separation especially for homo-polyelectrolyte, resulting in the formation of bulk polyelectrolyte complexes. Since my doctorate research was centered around bulk systems, the introduction part of this dissertation would also focused on recent progress in the understanding of the thermodynamics, kinetics, phase behavior, rheology and interfacial properties of bulk PECs, including insights from fundamental polymer physics and chemistry perspectives, and introduce promising applications of PEC-based materials in various settings.

1.2 Polyelectrolyte Complexation in Nature and Industrial Settings

The terminology of polyelectrolyte complexation may seem remote for the general public; however, this phenomenon is omniscient in both nature and industrial settings. On the cellular level, the genetic carrier DNA is complexed with histone proteins and further folds into Chromatin fibers. Recently, there has been resurgent interests in using polyelectrolyte complexation as ideal prototypes to study the morphological changes and biological signaling in membraneless organelles.[9] In vitro form of the polyelectrolyte complexation consisting of oppositely charged proteins could be utilized by sandcastle worms, caddisfly larva, and barnacles as natural adhesives.[4] Distinctive differences of pH and ionic strength between their living environments, such as seawater, and secretary systems of those animals could prevent premature solidification of the glue within the secretory systems, but trigger rapid solidification after secretion. Moreover, the underwater adhesives could be further strengthened by additional covalent curing as well.[5]

In the artificial world, polyelectrolyte complexation has been adopted for industrial uses starting from the 1970s. For example, it can be applied to improve the binding performance for the paper-making industry.[10] Since actual molecular contact area in the fiber-fiber joint is the most crucial factor in paper-making, people could use the method of depositing alternating layers of cationic and anionic polyelectrolytes that further forming a polyelectrolyte coating on the fiber surface to increase the paper strength.[11,12] Furthermore, in the food industry, electrostatic complexation between milk proteins and polysaccharides is currently utilized to enhance the functional properties of dairy products, such as solubility, gel-forming ability, and foaming as well as stabilization behaviors.[13] Weinbreck et al[14–16] and Ye et al[13] have shown that by adding polysaccharides, like pectin or gum arabic, in solutions containing whey proteins or caseins

Figure 1-1. Thermodynamic investigation of polyelectrolyte complexation

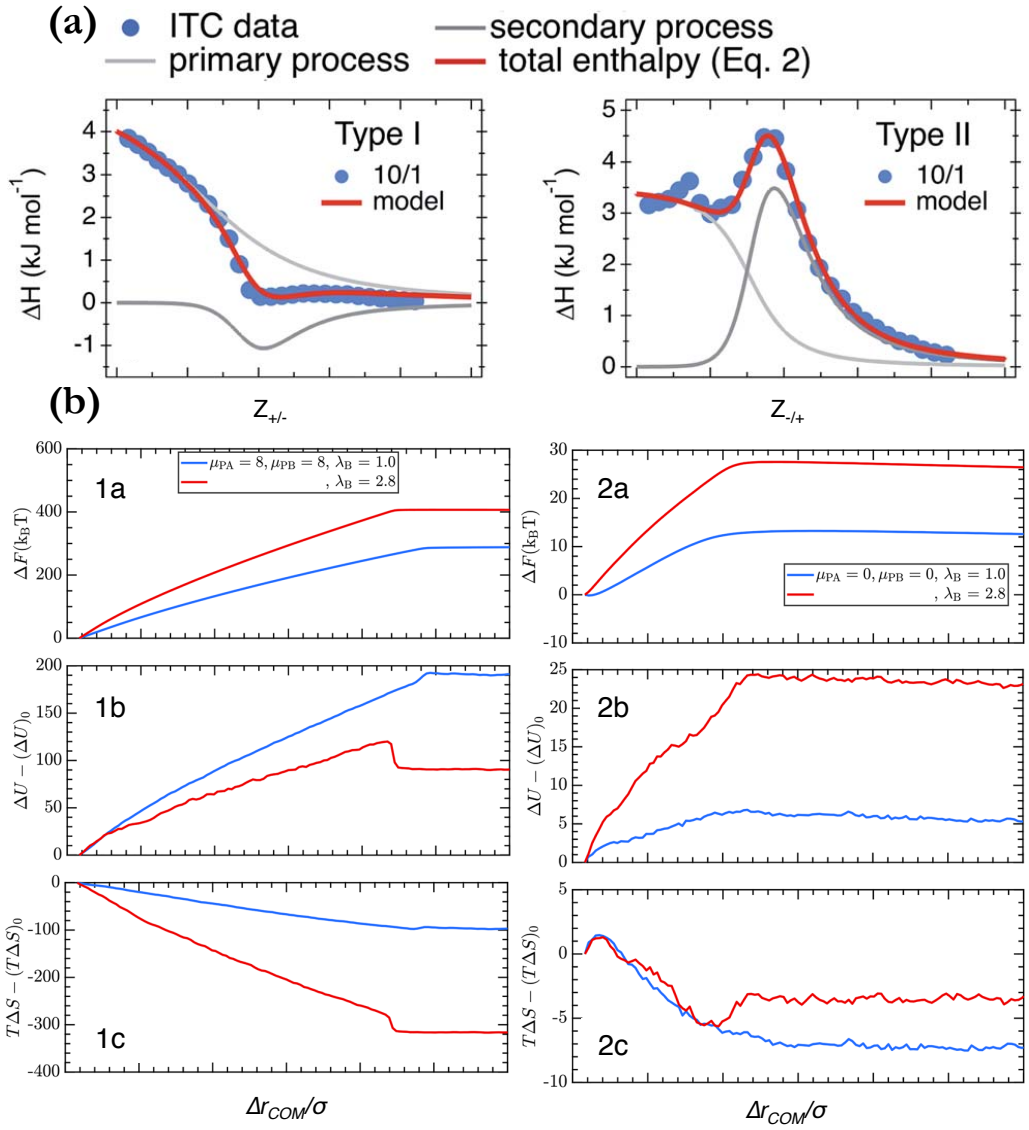

(a). Binding isotherms for PDADMAC/PAANa system. PDADMAC was used as titrant in Type I and PAANa was used as titrant in Type II. The concentration of titrant and the polymer to be titrated is 10 to 1. (b). Thermodynamic properties of complexing polyelectrolytes in strong charging limit (1a for total free energy, 1b for enthalpy, 1c for entropy) and weak associative charging limit (2a for total free energy, 2b for enthalpy, 2c for entropy). Δr_{COM} is the center of mass distance between polyacid and polybase. σ is the the distance between charged sites along the polyelectrolytes.

could lead to formation of stable complex coacervates micelles at low pH to avoid self-associates and precipitation of casein protein and promote the solubility of milk proteins at low

pH or larger temperature range.[17,18] Interestingly, Weinbreck et al also reported that oil of different flavors could be encapsulated in the complex coacervation of whey protein and gum arabic as food addictive to achieve desirable mouth feel.[19]

1.3 Advances in Polyelectrolyte Complexation Research

1.3.1 Thermodynamics and Kinetics of Polyelectrolyte Complexation

Polyelectrolyte complexation is a spontaneous process driven by a net decrease in the total free energy of the system. However, the relative magnitudes of the entropic and enthalpic contributions that drive complexation are still debated actively in the literature. Even though electrostatic interactions were intuitively identified as the major driving force in the early reports investigating complexation among polyelectrolytes,[20–23], most recent studies conclude that entropy gains from counterion release contribute significantly towards the phenomena.[24–26] Furthermore, the specific contributions to free energy have been argued to closely depend on the chemical structures of individual polyelectrolytes,[27] ionic strength and pH of the environment,[28] polyelectrolyte charge density and formulation pathways.[23,28–30] Recent efforts have quantitatively evaluated the respective contributions of enthalpy and entropy for different polyelectrolyte systems[26,31], thus providing a clearer understanding of the complexation phenomena.

Experimental approaches, like isothermal titration calorimetry (ITC)[24,32] and frontal continuous capillary electrophoresis,[31] have been used to extract thermodynamic parameters during complexation, with ITC being the most widespread technique of choice. In most commonly reported setups for ITC, the heat absorbed/supplied to keep the reservoir containing one polyelectrolyte solution (as substrate) at constant temperature is measured when the other

oppositely polyelectrolyte solution is added in aliquots (as titrant) [33]. Both *single set of identical sites* model[34,35] and *two sets of independent sites* model[36,37] have been employed in the past to describe the ITC data, but with limited success owing to the presence of multiple binding sites available between the oppositely charged polyelectrolyte chains in a complexed system. In a recent work, Vitorazi et al. modified *multiple non-interacting sites* model to capture the nature of polyelectrolyte complexation between poly(acrylic acid) sodium salt (PAANa) and poly(diallyldimethylammonium chloride) (PDADMAC) wherein binding of one site on the substrate macromolecule with the oppositely charged ligand macromolecule was considered independent from similar charged sites on the same polymer chain[32]. Complexation was described as a two-step process consisting of formation of charged polyelectrolyte complexes due to electrostatic interactions and coalescence of the charged complexes into secondary phases. Two comparative experiments of using either PDADMAC (type I) or PAANa (type II) as the titrant were conducted to investigate the influence from mixing order on the thermodynamic parameters. Representative thermograms from these experiments are shown in **Figure 1-1(a)**. After extracting thermodynamic parameters from measurements, the first step (complexation, fitted curve shown in light grey) was reported to be endothermic for both experiments but the second coalescence step was found to be exothermic for the addition of PDADMAC in PAANa and endothermic for the inverse case (fitted curve shown in dark grey). The stoichiometry coefficients, meaning the concentration ratio between PDADMAC and PAANa represented by $\frac{[+]}{[-]}$, for both mixing orders of the first step, n_A, were found to be both around 0.8, of 0.8 and 1.25 for the two types. On the other hand, the stoichiometry coefficient for the second step, n_C, were 1.1 and 1.05 respectively, suggesting neutralization of opposite charges in the complex phase.

The change in stoichiometry of the first type $\frac{[+]}{[-]}$ from 0.8 to 1.1 and $\frac{[+]}{[-]}$ from 1.25 to 0.95 was proposed as the reason for the exo/endothermic difference observed in the two kinds of the mixing order. Additionally, if the thermo-energy was converted to per titrating charge, the enthalpy was measured to be around $1k_BT$, whereas the entropy was $10k_BT$, highlighting the entropic nature of the complexation process for this polyelectrolyte pair. The entropic drive for complexation was also demonstrated by Lounis et al. wherein frontal continuous capillary electrophoresis (FACCE) was employed to investigate the complexation between poly(L-lysine) (PLL) and statistical copolymers of acrylamide and 2-acrylamido-2-methyl-1-propanesulfonate (PAMAMPS).[31] The binding site constant for interaction between each available independent binding site $-s$ on PAMAMPS chain and one PLL chain was defined as $k = \frac{[PLL-s]}{[-s][PLL]}$, with [PLL-s], [-s] and [PLL] being the concentrations of bounded sites, free sites, and free PLL chains. k exhibited a linear dependence with ionic strength on a double logarithmic scale, implying the dominant role of entropy to the formation of PECs. The slope of the linear correlation could be directly envisioned as the number of counterions released.

An extensive study by Fu et al. investigated the thermodynamic drivers of complexation among poly(styrenesulfonate) (PSSNa) with poly(diallyldimethylammonium) (PDADMA) in the presence of a series of counterions.[29] ITC measurements were conducted, but instead of fitting the data into any presumed model, the heat peaks were integrated as enthalpy ΔH_{PEC} for a systematic comparison. To further track the origins of enthalpic gain to be electrostatic or hydrogen bonding from water layer around the polyelectrolytes, the authors used the model developed by Green, Kitano and coworkers[38,39] to quantify the degree of H-bonds perturbed by complexation by Raman spectrum defined as ΔN_{corr}. It was found that ΔH_{PEC} was directly

proportional to ΔN_{corr}, with $\Delta H_{PEC} \rightarrow 0$ when $\Delta N_{corr} \rightarrow 0$. This led to the fact that the small enthalpic contribution to the total free energy was largely due to water perturbation instead of electrostatic interactions. After calculating the entropy gain as the difference between the measured enthalpies by ITC and total free energy calculated by the ion-pairing model using salt activities and swelling ratio as variants, entropy was reported to contribute 90 to 100% for complexation formation between PSS and PDADMAC polyelectrolytes in the NaCl salt range of 0.1 to 2M.

While the recent experimental results have identified entropy as the major driving force for complexation in the particular systems investigated, Monte Carlo simulation with implicit solvent reported by Rathee et al. [27] have perhaps provided a more complete picture by delineating the roles of enthalpy and entropy as a function of polymer charge densities and ionization. While entropy indeed was found to contribute majorly towards complexation of strong polyelectrolytes, enthalpy played a significant role in complexation in systems with weak electrostatic coupling or involving weak polyelectrolytes. Specifically, as shown in **Figure 1-1(b).** from 1a to 1c, for strong polyelectrolytes, at strong coupling strength of $l_B = 2.8\sigma$ (l_B is the Bjerrum length and σ is the distance between charged sites on polymer chain), the enthalpic contribution was roughly 1/3 of the entropic contribution. However, at weaker coupling strength of $l_B = \sigma$, the enthalpic contributions became twice the value of entropy. Conversely, for weak polyelectrolytes (shown in **Figure 1-1(b).** 2a to ac), in the case of strong coupling strength ($l_B = 2.8\sigma$), the entropic contribution (~$5k_BT$) was decidedly minor as compared to the enthalpic contribution (~$25k_BT$) in driving complexation. These findings were ascribed mainly to significant reduction in counterions condensed around polyelectrolytes and higher tendency of

each polymer chain to acquire charge when complexed for weak polyelectrolytes. More importantly, these findings highlight the complex interplay of various parameters that influence the energetics of the complexation phenomena that must be acknowledged in design strategies of PEC-based materials.

1.3.2 Kinetics of Polyelectrolyte Complexation

The strong drive for complexation, with free energy reductions on the order of 5~50kJ/mole, manifests as very fast kinetics of complexation processes. Regardless of the fact that complexation occurs almost instantaneously, even as fast as within milliseconds upon mixing of the solutions of oppositely charged polyelectrolytes, innovative experimental approaches have been devised to track the kinetics of complexation, revealing the true physical pathway. Liu et al. employed stopped-flow light scattering technique to monitor the early stages for PAA and PDADMAC complexation.[40] Specifically, they observed three distinct processes, with the first stage at low mixing charge ratio (z) mainly comprising relaxation and reorganization of small polyelectrolyte complexes through the initial fast mixing, the second stage at higher z comprising aggregation and rearrangement of small soluble complexes into larger structures, and finally the last step of formation of larger charge-neutralized coacervate droplets featuring bell-shaped curves in the light intensity versus time diagrams, indicating speeding up of coacervation when charge neutrality was approached. Interestingly, by manipulating the ionic strength in the solution, even though the position of the bell-shaped curve shifted, which corresponded to higher mobility of the complexed polymer at high ionic strength, the scaling factors for the decay of the curve remained constant, demonstrating that even though the rate of first stage could be adjusted by ionic strength, the last two steps followed a universal kinetic mechanism without pronounced influences from small counterions. Time-resolved ultra-

small angle X-ray scattering studies by Takahashi et al. also indicated similar kinetic pathways for PAANa and poly(allylamine hydrochloride) (PAH) complexes.[41] The growth rate of molecular weight of the global complexes formed (with time) was compared with the theoretical model for coagulation kinetics of spherical colloidal particles induced by salt. While the measured data agreed well with theoretical curves in the early stages in presence of NaCl, molecular weight of the complexes was much smaller in salt free circumstances, which suggested stronger repulsive interactions between complexes and higher viscosity of the solution. The authors proposed that the mismatch for the later stage might come from the fact that when conducting the stopped-flow mixing experiments, small amounts of excess residual component in the solution could attached to the formed complexes and cause extra repulsive interactions.

1.3.3 Phase Behavior and Morphology of Bulk Polyelectrolyte Complexes

A precise description of the phase behavior for the polyelectrolyte complexation system has been elusive ever since the first description of the phenomenon[1]. A complete description of the complex phase behavior can further facilitate accurate control of structures and properties of the resultant PEC materials and enable design of hybrid self-assembled structure that serve unique applications. The first theoretical model to quantitatively describe the system was proposed by Voorn and Overbeek in 1950s,[20,42] in which the total free energy of the solution mixture was described as a combination of a Debye-Hückle term for electrostatic interactions and a Flory-Huggins expression for entropy gain. While this simple model is an effective crude description and provided rough agreement with early experimental studies,[43,44] there are several inherent shortcomings associated with this model that were exposed in subsequent experimental studies.[5,45] Namely, the formalism is based on the Debye-Hückle framework, which neglects charge connectivity and charge distribution along the polymer chain, does not account for high

Figure 1-2. Phase behavior and morphology of polyelectrolyte complexation

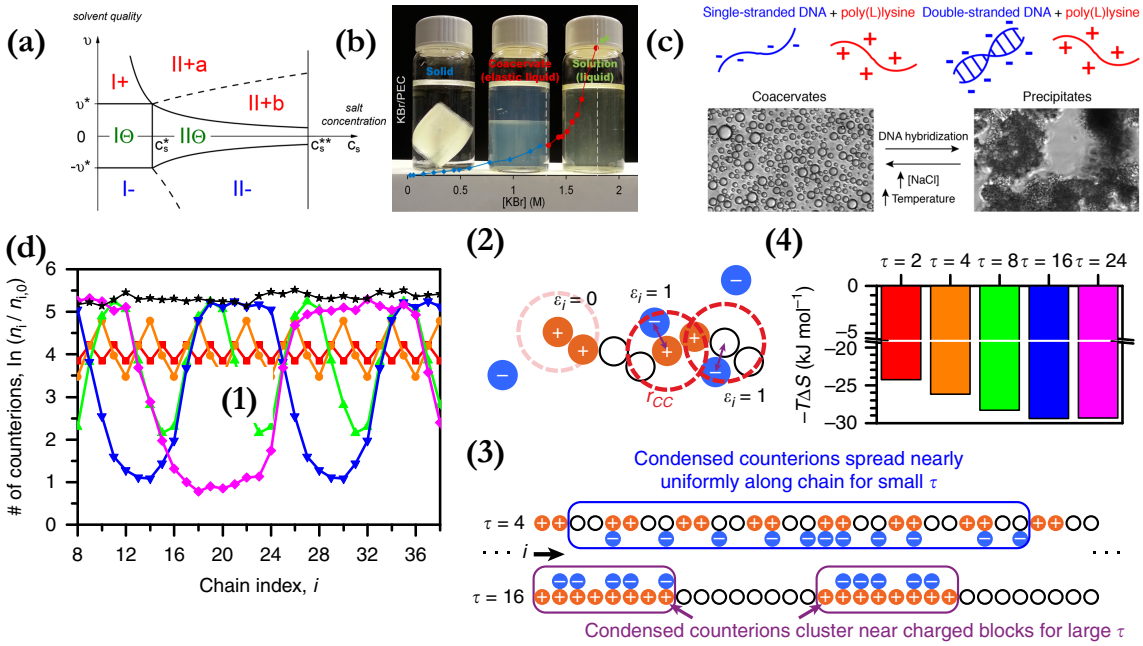

(a). Different regimes of the phase diagram divided by solvent quality and salt concentration based on scaling laws (b). Morphological transition from solid to liquid to one homogenous solution state for PSS+PDADMAC complexes with gradual addition of KBr salt. (c). Morphology of the complex phase was controlled by hybridization state of nucleic acid for single-stranded DNA formed coacervates droplets and double-stranded DNA formed precipitates. (d) Effect of charge sequence for counterion confinement entropy. (1). The number of counterions condensed along the chain index. (2). Schematic showing the criterion for a condensed counterion as the one that is within r_{CC} of a charged site on the polymer backbone. (3). Conceptual schematic illustrating the effect of charge sequence distribution on complexation. (4). Calculated entropic contribution to the total free energy for different periodicity τ.

charge density correlation effect, and is not an appropriate description of electrostatic correlation in solutions with high ionic strengths. Furthermore, it does not have inclusion of solvent effect and excluded volume interactions for ionic interactions. Recently, Larson, Qin and coworkers have also highlighted that using Debye-Hückle free energy for electrostatic correlations resulted in a reduction in the degree of ion binding at high concentrations of polyelectrolytes, and could be accounted for through charge-smearing by assigning finite sizes to each charge.[46] Several

theoretical improvements have been attempted aiming at more appropriate descriptions of the phase behavior of polyelectrolyte complexation, with early works updating versions of the Voorn-Overbeek (V-O) model to include Flory-Huggins χ parameter as non-electrostatic contribution for interactions between polymers and solvents.[44,47,48] More recently, Larson and coworkers have extended V-O model by incorporating counterion condensation, ion-pairing formation and protonation/deprotonation effects for weak polyelectrolyte as well as a χ parameter and composition-dependent dielectric constants to capture the specific physico-chemistry of different polyelectrolytes and salt identities[46,49]. At the same time, Qin et al. improved V-O model by considering full intramolecular structural correlation among charges along the backbone to account for charge connectivity and polyelectrolyte architecture.[48,49] Beyond these improvements to the V-O model, random phase approximation based theories by several groups has successfully optimized the charge concentration fluctuation via correlation function and accounted the hardcore interaction via incorporating finite particle size[50–54]; field theoretic simulation have been especially helpful in understanding inhomogeneous phases like micelle structures for block copolymers[55–57]; and PRISM along with liquid state theory have better captured the local charge density and counterion condensation profiles.[58–62] These theoretical advancements have furthered our fundamental understanding of the phase behaviors for the PEC system, and in combination with advanced experimental techniques have enabled quantitative comparisons between theoretical predictions and experimental data. Before our work, the first thorough experimental description of PEC binodal phase behavior was provided by Spruijt et al., who investigated complexation between fluorescently labeled PAA and poly(N,N-dimethylaminoethyl methacrylate) (PDMAEMA).[44] The polymer contents in the complex and the supernatant phases were estimated by measuring the fluorescent signal in the supernatant

phase, and it was assumed that salt partitioned equally into the two respective phases. Surprisingly good agreement between the experimental results and predictions form the V-O model including χ as an adjustable parameter was achieved. Besides, Tirrell and coworkers have thoroughly investigated the phase behaviors of polypeptide systems in a qualitative and semi-quantitative way via turbidity measurement and microscopic observations. In general addition of external salt and temperature increment suppressed the two phase-separated regions and interrupt the physical cross-linked networks of the formed complexes.[24,64]

Due to the essential roles of electrostatic interactions and counterions in complexation, ionic strength as well as pH of the solution, chemical nature of the counterions, charge density, molecular weight and backbone hydrophobicity of the polyelectrolytes all affect the compositions as well as the structure and properties of the complexes (and their inter-relationships).[3,47,68–79] As a general rule, moving the pH of solution away from the pKa of the polyelectrolytes, increasing chain length and increasing polyelectrolyte charge density enhance complexation and result in denser polyelectrolyte-rich complexes.[63,64,80] Additionally, increasing the salt concentration (ionic strength) in the solution screens the electrostatic interactions, lowers the entropy gain from counterion release, and thus leads to progressive decay of polyelectrolyte fraction in complexes. The ability for sodium halide salts to dissolve complexes decreased in the order of Cl^-, Br^-, I^-, generally following the Hofmeister order[73]. Moreover, divalent salt, like $CaCl_2$ and Na_2SO_4, were found to be more effective than monovalent salt in preventing complexation. Charge density of the counterions also influences their impact on the complexes – $CaCl_2$ had stronger inhibitory impact than $NaSO_4$ since Ca^{2+} ions have higher charge density than Na^+ ions whereas charges on SO_4^{2-} ion are less localized than on Cl^- ions. In a recent work by Chang et al., the blockiness of the charge sequence in non-uniformly charged polyelectrolytes

was also shown to have a profound effect on the complex compositions and phase behavior[25]. Precise sequence control in poly(glycine-co-lysine) and poly(glutamate) was enabled by solid-phase peptide synthesis; The charge distribution in sequence-controlled poly(glycine-co-lysine) was characterized its periodicity τ, with blocky polymers having larger τ and alternating polymers having smaller τ values. With increasing blockiness of charged groups (increasing values of τ), the two-phase region expanded – polymer content in the complexes and their salt resistances increased. These observations were ascribed to the disparate distribution of counterions along the polymer backbone – the counterions were evenly distributed along the chain with low τ but restricted to charged blocks with high τ (Figure 2(e)). Accordingly, larger entropy gains accompanied complexation of high τ polyelectrolytes, leading to a stronger drive for complexation (Figure 2(e)). Moreover, by the same group, Sing and coworkers, identified that architecture, stiffness and counterion valency were also essential factors affecting complexation behaviors by using a combinatorial method of transfer matrix theory and coarse-grained simulation in high charge density regime. For example, complexation would be suppressed with increasing polymer stiffness, due to the entropic penalty of aligning neighboring polyelectrolyte chains.[81]

The distinction between liquid coacervate complexes or solid precipitate complexes is debatable, with the most distinct clarification coming from Schlenoff and coworkers who proposed the crossover of storage modulus with loss modulus in frequency sweeps in the linear viscoelastic regime (as investigated through rheometry) as the transition point from liquid state to glassy state[82]. The morphology of the dense phase has also been explored through optical microscopy, wherein liquid complex coacervates appear as spherical droplets while precipitates

appear as inhomogeneous sediments[4,6]. The recovery from photo-bleaching provided another route, within the time scale of several minutes denoting the transition between solid precipitates and liquid coacervates.[83] Generally, denser complexes are more solid-like while water-rich complexes are more liquid-like. Modulation of electrostatic interactions can enable a tuning of the PEC morphology, as was demonstrated by Wang et al., wherein increasing ionic strength of the solution led to a solid-liquid-solution transition in PSS and PDADMAC PECs, seen from Figure 2(c).[3] Besides, Vieregg et al. showed that hybridization state of the nucleic acid can control the morphology of the complex phase as well for DNA(or RNA) and poly(L-lysine) system.[83] Specifically, double-stranded nucleic acids formed solid precipitates, and single-stranded nucleic acids formed liquid coacervates, and can be ascribed to the different charge densities (double-stranded DNA has a charge density ~2.4 times higher than that of the single-stranded DNA), shown in Figure 2(d).

PEC morphology is also strongly influenced by polyelectrolyte-solvent interactions and secondary intermolecular interactions among the pair of polyelectrolytes. Hydrogen bonding between chiral polypeptides lead to solid precipitates upon complexation of poly(lysine) and poly(glutamic acid), while liquid coacervate droplets were reported when either or both of the polyelectrolytes were racemic[7]. The formation of solid precipitates for chiral polypeptides was attributed to the formation of β-sheet secondary structures along the polymer chains following formation of hydrogen bonds between chiral polymers, demonstrated via FTIR, circular dichroism (CD) measurements and molecular dynamics simulations. Solvent effect or hydrophobicity of the polyelectrolyte backbone can also profoundly affect the phase behavior of the complexes. Jha et al. found experimentally that for PAA and PDADMAC complexes, as the pH decreased below 7 and PAA monomers became protonated, the salt resistance concentration

(also termed critical salt concentration) increased while the opposite trend was observed when pH was raised above 7. These trends were described by the V-O model, albeit only after incorporating a large positive χ parameter (=0.75) in V-O model. The increased hydrophobicity of neutralized PAA in acidic environment was identified to contribute towards phase separation despite reduced ionic interactions between oppositely charge polyelectrolytes.[47] Sadman et al. systematically studied the effect of backbone hydrophobicity by investigating the complexation of sodium salt of PSS with poly(4-vinylpyridine) wherein the ammonium groups were quaternized with methyl, ethyl and propyl groups, and reported increasing resistance against doping salt for swelling of complexes with increasing hydrophobicity, along with functional group-independent rheological behavior of the complexes.[6] From a theoretical perspective, Rumyantsev et al. studied the effect of salt concentration c_S and solvent quality, characterized by second virial coefficient ν, on polymer density φ, surface tension γ, salt partitioning δ and correlation lengths ξ for weakly charged polyelectrolytes with equal degrees of ionization. Power laws for ν, φ, γ, δ, ξ were derived based on scaling theory for different regimes on c_S-ν diagram, corresponding to high/low salt concentrations with poor/Θ/good solvents shown by (b) in Figure 2. As a note, subregimes of IIa and IIb were divided by the fact that Debye blobs can be either swollen for the former or Gaussian for the later. [54] The results for different regimes distinguished in Figure 2(b) were summarized in Table 1., wherein u is dimensionless Bjerrum length of l_B/unit length, f is the degree of ionization, v is the second viral coefficient, w is the third viral coefficient and c_s is the salt concentration. Thus, it cannot be straightforwardly concluded that weak polyelectrolytes always form water-rich liquid coacervates and strong polyelectrolytes yield denser precipitates.

Regime	ϕ	ξ	γ	$\delta c_s/c_s$
IΘ	$u^{1/3}f^{2/3}w^{-4/}$	$u^{-1/3}f^{-2/3}w^{1/9}$	$u^{2/3}f^{4/3}w^{-7/18}$	$u^{4/3}f^{2/3}w^{-1/9}$
IIΘ	$f^2{c_s}^{-1}w^{-2/3}$	$f^{-2}c_s w^{1/3}$	$f^4{c_s}^{-2}w^{-5/6}$	$u^{1/2}f^4{c_s}^{-5/2}w^{-2/3}$
II-	$\lvert v\rvert w^{-1}$	$\lvert v\rvert^{-1}w^{2/3}$	$\lvert v\rvert^2 w^{-3/2}$	$u^{5/4}f^{1/2}\lvert v\rvert^{1/4}w^{-1/4}$
II-				$u^{1/2}f^2{c_s}^{-3/2}\lvert v\rvert w^{-1}$
II+	$u^{4/7}f^{8/7}v^{-5/}$	$u^{-3/7}f^{-6/7}v^{2/7}$	$u^{6/7}f^{12/7}v^{-4/7}$	$u^{10/7}f^{6/7}v^{-2/7}$
II+a	$f^8{c_s}^{-4}v^{-3}$	$f^{-6}{c_s}^3v^2$	$f^{12}c^{-6}v^{-4}$	$u^{2/3}f^{10}{c_s}^{-16/3}v^{-10/}$
II+b				$u^{1/2}f^{10}{c_s}^{-11/2}v^{-3}$

Table 1-1. Scaling laws for coacervates physical properties

While most of the past as well as recent works have focused on symmetric complexes wherein the polyelectrolyte charges and concentrations are matched, researchers have also begun investigating the more intricate but, at the same time, more practically relevant cases of asymmetric complexes wherein non-stoichiometric or overcharged complexes can form.[74,84,85] Notably, Wang and coworkers have extensively studied the phase behavior of asymmetric systems based on liquid state theory by constructing 3D polyanion-polyanion-cation phase diagrams, which could be related to experimentally accessible parameters of the initial polyelectrolyte concentration $\rho_{P,0}$, the extra salt concentration $\rho_{S,0}$, and the asymmetry factor r, defined as $r = \frac{V_1 - V_2}{V_1 + V_2}$ wherein V_1 is the volume of polycation solution with initial polyelectrolyte concentration $\rho_{P,0}$ and V_2 is the volume of polyanion solution with the same initial polyelectrolyte concentration $\rho_{P,0}$. Accordingly, r=0 corresponded to symmetric case and r=1 meant pure polycation solution. Specifically, they found that the phase separation region along r

axis would shrink with increasing $\rho_{P,0}$ and $\rho_{S,0}$ and eventually vanish for sufficiently large $\rho_{P,0}$ and $\rho_{S,0}$, which could be seen from (a) in Figure 3. Additionally, the composition of the complex

Figure 1-3. Polymer conformation and structures

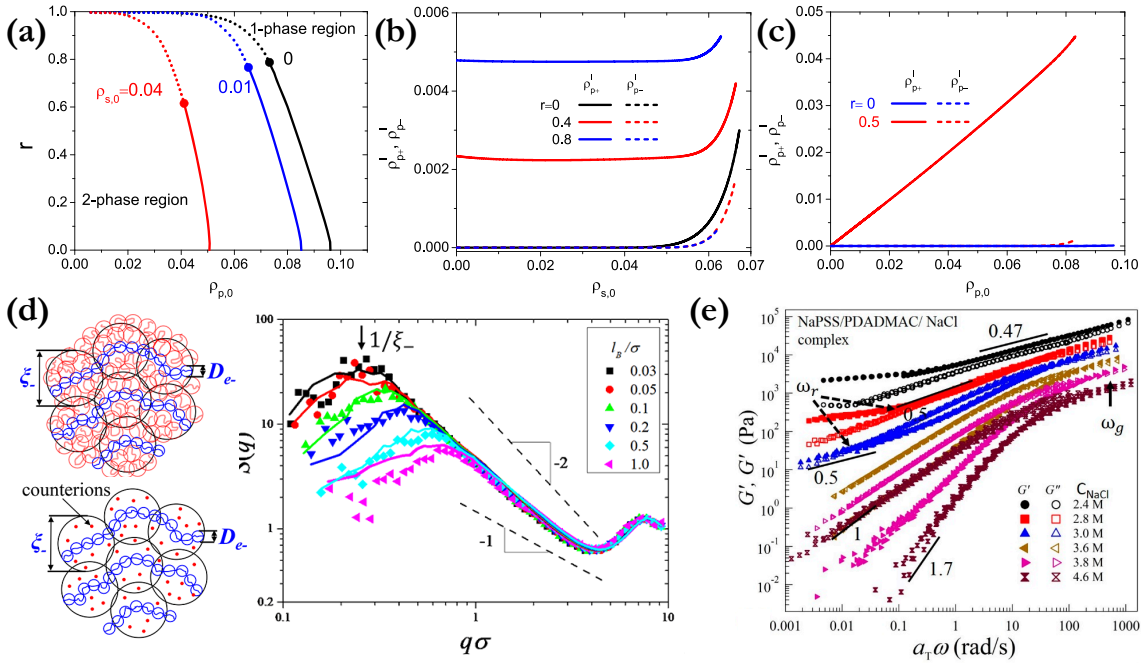

(a) Phase separation region obtained from systems with different asymmetric factor, initial polymer concentration and extra salt concentration. (b)(c) The concentrations of polycation and polyanion in the supernatant phases at different asymmetric factor, initial polymer concentration and extra salt concentration. (d). Conformations of polyanions in the coacervate (top) are analogous to their conformations in solutions of only polyanions (bottom) at the same concentration. The scattering figure compared the structure factors of polyanions in coacervates (symbols) and in semidilute solutions (lines) with the same polyanion concentration at different Bjerrum length l_B. (e) Plots of frequency-dependent viscoelastic moduli G' and G'' for PSS+PDADMAC complexes prepared at different NaCl concentrations, where the solid-to-liquid transition by addition of salt could be observed.

phase was found to only weakly vary with r but decreased monotonically with increasing $\rho_{P,0}$ and $\rho_{S,0}$, which can be understand as self-suppression and screening effects. However, for the supernatant phase shown by (b) and (c) in Figure 3, except the regions near the critical points,

the major polyelectrolytes (the one in excess) nearly remained constant with $\rho_{S,0}$, but increased with $\rho_{P,0}$ and r while the minor polyelectrolyte was nearly 0 always.

1.3.4 Structures and Properties of Bulk Polyelectrolyte Complexes

Michaels proposed two possible conformations of polyelectrolytes existing in the complexes in 1965 as ladder-like or scrambled-egg structures.[86] Since then, small angle neutron, X-ray and light scattering techniques have been utilized to characterize the polyelectrolyte chain conformations in PECs. The general consensus is that the chains preserve their Gaussian conformation upon complexation leading to coacervates.[87–90] Tirrell and coworkers recently presented an in-depth comparison of the polyelectrolyte structure in solution and in complexes for PECs comprising poly(lysine) and poly(glutamic acid) using small angle X-ray scattering studies.[91] For this polymer pair, liquid coacervates formed if one of the polyelectrolytes in the complex was racemic and solid precipitates formed if both polyelectrolytes were chirally pure.[7] In solution, the individual polyelectrolytes exhibited strong correlation peaks associated with the intra-chain repulsion along with the inverse of the peak position (corresponding to correlation length) decreasing quadratically with increasing polyelectrolyte concentration. The correlation peaks were severely suppressed in the scattering from liquid complex coacervates, and the correlation length extracted from the scattering patterns denoted a homogenous semi-dilute solution of juxtaposed oppositely charged polyelectrolytes maintaining their self-avoiding random walk conformation, pointing towards a scrambled egg like arrangement of the chains. However, in the solid precipitates, hydrogen bonding resulted in β sheet formation and manifested as aggregation of chains in the complexes, indicating possible formation of ladder-like structure. At the same time, neutron scattering investigations by Fare et al. revealed that

regardless of the strong swelling of complexes upon addition of KBr into PDADMA/PSS complexes, the coil size of the PSS polymer remained constant up to 1.4 M KBr, which was unexpected and significantly different from the polyelectrolyte behavior in simple solution state.[92] Cryo-electron microscopy images revealed the existence of polymer-rich and polymer-deficient micro-phases with excess water and salt squeezed into adjacent pores in the complex phase, thus leading to the unexpected independence of polyelectrolyte coil size with increasing KBr concentrations.

At the same time, recent theoretical and simulation works have identified that the polymers in the coacervates could form interpenetrating networks and adopt conformations analogous to quasi-neutral and polyelectrolyte solutions for polymers having low and high charge densities respectively.[93] For symmetric case of weak polyelectrolytes with equally sized electrostatic blobs [93], the coacervate phase could be envisaged as a dense packing of electrostatic blobs with electrostatic attractions between the oppositely charged chains stabilized by short-range non-electrostatic repulsion from excluded-volume effect between neighboring blobs. For asymmetric case of stronger intramolecular electrostatic repulsion in polyanions than in polycations (polyanion blob size < polycation blob size), polycations in the complex coacervates would adopt the ideal chain conformation in a Θ solvent with correlation length ξ_+ smaller than polycation blob size$_+$, and polyanion, with blob size (D_{e-}) larger than the correlation length ξ_-, would stretch on length scales between D_{e-} and ξ_- owing to strong intramolecular repulsion. In this case, for weakly charged polyelectrolytes with electrostatic interaction energy per charge less than thermal energy kT, conformations of both oppositely charged polyelectrolytes in coacervates resembled to those in their respective pure solutions containing only one kind of polyelectrolytes. For example, as shown by Figure (d), the conformation of the polyanion in

PEC is analogous to that of solution containing only polyanions at the same polymer concentration, supported by the measured structure factors of the coacervates and polyanion solutions.

The dynamics of individual polymer chains and water molecules have been investigated using dynamic nuclear polarization enhanced nuclear magnetic resonance (DNP) and electron paramagnetic resonance (EPR) measurements.[94,95] In the complexes formed by PAA and poly(ethylene-alt-maleic acid),[95] the segmental mobility of PAA was found to be nearly constant in the pH range from 5 to 10 but decreased heavily in acidic conditions, which was reasoned to be caused by formation of hydrogen bonding among carboxyl groups. Thus, counterintuitively, the strength of attractive interactions did not have significant influence upon the polymer dynamics in the complex phase under neutral and basic conditions.

The composition and the morphology of the complexes is strongly correlated with their viscoelastic behavior which ranges from simple Maxwell liquids wherein the loss (G'') and the storage (G') moduli follow a linear and quadratic dependencies on the frequency ω of the oscillatory flow field, respectively ($G' < G''$)[8,96,97] to solid-like glassy state wherein $G' > G''$ and both the moduli are nearly independent of ω.[6,97–99] In general, increasing the chain length, employing stronger polyelectrolytes and lowering the ionic strength in the environment are accompanied with an increase in the absolute values of both G' and G''.[6,8,80,97] Unlike the permanently cross-linked polymers by covalent bonds, PECs exhibit reversible viscoelasticity due to the electrostatic nature of the interactions among polyanions and polycations capable of forming and breaking continuously. The ionic bonds hinder polymer mobility in the complex phase and serve as "sticky points". Accordingly, addition of salt or pH variation influence the strength of electrostatic interactions and rheological behaviors.[97,99,100] Consequently, time-salt or

time-pH superposition could be used to produce master curves with broader accessible frequency range of 2 to 5 more orders of magnitude.[6,91,96] Spruijt et al. proposed that the horizontal shift factor was proportional to $\exp(-A\sqrt{c_s}+B)$ (c_s is salt concentration, A and B are constants), and showed good agreement with experimental data for PDMAEMA and PAA complexes in the salt range of 0.4 to 1.2M at different polymer chain length, chain length matching, and mixing stoichiometry. The dependence on salt of shift factor was further illustrated more explicitly by Hamad et al. by $\exp(1/a-\sqrt{8\pi l_B c_s N_A})$ (a is bond length, l_B is Bjerrum length), derived from the assumption that the activation energy for dissociation of one ionic pair equals the energy needed to separate one ion pair from bond length a to Debye length ($(8\pi l_B c_{salt} N_A)^{-0.5}$). This model adequately described the rheological behavior of PDADMAC and poly(isobutylene-alt-maleate sodium) (PIBMANa) complexes at different salt concentrations and chain length.[97] However, an exponential dependence of the shift factor on c_{salt} (as opposed to previously reported $\exp\sqrt{c_s}$) was demonstrated by Marciel et al., possibly due to the different salt range investigated and the hydrophilicity of the peptide backbones.[8] Moreover, the solid-to-liquid transition could be quantitatively captured by rheological characterization as well.[101,102] Liu et al. utilized time-salt superposition to expand the range of frequency space in viscoelastic measurements for both liquid and solid state of PSS and PDADMAC complexes, and proposed that gelation occurred at low salt concentrations when the network of trapped cross-linked ionic interactions percolated the materials with insufficient salt molecules to facilitate the chain motion.[101] Additionally, for the same system, Ali and Prabhu achieved time-temperature-salt superposition over the entire range of frequencies at high salt concentrations. However, limited overlapping was observed at low salt concentrations or low frequency in Figure 3(e), which was

mainly resulted from impaired mobility and correlated collective dynamics of longer segments between ion pairs or polymers entanglements.[102]

1.3.5 Interfacial Properties

Low interfacial tension of the liquid coacervates has long been identified. Surface forces apparatus (SFA) measured the interfacial tension γ to be in the range of 0.1 to 10 mJ/m^2 for poly(L-glutamic acid sodium salt) and poly(L-lysine hydrochloride) coacervates.[103] γ was found to decrease with increasing salt concentration and decreasing chain length. Theoretical work by Qin et al. derived explicit expression of the interfacial tension by using Debye-Hückle approximation for Cahn-Hilliard theory as

$$\gamma = \left(\frac{k_B T_c a}{\nu}\right) \frac{(1 - \psi_0/\psi_c)^{3/2}}{N^{1/4}}$$

with T_c, a, ν, ψ_c, and N being the critical temperature, width of the interface, the swelling exponent, critical salt concentration and polymer chain length.[104] Molecular weight and salt concentration were thus identified as accessible parameters to control in experiments to manipulate interfacial tension of coacervates. More recently, Lytle et al. have showed consistent results from both Monte-Carlo simulations and transfer matrix theory to reproduce interfacial features, including the effect of salt concentration on interfacial tension, interfacial width, and interfacial excess of salt, present in large-scale molecular dynamics simulation. Similarly, utilizing the analogous interface between a coacervate and a neutral polymer, they further investigated the phase behavior of coacervation-driven self-assemblies, which are unlike the classical simple polymer-polymer interface driven by a positive short-range χ parameter They found adding a neutral polymer or increasing neutral polymer density could also expand the

immiscible regions on the phase diagram and result in large regions of small but positive surface tension, due to the interplay between the excluded volumes of polymeric species. [105]

1.4 Applications

1.4.1 Artificial Underwater Adhesives

Inspired by the naturally occurring PEC underwater adhesives produced by sandcastle worms and mussels,[106] [107] researchers have synthesized macromolecular adhesives that harness electrostatic or cation-π interactions enhanced by subsequent covalent crosslinking to provide robust binding in aqueous environments. Zhao et al. employed bis(trifluoromethane-sulphonyl)imide (Tf_2N^-) (QCS-Tf_2N) polycation and catechol-functionalized PAA polyanion to create underwater adhesives wherein rapid complexation and catechol based adhesion was achieved via solvent exchange. The polyelectrolytes, initially dissolved in low dielectric constant DMSO, formed complex coacervates rapidly (within a minute) upon switching to aqueous media, and formed strong bonding with substrates in ~30 minutes (the process is shown in **Figure 1-4(a)**). SEM images revealed the morphology of the setting substance to be porous-like, whose porosity was directly related with the fraction of catechol in the system.[108] Gebbie et al. have harnessed complexation driven by cation-π interactions to achieve reversible adhesion interaction between lysine-rich and phenylalanine containing polypeptides providing stronger adhesives in comparison to the mussel-mimetic polypeptides with Dopa sequences.[109] Surprisingly, Kim et al. demonstrated liquid-liquid coacervation could also form between both positively charged macromolecules with two adapted recombinant mussel foot protein of Rmfp-1 with π-rich structures and MADQUAT with its trimethylammonium group.[110] The strong short-

range cation-π interaction could trigger underwater adhesion, which was inspired by marine mussels.

1.4.2 Multifunctional Membranes

Polyelectrolyte complexes membranes have long been assembled using layer-by-layer (LbL) assembly,[111,112] but sophisticated fabrication process in the LbL fabrication and low yield rates have promoted alternative strategies to produce PEC membranes, including electro-spinning,[113,114] spin-coating,[115] electrochemical deposition[116] and other one-step protocols.[117,118] Sadman et al. deposited PEC films consisting of PAA and PAH by carrying out electrochemical reduction at quartz crystal microbalance electrodes.[116] Kelly et al. have doped PSS and PDADMAC complexes with KBr to reduce viscosity and impart processability followed by spin-coating the complexes to form uniform and smooth membranes, and subsequently vitrification by removing KBr upon immersion in water baths.[115] The schematics demonstrating the spin-coating process, an exemplary photo of the formed PEC membrane, and the effects of spinning speed as well as time on membrane thickness were shown by **Figure 1-4(d)**. Those high-throughput methods enabled future application of electrodeposited paints and smart coatings. Smith et al. obtained thin films of PDADMAC and PAA by consecutively dipping the PET substrate into polyelectrolyte solution mixture maintained at pH = 2 and then into a pH = 3 citric buffer solution for curing to obtain ~ 2 μm thick PEC coatings that exhibited more than 2 orders of magnitude reduction in oxygen transmission rate than uncoated PET substrate by increasing cohesive forces within PEC with presence of ionic crosslinking as small molecule barrier.[117] Cain et al. coated cotton fibers with PECs by immersing them in poly(phosphate sodium salt) and branched polyethylenimine (PEI) mixtures to enhance flame-retardant attributes.[118] Evaluated by TGA, vertical flame testing and micro-combustion calorimeter, the percentage of

the unburned residue increased with increasing PEC coating weight, afterglow was not observed for any of the coated fabrics when flame was removed while the uncoated sample was consumed

Figure 1-4: Innovative applications by PEC materials

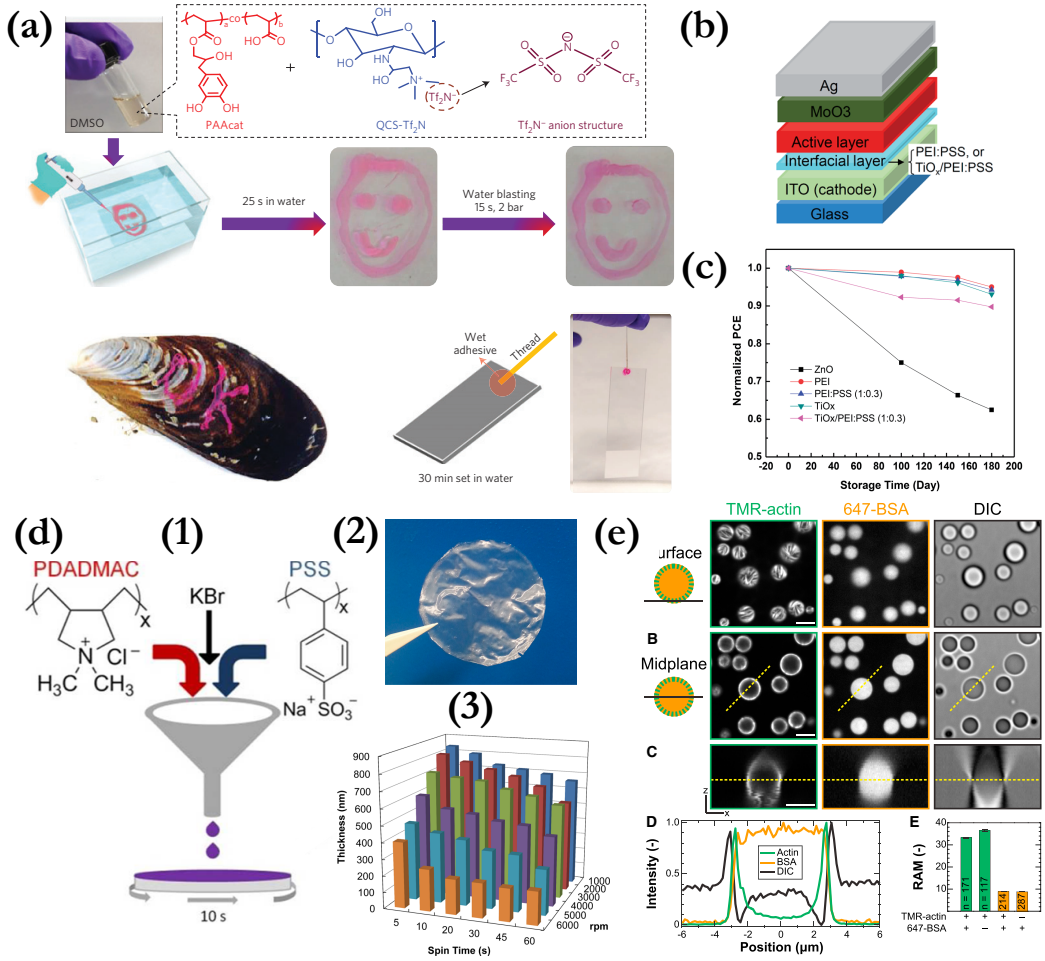

(a). Water-DMSO solvent exchange triggered wet-adhesion process. (b). Device structure of high-efficiency inverted polymer solar cells utilizing PEC materials. (c) Power conversion efficiency of different materials for solar cells. (d) (1) Demonstration of the spin-coating device using PSS+PDADMAC coacervates with KBr. (2) Standalone PEC film (1 inch diameter and 15 μm thickness) spun from PSS+PDADMAC in 1.7M KBr at 1000rpm (3) Thickness of the spun films of PSS+PDADMAC in 1.9M KBr at different spinning speed and time. (e) Encapsulation of action and BSA in polypeptide coacervates. Confocal fluorescence (left and middle) and differential interference contrast (DIC) microscopy (right) showed accumulation of actin on the periphery of coacervates droplets while BSA was distributed uniformly.

with ashes radiating for another 21 seconds after removal of the flame. Additionally, the heat release rate as well as total heat released were all reduced by up to 70% in coated vs. uncoated fibers. Meng et al. have demonstrated electrospun PSS and PDADMAC fibers to make stable fiber mats for a range of pH values, ionic strength and different organic solvents. These multifunctional membranes can be promising candidates for various industries, like food or pharmaceutical production, water treatment and electronics packaging process.

1.4.3 Encapsulants

PECs, and specifically complex coacervates, have long been posited as models for proto-cellular environments owing to their rapid self-assembly and spontaneous partitioning (nearly resembling complete encapsulation) of charged (macro)molecules, leading to dense, polymer-rich environments with high concentration of charged species.[9,119,120] These attributes have also been harnessed in synthetic systems to *encapsulate* biologically relevant molecules, like short therapeutic nucleotide-sequences and proteins, as well as small synthetic molecules into the complex phases in both bulk[121–123] or micellar assemblies[124]. Black et al. demonstrated strong encapsulation of bovine serum albumin (BSA) in poly(lysine) and poly(glutamic acid) coacervate droplets.[125] The negatively-charged fluorescently-labeled BSA were first complexed with poly(lysine) to form intermediate complexes, and then poly(glutamic acid) was added to form coacervate droplets. The fluorescent signals indicated accumulation of BSA mostly in the coacervates droplets along with a preservation of the secondary structure of the protein, as confirmed by CD spectra. McCall et al. employed the same coacervate material platform to co-encapsulate BSA and globular actin in coacervate droplets and investigated the assembly of actin filaments as a proxy for protein activity in these systems. Actin filaments were found to form at rates 50-folds faster than solution assembly of actin filaments, and the filaments were found to

concentrate near the droplet peripheries leading to spherical shells of actin filaments while BSA was found to be uniformly distributed inside the coacervate droplets, shown in Figure 3 (e). Synthetic dyes of varying chemical structures with different electrostatic strength, hydrophobicity and aromaticity have also been employed as model encapsulants in PEC materials owing to their viable traceability. Partitioning of methylene blue into the complexes formed by PSS was found to be 3~8 times stronger compared with other polyanions like PAA or poly(vinyl sulfonate) depending on solution pH, and has been ascribed to $\pi - \pi$ stacking between benzene rings.[126] Recently, Meng et al. demonstrated successful incorporation of two families of six individual dyes, with different chemical structures and electrostatic strength, into electrospun fibers made from PSS and PDADMAC complexes.[127]

1.4.4 Other Applications

Apart from the major application areas mentioned above, there are several innovative reports exploring unconventional use of PEC materials. Since microencapsulation has been actively explored in this field, encapsulating liquids inside the PECs has enabled the use of PECs as oil-water emulsion stabilizers.[128] Rodriguez et al. illustrated the potential of using PAA and PDADMAC complexes over the pH range from 2 to 10 to stabilize 5 different kinds of organic reagents in water. It turned out that no stable emulsion was formed for low and intermediate pH, since the number of coacervate droplets/precipitate particles showing positive zeta potential was not sufficient for stabilization or the precipitate aggregates were too large to attach to droplet surfaces. Only at higher pH from 7 to 10, when the coacervates were nearly neutral in charge status, stable dodecane-water emulsion was formed. The stabilization ability of the oil droplets coated by coacervates was further compared with theoretical predictions using equilibrium spreading coefficients. While agreement was achieved for dodecane and toluene, deviation was

observed for other oils owning to not accounting kinetic variation by viscosity change of coacervate formation in the equilibrium spreading coefficients. The mechanical and electronic responses of PEC materials have also been adjusted by changing polyelectrolyte chemistry, concentration and charge density, pH and salt chemistry and concentrations to boost their utility in unique applications. Bulk PEC materials with appropriate viscosity and gelation rates have been used as extruding materials to construct complex structures in 3D printing.[129] PEI:PSS PEC films have also been demonstrated to enhance power conversion efficiency (PCE) in polymeric solar cells from 3.01% of PEI-only interlayer to 3.68% by enhancing the cell short circuit current, owning to improved electron extraction at the PEI:PSS-active-layer interfaces.[130] The architecture of the optimized solar cell was shown by **Figure 1-4(b)**. The cell performance could be further enhanced by TiO_x-PEI:PSS combined interfacial layer without the need for light-soaking treatment for TiO_x. **Figure 1-4(c)** exhibited the improved PCE values for different kinds of layer materials. Additionally, the complex coacervation of PSS and poly(3-[6'-{N-butylimidazolium}hexyl]thiophene) bromide formed in tetrahydrofuran-water mixture was used to form dense suspensions of π-conjugated materials, which could be used for large-scale processing of optoelectronic devices, chemical sensors and bioelectronics applications.

1.5 References

1. Jong, B. de, Kruyt, H. G. & R, H. Koazervation. *Proc. K. Ned. Akad. Wet.* **32**, 849–856 (1929).

2. Bungenberg De Jong, H. G. & Kruyt, H. R. Coacervation. (Partial miscibility in colloid systems). (Preliminary Communication). *Chemistry (Easton)*. (1929).

3. Wang, Q. & Schlenoff, J. B. The polyelectrolyte complex/coacervate continuum. *Macromolecules* (2014). doi:10.1021/ma500500q

4. Chollakup, R., Smitthipong, W., Eisenbach, C. D. & Tirrell, M. Phase behavior and coacervation of aqueous poly(acrylic acid)-poly(allylamine) solutions. *Macromolecules* **43**, 2518–2528 (2010).

5. Li, L. *et al.* Phase Behavior and Salt Partitioning in Polyelectrolyte Complex Coacervates. *Macromolecules* **51**, 2988–2995 (2018).

6. Sadman, K. *et al.* Influence of Hydrophobicity on Polyelectrolyte Complexation. *Macromolecules* **50**, 9417–9426 (2017).

7. Perry, S. L. *et al.* Chirality-selected phase behaviour in ionic polypeptide complexes. *Nat. Commun.* (2015). doi:10.1038/ncomms7052

8. Marciel, A. B., Srivastava, S. & Tirrell, M. V. Structure and rheology of polyelectrolyte complex coacervates. *Soft Matter* **14**, 2454–2464 (2018).

9. Brangwynne, C. P., Tompa, P. & Pappu, R. V. Polymer physics of intracellular phase transitions. *Nat. Phys.* (2015). doi:10.1038/nphys3532

10. Müller, M. *Polyelectrolyte Complexes in the Dispersed and Solid State II Application Aspects*. (Springer, 2013).

11. Decher, G., Hong, J. D. & Schmitt, J. Buildup of ultrathin multilayer films by a self-assembly process: III. Consecutively alternating adsorption of anionic and cationic polyelectrolytes on charged surfaces. *Thin Solid Films* **210–211**, 831–835 (1992).

12. Wagberg, L., Forsberg, S. & Johansson, A. Engineering of fibre surface properties by application of the polyelectrolyte multilayer concept. Part I: modification of paper strength. *J Pulp Pap Sci* **28**, 222–227 (2002).

13. Ye, A. Complexation between milk proteins and polysaccharides via electrostatic interaction: Principles and applications - A review. *Int. J. Food Sci. Technol.* **43**, 406–415 (2008).

14. Weinbreck, F., de Vries, R., Schrooyen, P. & de Kruif, C. G. Complex coacervation of whey proteins and gum arabic. *Biomacromolecules* **4**, 293–303 (2003).

15. Weinbreck, F., Nieuwenhuijse, H., Robijn, G. W. & De Kruif, C. G. Complex Formation of Whey Proteins: Exocellular Polysaccharide EPS B40. *Langmuir* **19**, 9404–9410 (2003).

16. Weinbrreck, F., Tromp, R. H. & de Kruif, C. G. Composition and structure of whey protein/gum arabic coacervates. *Biomacromolecules* **5**, 1437–1445 (2004).

17. Tromp, R. H., De Kruif, C. G., Van Eijk, M. & Rolin, C. On the mechanism of stabilisation of acidified milk drinks by pectin. *Food Hydrocoll.* **18**, 565–572 (2004).

18. Dalgleish, D. G. Casein Micelles as Colloids: Surface Structures and Stabilities. *J. Dairy Sci.* **81**, 3013–3018 (2010).

19. Weinbreck, F., Minor, M. & de Kruif, C. G. Microencapsulation of oils using whey protein/gum arabic coacervates. *J. Microencapsul.* **21**, 667–679 (2004).

20. Overbeek, J. T. G. & Voorn, M. J. Phase separation in polyelectrolyte solutions. Theory of complex coacervation. *J. Cell. Comp. Physiol.* **49**, 7–26 (1957).

21. Arthur Veis, C. A. Phase separation in polyelectrolyte systems. I. complex coacervates of gelatin. *J. Phys. Chem.* **64**, 1203–1210 (1960).

22. Veis, A. Phase separation in polyelectrolyte solution. II. interaction effect. *J. Phys. Chem.* **65**, 1798–1803 (1961).

23. Veis, A. A review of the early development of the thermodynamics of the complex coacervation phase separation. *Adv. Colloid Interface Sci.* **167**, 2–11 (2011).

24. Priftis, D., Laugel, N. & Tirrell, M. Thermodynamic Characterization of Polypeptide Complex Coacervation. *Langmuir* **28**, 15947–15957 (2012).

25. Chang, L. W. *et al.* Sequence and entropy-based control of complex coacervates. *Nat. Commun.* (2017). doi:10.1038/s41467-017-01249-1

26. Lytle, T. K. & Sing, C. E. Tuning chain interaction entropy in complex coacervation using polymer stiffness, architecture, and salt valency. *Mol. Syst. Des. Eng.* (2018). doi:10.1039/c7me00108h

27. Rathee, V. S., Sidky, H., Sikora, B. J. & Whitmer, J. K. Role of Associative Charging in the Entropy−Energy Balance of Polyelectrolyte Complexes. *J. Am. Chem. Soc* **140**, 19 (2018).

28. Priftis, D., Laugel, N. & Tirrell, M. Thermodynamic Characterization of Polypeptide

Complex Coacervation. *Langmuir* **28**, 15947–15957 (2012).

29. Fu, J. & Schlenoff, J. B. Driving Forces for Oppositely Charged Polyion Association in Aqueous Solutions: Enthalpic, Entropic, but Not Electrostatic. *J. Am. Chem. Soc.* (2016). doi:10.1021/jacs.5b11878

30. Tang, J. D., Caliari, S. R. & Lampe, K. J. Temperature-Dependent Complex Coacervation of Engineered Elastin-like Polypeptide and Hyaluronic Acid Polyelectrolytes. *Biomacromolecules* (2018). doi:10.1021/acs.biomac.8b00837

31. Lounis, F. M., Chamieh, J., Leclercq, L., Gonzalez, P. & Cottet, H. The effect of molar mass and charge density on the formation of complexes between oppositely charged polyelectrolytes. *Polymers (Basel).* (2017). doi:10.3390/polym9020050

32. Vitorazi, L. *et al.* Evidence of a two-step process and pathway dependency in the thermodynamics of poly(diallyldimethylammonium chloride)/poly(sodium acrylate) complexation. *Soft Matter* (2014). doi:10.1039/c4sm01461h

33. Kayitmazer, A. B. Thermodynamics of complex coacervation. *Advances in Colloid and Interface Science* (2017). doi:10.1016/j.cis.2016.07.006

34. Bucur, C. B., Sui, Z. & Schlenoff, J. B. Ideal mixing in polyelectrolyte complexes and multilayers: Entropy driven assembly. *J. Am. Chem. Soc.* **128**, 13690–13691 (2006).

35. Feng, X., Leduc, M. & Pelton, R. Polyelectrolyte complex characterization with isothermal titration calorimetry and colloid titration. *Colloids Surfaces A Physicochem. Eng. Asp.* **317**, 535–542 (2008).

36. Aberkane, L., Jasniewski, J., Gaiani, C., Scher, J. & Sanchez, C. Thermodynamic characterization of acacia gum-β-Lactoglobulin Complex Coacervation. *Langmuir* **26**, 12523–12533 (2010).

37. Kim, W., Yamasaki, Y., Jang, W. D. & Kataoka, K. Thermodynamics of DNA condensation induced by poly(ethylene glycol)- block -polylysine through polyion complex micelle formation. *Biomacromolecules* **11**, 1180–1186 (2010).

38. Tsukida, N., Muranaka, H., Ide, M., Maeda, Y. & Kitano, H. Effect of Neutralization of Poly (acrylic acid) on the Structure of Water Examined by Raman Spectroscopy. *J. Phys. Chem. B* **101**, 6676–6679 (1997).

39. Green, J. L., Lacey, A. R. & Sceats, M. G. Determination of the intrinsic netwrok defect density in liquid water. *Chem. Phys. Lett.* **130**, 67–71 (1986).

40. Liu, X. *et al.* Early stage kinetics of polyelectrolyte complex coacervation monitored through stopped-flow light scattering. *Soft Matter* (2016). doi:10.1039/c6sm01979j

41. Takahashi, R., Narayanan, T. & Sato, T. Growth Kinetics of Polyelectrolyte Complexes Formed from Oppositely-Charged Homopolymers Studied by Time-Resolved Ultra-Small-Angle X-ray Scattering. *J. Phys. Chem. Lett.* (2017). doi:10.1021/acs.jpclett.6b02957

42. Voorn, M. J. *Complex Coacervation.* (Wiley-VCH Verlag GmbH Co., 1956).

43. Arthur, V., Edward, B. & Shirley, M. Molecular weight fractionation and the self-suppression of complex coacervation. *Biopolymers* **5**, 37–59 (1967).

44. Spruijt, E., Westphal, A. H., Borst, J. W., Cohen Stuart, M. A. & Van Der Gucht, J. Binodal compositions of polyelectrolyte complexes. *Macromolecules* **43**, 6476–6484 (2010).

45. Meng, X., Perry, S. L. & Schiffman, J. D. Complex Coacervation: Chemically Stable Fibers Electrospun from Aqueous Polyelectrolyte Solutions. *ACS Macro Lett.* **6**, 505–511 (2017).

46. Friedowitz, S., Salehi, A., Larson, R. G. & Qin, J. Role of electrostatic correlations in polyelectrolyte charge association. *J. Chem. Phys.* **149**, (2018).

47. Jha, P. K., Desai, P. S., Li, J. & Larson, R. G. pH and salt effects on the associative phase separation of oppositely charged polyelectrolytes. *Polymers (Basel).* (2014). doi:10.3390/polym6051414

48. Qin, J. & De Pablo, J. J. Criticality and connectivity in macromolecular charge complexation. *Macromolecules* (2016). doi:10.1021/acs.macromol.6b02113

49. Salehi, A. & Larson, R. G. A Molecular Thermodynamic Model of Complexation in Mixtures of Oppositely Charged Polyelectrolytes with Explicit Account of Charge Association/Dissociation. *Macromolecules* (2016). doi:10.1021/acs.macromol.6b01464

50. Kudlay, A. & De la Cruz, M. O. Precipitation of oppositely charged polyelectrolytes in salt solutions. *J. Chem. Phys.* **120**, 404–412 (2004).

51. Kudlay, A., Ermoshkin, A. V. & De La Cruz, M. O. Complexation of oppositely charged polyelectrolytes: Effect of ion pair formation. *Macromolecules* **37**, 9231–9241 (2004).

52. Ermoshkin, A. V. & Olvera De La Cruz, M. A modified random phase approximation of polyelectrolyte solutions. *Macromolecules* **36**, 7824–7832 (2003).

53. Rumyantsev, A. M. & Potemkin, I. I. Explicit description of complexation between oppositely charged polyelectrolytes as an advantage of the random phase approximation over the scaling approach. *Phys. Chem. Chem. Phys.* (2017). doi:10.1039/c7cp05300b

54. Rumyantsev, A. M., Zhulina, E. B. & Borisov, O. V. Complex Coacervate of Weakly Charged Polyelectrolytes: Diagram of States. *Macromolecules* (2018). doi:10.1021/acs.macromol.8b00342

55. Lee, J., Popov, Y. O. & Fredrickson, G. H. Complex coacervation: A field theoretic simulation study of polyelectrolyte complexation. *J. Chem. Phys.* **128**, (2008).

56. Audus, D. J. *et al.* Phase Behavior of Electrostatically Complexed Polyelectrolyte Gels Using an Embedded Fluctuation Model. *Soft Matter* **1**, 1–13 (2010).

57. O, P. Y., Lee, J. & Fredrickson, G. H. Field-Theoretic Simulations of Polyelectrolyte Complexation. *J. Polym. Sci. B Polym. Phys.* **45**, 3223–3230 (2007).

58. Perry, S. L. & Sing, C. E. PRISM-Based Theory of Complex Coacervation: Excluded Volume versus Chain Correlation. *Macromolecules* (2015). doi:10.1021/acs.macromol.5b01027

59. Radhakrishna, M. *et al.* Molecular Connectivity and Correlation Effects on Polymer Coacervation. *Macromolecules* **50**, 3030–3037 (2017).

60. Zhang, P., Shen, K., Alsaifi, N. M. & Wang, Z. G. Salt Partitioning in Complex Coacervation of Symmetric Polyelectrolytes. *Macromolecules* (2018). doi:10.1021/acs.macromol.8b00726

61. Zhang, P., Alsaifi, N. M., Wu, J. & Wang, Z. G. Salting-Out and Salting-In of Polyelectrolyte Solutions: A Liquid-State Theory Study. *Macromolecules* (2016). doi:10.1021/acs.macromol.6b02160

62. Shen, K. & Wang, Z. G. Polyelectrolyte chain structure and solution phase behavior. *Macromolecules* (2018). doi:10.1021/acs.macromol.7b02685

63. Li, L. *et al.* Phase Behavior and Salt Partitioning in Polyelectrolyte Complex Coacervates. *Macromolecules* (2018). doi:10.1021/acs.macromol.8b00238

64. Priftis, D. & Tirrell, M. Phase behaviour and complex coacervation of aqueous polypeptide solutions. *Soft Matter* **8**, 9396–9405 (2012).

65. Arthur, V., Edward, B. & Shirley, M. Molecular weight fractionation and the self-suppression of complex coacervation. *Biopolymers* **5**, 37–59 (1967).

66. Zhang, P., Shen, K., Alsaifi, N. M. & Wang, Z. G. Salt Partitioning in Complex Coacervation of Symmetric Polyelectrolytes. *Macromolecules* **51**, 5586–5593 (2018).

67. Andreev, M., Chremos, A., De Pablo, J. & Douglas, J. F. Coarse-Grained Model of the

Dynamics of Electrolyte Solutions. *J. Phys. Chem. B* **121**, 8195–8202 (2017).

68. Priftis, D. *et al.* Ternary, tunable polyelectrolyte complex fluids driven by complex coacervation. *Macromolecules* (2014). doi:10.1021/ma500245j

69. Lappan, U. & Scheler, U. Influence of the Nature of the Ion Pairs on the Segmental Dynamics in Polyelectrolyte Complex Coacervate Phases. *Macromolecules* (2017). doi:10.1021/acs.macromol.7b01858

70. Chollakup, R., Beck, J. B., Dirnberger, K., Tirrell, M. & Eisenbach, C. D. Polyelectrolyte molecular weight and salt effects on the phase behavior and coacervation of aqueous solutions of poly(acrylic acid) sodium salt and poly(allylamine) hydrochloride hydrochloride. *Macromolecules* **46**, 2376–2390 (2013).

71. Tirrell, M. Polyelectrolyte Complexes: Fluid or Solid? *ACS Cent. Sci.* **4**, 532–533 (2018).

72. Priftis, D. *et al.* Self-Assembly of α-Helical Polypeptides Driven by Complex Coacervation. *Angew. Chemie - Int. Ed.* **54**, 11128–11132 (2015).

73. Perry, S. L., Li, Y., Priftis, D., Leon, L. & Tirrell, M. The effect of salt on the complex coacervation of vinyl polyelectrolytes. *Polymers (Basel).* (2014). doi:10.3390/polym6061756

74. Kremer, T., Kovačević, D., Salopek, J. & Požar, J. Conditions leading to polyelectrolyte complex overcharging in solution: Complexation of poly(acrylate) anion with poly(allylammonium) cation. *Macromolecules* (2016). doi:10.1021/acs.macromol.6b01892

75. Fares, H. M. & Schlenoff, J. B. Diffusion of Sites versus Polymers in Polyelectrolyte Complexes and Multilayers. *J. Am. Chem. Soc.* (2017). doi:10.1021/jacs.7b07905

76. Huang, S. *et al.* Effect of small molecules on the phase behavior and coacervation of aqueous solutions of poly(diallyldimethylammonium chloride) and poly(sodium 4-styrene sulfonate). *J. Colloid Interface Sci.* (2018). doi:10.1016/j.jcis.2018.02.029

77. Zhang, Y., Li, F., Valenzuela, L. D., Sammalkorpi, M. & Lutkenhaus, J. L. Effect of water on the thermal transition observed in poly(allylamine hydrochloride)-poly(acrylic acid) complexes. *Macromolecules* (2016). doi:10.1021/acs.macromol.6b00742

78. Fu, J., Fares, H. M. & Schlenoff, J. B. Ion-Pairing Strength in Polyelectrolyte Complexes. *Macromolecules* (2017). doi:10.1021/acs.macromol.6b02445

79. Drechsler, A., Elmahdy, M. M., Uhlmann, P. & Stamm, M. PH and Salt Response of Mixed Brushes Made of Oppositely Charged Polyelectrolytes Studied by in Situ AFM Force Measurements and Imaging. *Langmuir* (2018). doi:10.1021/acs.langmuir.8b00498

80. Samanvaya, S. & V., T. M. Polyelectrolyte Complexation. *Adv. Chem. Phys.* 499–544 (2016). doi:10.1002/9781119290971.ch7

81. Lytle, T. K. & Sing, C. E. Tuning chain interaction entropy in complex coacervation using polymer stiffness, architecture, and salt valency. *Mol. Syst. Des. Eng.* **3**, 183–196 (2018).

82. Fu, J., Abbett, R. L., Fares, H. M. & Schlenoff, J. B. Water and the Glass Transition Temperature in a Polyelectrolyte Complex. *ACS Macro Lett.* **6**, 1114–1118 (2017).

83. Vieregg, J. R. *et al.* Oligonucleotide-peptide complexes: Phase control by hybridization. *J. Am. Chem. Soc.* (2018). doi:10.1021/jacs.7b03567

84. Fares, H. M. & Schlenoff, J. B. Equilibrium Overcompensation in Polyelectrolyte Complexes. *Macromolecules* (2017). doi:10.1021/acs.macromol.7b00665

85. Oskolkov, N. N. & Potemkin, I. I. Complexation in asymmetric solutions of oppositely charged polyelectrolytes: Phase diagram. *Macromolecules* **40**, 8423–8429 (2007).

86. Alan S. Michaels. Polyelectrolyte Complexes. *Ind. Eng. Chem.* **57**, 32–40 (1965).

87. Krogstad, D. V. *et al.* Structural evolution of polyelectrolyte complex core micelles and ordered-phase bulk materials. *Macromolecules* (2014). doi:10.1021/ma5017852

88. Spruijt, E. *et al.* Structure and dynamics of polyelectrolyte complex coacervates studied by scattering of neutrons, X-rays, and light. *Macromolecules* **46**, 4596–4605 (2013).

89. Srivastava, S. *et al.* Gel phase formation in dilute triblock copolyelectrolyte complexes. *Nat. Commun.* **8**, 1–9 (2017).

90. Lueckheide, M., Vieregg, J. R., Bologna, A. J., Leon, L. & Tirrell, M. V. Structure-property relationships of oligonucleotide polyelectrolyte complex micelles. *Nano Lett.* (2018). doi:10.1021/acs.nanolett.8b03132

91. Marciel, A. B., Srivastava, S. & Tirrell, M. V. Structure and rheology of polyelectrolyte complex coacervates. *Soft Matter* (2018). doi:10.1039/c7sm02041d

92. Fares, H. M. *et al.* Scattering Neutrons along the Polyelectrolyte Complex/Coacervate Continuum. *Macromolecules* (2018). doi:10.1021/acs.macromol.8b00699

93. Rubinstein, M., Liao, Q. & Panyukov, S. Structure of Liquid Coacervates Formed by Oppositely Charged Polyelectrolytes. doi:10.1021/acs.macromol.8b02059

94. Ortony, J. H., Hwang, D. S., Franck, J. M., Waite, J. H. & Han, S. Asymmetric collapse in biomimetic complex coacervates revealed by local polymer and water dynamics. *Biomacromolecules* **14**, 1395–1402 (2013).

95. Lappan, U., Wiesner, B. & Scheler, U. Segmental dynamics of poly(acrylic acid) in polyelectrolyte complex coacervates studied by spin-label EPR spectroscopy. *Macromolecules* (2016). doi:10.1021/acs.macromol.6b01863

96. Tekaat, M., Bütergerds, D., Schönhoff, M., Fery, A. & Cramer, C. Scaling properties of the shear modulus of polyelectrolyte complex coacervates: A time-pH superposition principle. *Phys. Chem. Chem. Phys.* **17**, 22552–22556 (2015).

97. Hamad, F. G., Chen, Q. & Colby, R. H. Linear Viscoelasticity and Swelling of Polyelectrolyte Complex Coacervates. *Macromolecules* **51**, 5547–5555 (2018).

98. Krogstad, D. V. *et al.* Structural evolution of polyelectrolyte complex core micelles and ordered-phase bulk materials. *Macromolecules* **47**, 8026–8032 (2014).

99. Liu, Y., Winter, H. H. & Perry, S. L. Linear viscoelasticity of complex coacervates. *Advances in Colloid and Interface Science* (2017). doi:10.1016/j.cis.2016.08.010

100. Spruijt, E., Stuart, M. A. C. & Gucht, J. van der. Linear Viscoelasticity of Complex Coacervates. *Macromolecules* **46**, 1633–1641 (2013).

101. Liu, Y., Momani, B., Winter, H. H. & Perry, S. L. Rheological characterization of liquid-to-solid transitions in bulk polyelectrolyte complexes. *Soft Matter* **13**, 7332–7340 (2017).

102. Ali, S. & Prabhu, V. Relaxation Behavior by Time-Salt and Time-Temperature Superpositions of Polyelectrolyte Complexes from Coacervate to Precipitate. *Gels* **4**, 11 (2018).

103. Priftis, D., Farina, R. & Tirrell, M. Interfacial energy of polypeptide complex coacervates measured via capillary adhesion. *Langmuir* **28**, 8721–8729 (2012).

104. Qin, J. *et al.* Interfacial tension of polyelectrolyte complex coacervate phases. *ACS Macro Lett.* (2014). doi:10.1021/mz500190w

105. Lytle, T. K., Salazar, A. J. & Sing, C. E. Interfacial properties of polymeric complex coacervates from simulation and theory. *J. Chem. Phys.* **149**, (2018).

106. Stewart, R. J., Ransom, T. C. & Hlady, V. Natural underwater adhesives. *J. Polym. Sci. Part B Polym. Phys.* **49**, 757–771 (2011).

107. Hwang, D. S., Waite, J. H. & Tirrell, M. Promotion of osteoblast proliferation on complex coacervation-based hyaluronic acid - recombinant mussel adhesive protein coatings on titanium. *Biomaterials* **31**, 1080–1084 (2010).

108. Zhao, Q. *et al.* Underwater contact adhesion and microarchitecture in polyelectrolyte

complexes actuated by solvent exchange. *Nat. Mater.* (2016). doi:10.1038/nmat4539

109. Gebbie, M. A. *et al.* Tuning underwater adhesion with cation-φ interactions. *Nat. Chem.* (2017). doi:10.1038/nchem.2720

110. Kim, S. *et al.* Complexation and coacervation of like-charged polyelectrolytes inspired by mussels. *Proc. Natl. Acad. Sci.* (2016). doi:10.1073/pnas.1521521113

111. Selin, V., Ankner, J. & Sukhishvili, S. Ionically Paired Layer-by-Layer Hydrogels: Water and Polyelectrolyte Uptake Controlled by Deposition Time. *Gels* **4**, 7 (2018).

112. Salehi, A., Desai, P. S., Li, J., Steele, C. A. & Larson, R. G. Relationship between polyelectrolyte bulk complexation and kinetics of their layer-by-layer assembly. *Macromolecules* (2015). doi:10.1021/ma502273a

113. Boas, M., Burman, M., Yarin, A. L. & Zussman, E. Electrically-responsive deformation of polyelectrolyte complex (PEC) fibrous membrane. *Polymer (Guildf).* (2018). doi:10.1016/j.polymer.2018.10.064

114. Boas, M., Gradys, A., Vasilyev, G., Burman, M. & Zussman, E. Electrospinning polyelectrolyte complexes: PH-responsive fibers. *Soft Matter* **11**, 1739–1747 (2015).

115. Kelly, K. D. & Schlenoff, J. B. Spin-Coated Polyelectrolyte Coacervate Films. *ACS Appl. Mater. Interfaces* (2015). doi:10.1021/acsami.5b02988

116. Sadman, K., Wang, Q., Chen, S. H., Delgado, D. E. & Shull, K. R. pH-Controlled Electrochemical Deposition of Polyelectrolyte Complex Films. *Langmuir* (2017). doi:10.1021/acs.langmuir.6b04491

117. Smith, R. J., Long, C. T. & Grunlan, J. C. Transparent Polyelectrolyte Complex Thin Films with Ultralow Oxygen Transmission Rate. *Langmuir* (2018). doi:10.1021/acs.langmuir.8b02391

118. Cain, A. A., Murray, S., Holder, K. M., Nolen, C. R. & Grunlan, J. C. Intumescent nanocoating extinguishes flame on fabric using aqueous polyelectrolyte complex deposited in single step. *Macromol. Mater. Eng.* (2014). doi:10.1002/mame.201400022

119. Oparin. *The Origin of Life*. (Dover Publications, 1935).

120. Priftis, D. *et al.* Self-Assembly of ??-Helical Polypeptides Driven by Complex Coacervation. *Angew. Chemie - Int. Ed.* **54**, 11128–11132 (2015).

121. Black, K. A. *et al.* Protein encapsulation via polypeptide complex coacervation. *ACS Macro Lett.* **3**, 1088–1091 (2014).

122. Aumiller, W. M., Pir Cakmak, F., Davis, B. W. & Keating, C. D. RNA-Based Coacervates as a Model for Membraneless Organelles: Formation, Properties, and Interfacial Liposome Assembly. *Langmuir* **32**, 10042–10053 (2016).

123. Aumiller, W. M. & Keating, C. D. Phosphorylation-mediated RNA/peptide complex coacervation as a model for intracellular liquid organelles. *Nat. Chem.* (2016). doi:10.1038/nchem.2414

124. Kuo, C. H. *et al.* Inhibition of atherosclerosis-promoting microRNAs via targeted polyelectrolyte complex micelles. *J. Mater. Chem. B* **2**, 8142–8153 (2014).

125. Black, K. A. *et al.* Protein encapsulation via polypeptide complex coacervation. *ACS Macro Lett.* (2014). doi:10.1021/mz500529v

126. Zhao, M. & Zacharia, N. S. Sequestration of Methylene Blue into Polyelectrolyte Complex Coacervates. *Macromol. Rapid Commun.* (2016). doi:10.1002/marc.201600244

127. Meng, X., Schiffman, J. D. & Perry, S. L. Electrospinning Cargo-Containing Polyelectrolyte Complex Fibers: Correlating Molecular Interactions to Complex Coacervate Phase Behavior and Fiber Formation. *Macromolecules* (2018). doi:10.1021/acs.macromol.8b01709

128. Bago Rodriguez, A. M., Binks, B. P. & Sekine, T. Emulsion stabilisation by complexes of oppositely charged synthetic polyelectrolytes. *Soft Matter* (2018). doi:10.1039/c7sm01845b

129. Zhu, F. *et al.* 3D Printing of Ultratough Polyion Complex Hydrogels. *ACS Appl. Mater. Interfaces* (2016). doi:10.1021/acsami.6b09881

130. Lin, Z. *et al.* A work-function tunable polyelectrolyte complex (PEI:PSS) as a cathode interfacial layer for inverted organic solar cells. *J. Mater. Chem. A* **2**, 7788–7794 (2014).

CHAPTER 2. Phase Behavior and Salt Partitioning in the Hydrophilic Polyelectrolyte Complexation System

2.1 Introduction

Due to polyelectrolyte complexation's profound implication of biological systems and popularity in industrial applications, there have been continuous effort to capture the phase behaviors of different polymeric systems and understanding the fundamental physical interactions influencing the molecular interactions for PEC-based materials. Starting from 1960s, Veis et al have done extensive studies on natural macromolecules to illustrate the effect of chain length, salt concentrations and molecular chemistry on the phase behaviors.[1–3] Tirrell and coworkers have demonstrated the phase separation boundaries of binary and teriary systems of polypeptides and PAA-PDMAEMA-PDADMAC by turbidimetric and microscopic measurements under various temperature, pH, and salt environments.[4–7] However, the majority of macromolecular physics work in this field thus far has provided only a qualitative description of the thermodynamics and phase behavior of polyelectrolyte complexes.[8–10] Important physical properties of polyelectrolyte complexes are not well understood, like partitioning of different components in the two respective phases, the volume fraction of the complex phase, and molecular interactions governing the stability of the phase separated systems, impeding predictive design of end-use materials.[11] To our best knowledge, the most detailed work demonstrating the binodal phase behavior was done by Spruijt et al then, in which they used PAA-PDMAEMA as model polyelectrolyte pair. PAA was fluorescently labeled and used as indicator to measure the polymer content in the two separated phases, but salt was assumed to

partition equally in the two phases without direct measurements.[12] There is still a lack of quantitative data to test and establish an overarching physical model describing the phenomenon.

The general features of the polyelectrolyte phase diagram, not intended to represent any particular theory, are shown schematically in **Figure 2-1**. The first model to describe the system

Figure 2-1. Features of the binodal phase diagram.

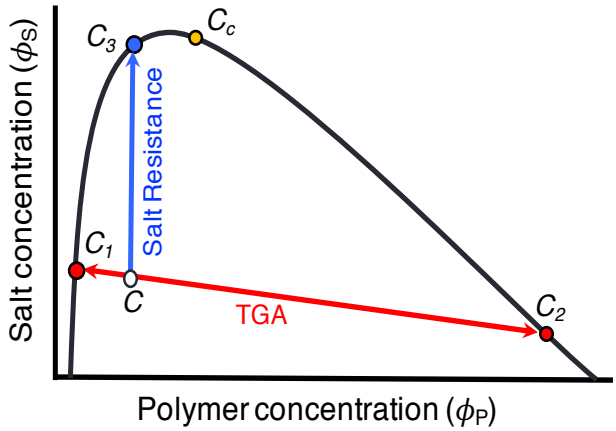

Schematic of a binodal phase boundary for polyelectrolyte complexes in the polymer concentration ($\boldsymbol{\phi_P}$) – salt concentration ($\boldsymbol{\phi_S}$) map. A solution with composition corresponding to point $\boldsymbol{C}$ will phase separate into a polymer-lean supernatant phase ($\boldsymbol{C_1}$) and a polymer-rich complex phase ($\boldsymbol{C_2}$). Phase separation can be completely suppressed by addition of salt ($\boldsymbol{C_3}$). $\boldsymbol{C_c}$ is the critical point, which lies on the right side of the maximum in the binodal phase boundary. The two complementary experimental approaches adopted to elucidate the phase boundary are represented with red arrow indicating composition measurements by thermogravimetric analysis and conductivity measurements, and blue arrow indicating salt resistance measurements by microscopic and turbidimetric evaluations.

was proposed by Voorn and Overbeek, wherein the total free energy of the system was written as an ad hoc combination of a Debye-Hückel term to represent the electrostatic interactions among the charges on the chains and the counterions (enthalpic) and a Flory Huggins expression (entropic) as $f_{total} = -\alpha[\sum_i \sigma_i \phi_i]^{3/2} + \sum_i (\phi_i/N_i) \ln \phi_i$, with σ_i, ϕ_i, and N_i being the charge density, volume fraction and degree of polymerization of the each of the species present in the

solution, and α being a medium-dependent interaction constant.[13,14] The predictions of the binodal phase behavior from the Voorn-Overbeek theory agreed apparently well with early experimental results.[3,12,15–17] However, these earlier studies were limited to either naturally-derived macromolecules with high polydispersity, uncontrolled and complicated chemical structures, or synthetic polymers with hydrophobic backbones[12] leading to deviations from expected behavior.[11] These factors, combined with the incompleteness of the Voorn-Overbeek model with no accounting for important features such as charge connectivity on the polymer chains, excluded volume interactions, and explicit polymer-solvent interactions, have to date made a systematic comparison between experiments and theory nearly impossible. At the same time, recent disagreements with the Voorn-Overbeek model have also been reported, including negatively sloped tie-line[18–22] and underestimation of the polymer content in the complex.[23,24] In parallel, various improvements of the Voorn-Overbeek theory have been proposed,[19–21,23,25–28] but a lack of model experimental data has prevented meaningful comparisons between experiments and theory.

Here, we present a combined study with extensive experiments and realistic simulations of the phase behavior of *as-formed* polyelectrolyte complexes comprising model polyelectrolytes, charged polypeptides Poly(L-lysine hydrochloride) (PLK) and sodium salt of poly(D,L-glutamic acid sodium salt) (PRE). This pair of polymers, with identical hydrophilic backbones, similar side-group structures and controlled length distributions, allowed for a systematic investigation of the complex phase behaviors and compositions. They were intentionally chosen due to the hydrophilic nature of backbone to avoid possible complication by hydrophobicity, which will be discussed in further details in Chapter 3. Additionally, the racemic form of the poly(glutamic acid) was used to interrupt the formation of hydrogen-bonding among

chiral polypeptides that could lead to solid precipitates instead of liquid coacervates.[29] In our work, two distinct and complementary experimental approaches, involving multiple methodologies, were employed to determine the binodal phase boundary. Most importantly, minimal processing of the complexes was carried out to achieve a true description of the

Figure 2-2. Complete polyelectrolyte complexation phase diagrams.

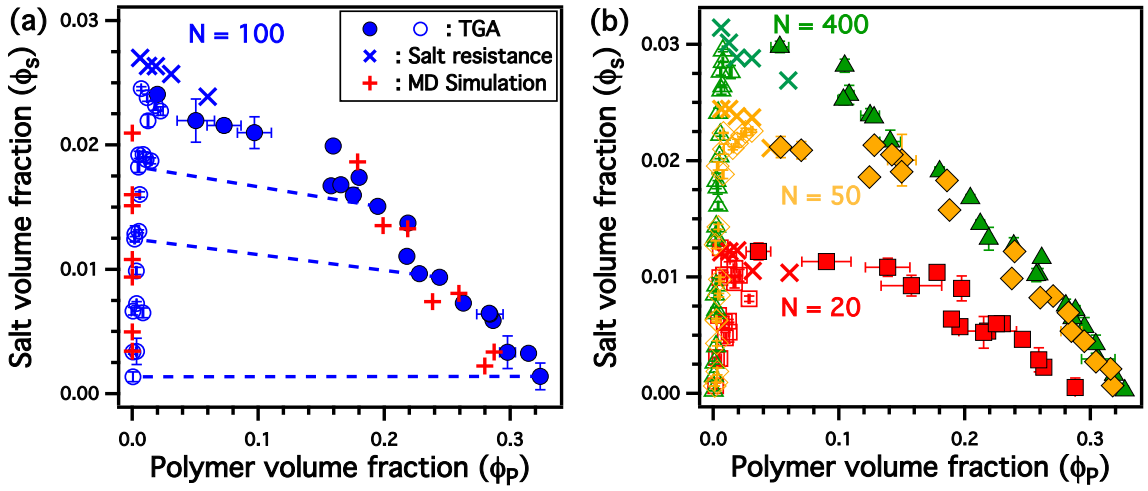

(a) Phase diagram for solutions comprising PLK_{100} and PRE_{100}. Two experimental approaches were employed to map the phase boundaries (blue symbols) and were in excellent agreement with the simulation results (red + symbols). The filled circles (complex phase) and open circles (supernatant phase) are the results from TGA; × are the results from salt resistance methods. Representative tie-lines are shown as dotted lines to demonstrate their negative slopes, which are contrary to the predictions from the Voorn-Overbeek theory. (b) Phase diagram for PLK_{20}+PRE_{20} (red), PLK_{50}+PRE_{50} (yellow), and PLK_{400}+PRE_{400} (green). The solid (complex phase) and open (supernatant phase) squares, diamonds and triangles are the results from TGA on the three respective systems; × are the results from salt resistance methods. The overall shape of the binodal phase boundary was preserved, while the two-phase region became larger with increasing polymer chain lengths.

complexation. At the same time, molecular dynamics/Monte Carlo (MD/MC) hybrid simulations accurately revealed the essential physics for polyelectrolyte complexation by incorporating long-range electrostatic interactions, excluded volume interactions, and an explicit, realistic description of the polymer chains (with monomer resolution, bending potential and finitely

extensible bonds), salt ions and solvent molecules. Excellent agreement between the experiments and the simulations is demonstrated, further enabling investigations of several key features of complexation-driven phase separation.

2.2 Results and Discussion

2.2.1 Binodal Phase Diagram of PRE-PLK System

The compositions of the complex and supernatant phases are presented on a polymer concentration (ϕ_P)-salt concentration(ϕ_S) map in **Figure 2-2**. Solutions of PLK and PRE of the same chain lengths, with known polymer and added salt (NaCl) concentrations, $\phi_{P,0}$ and $\phi_{S,added}$, were mixed together at ratios corresponding to matching polyelectrolyte charge concentrations, and the resulting mixtures(C in **Figure 2-1**) separated into the complex (C_2 in **Figure 2-1**) and the supernatant (C_1 in **Figure 2-1**) phase. Independent thermogravimetric analysis (TGA) of the two phases was carried out to determine water, polymer and salt weight fractions. The amounts of salt in both phases were small, and were further confirmed by solution conductivity measurements. **Figure 2-2(a)** shows the composition results for PLK_{100} +PRE_{100} (N = 100) complexes (blue solid symbols) and corresponding supernatants (blue open symbols). Expectedly, most of the polyanions and polycations complexed with each other and condensed in the complex, leading to an exceptional disparity between the polymer concentrations in the two phases (especially at low ϕ_S). Phase separation in multiple systems with varying polymer and salt concentrations ($\phi_{P,0}$ and $\phi_{S,added}$) was examined to achieve the first complete description of the binodal phase boundary, including regions near the critical point (C_C in **Figure 2-1**) where the complex and the supernatant branches met. The general shape of the binodal phase boundary bears a superficial resemblance to the predictions from the Voorn-Overbeek theory. However,

the theory significantly underestimates ϕ_P in the complexes at low ϕ_S (**Figure 2-3(a)**), and was clearly unable to accurately describe complexation quantitatively. At the same time, enabled with an accurate representation of the polymer chains as well as explicitly incorporated solvent molecules and excluded volume interactions, MD/MC simulations accurately reproduced the experimental results (red + signs), highlighting the ability of the model to describe the interactions and thermodynamics of the complexation phenomena.

Two further key departures from the Voorn-Overbeek theory were also revealed. Select

Figure 2-3. Comparison between experimental data and fitting based on V-O theory & Binodal phase diagrams on logarithm scale.

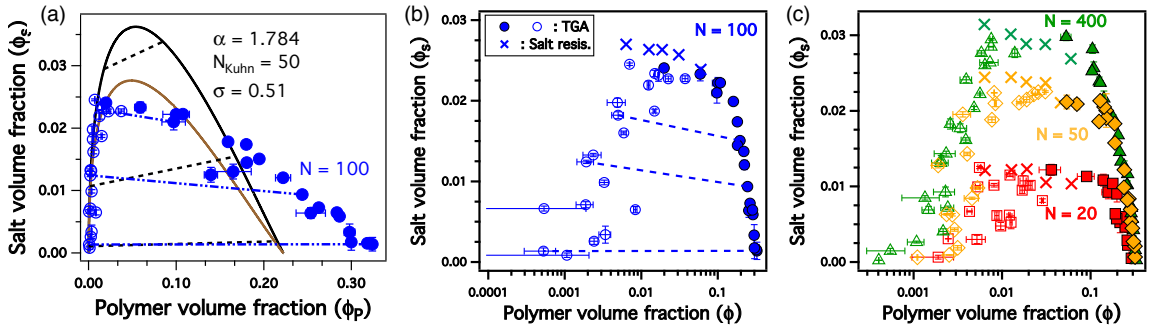

(a) Fits from the Voorn-Overbeek model (black curve) and modified Voorn-Overbeek model assuming equal amount of salt in complex and supernatant phases (brown curve) to the experimental data (blue symbols) for PLK_{100}+PRE_{100}. The model parameters were optimized to obtain the best-fit to the experimental data by the modified Voorn-Overbeek model. The two fits severely underestimated ϕ_P in the complexes at low ϕ_S. Select tie-lines from experiments (blue dotted lines) and Voorn-Overbeek calculations (black dotted lines) showed opposite signs of slopes, indicating shortcomings of Voorn-Overbeek model. (b) Phase diagrams for PLK_{100}+PRE_{100}. The horizontal ϕ_P axis was represented on a logarithmic scale to highlight the features at low ϕ_P values. Two sets of experimental data from TGA (blue solid symbols for complex phase and blue open symbols for supernatant phase) and salt resistance measurements (×) of ϕ_S were plotted against ϕ_P. (c) Similar phase diagrams for PLK_{20}+PRE_{20} (red), PLK_{50}+PRE_{50} (yellow), and PLK_{400}+PRE_{400} (green). Logarithm scale was used to better illustrate compositional differences in the supernatant phase. Clearly, the systems with shortest chains (PLK_{20}+PRE_{20} in red) have the highest polymer concentration in supernatant phases.

representative tie-lines connecting the complementary complex and supernatant composition states are shown in the **Figure 2-2(a)** (blue dashed lines). The negatively sloped tie-lines demonstrate the preferential partitioning of salt in the supernatant phase, in stark contrast to the predictions of positively sloped tie-lines from the Voorn-Overbeek theory. Furthermore, negatively-sloped tie-lines imply that the critical point must lie to the right of the maximum in the binodal phase boundary ($\phi_{P,C} > \phi_{P,max}$, C_C in **Figure 2-1**), contrary to the predictions from the Voorn-Overbeek theory ($\phi_{P,C} < \phi_{P,max}$). Here $\phi_{P,C}$ and $\phi_{P,max}$ are ϕ_P at the critical point and at the maximum in the $\phi_P - \phi_S$ phase boundary.

2.2.2 Effect of Chain Length on the Phase Behavior

The binodal phase boundaries for three more systems, PLK_{20} + PRE_{20} (N = 20), PLK_{50} + PRE_{50} (N = 50) and PLK_{400} + PRE_{400} (N = 400) are shown in **Figure 2-2(b)**. It can be seen from

Figure 2-4. Phase diagram for PLK_{50}+PRE_{50} and PLK_{400}+PRE_{400} by experiments and simulation.

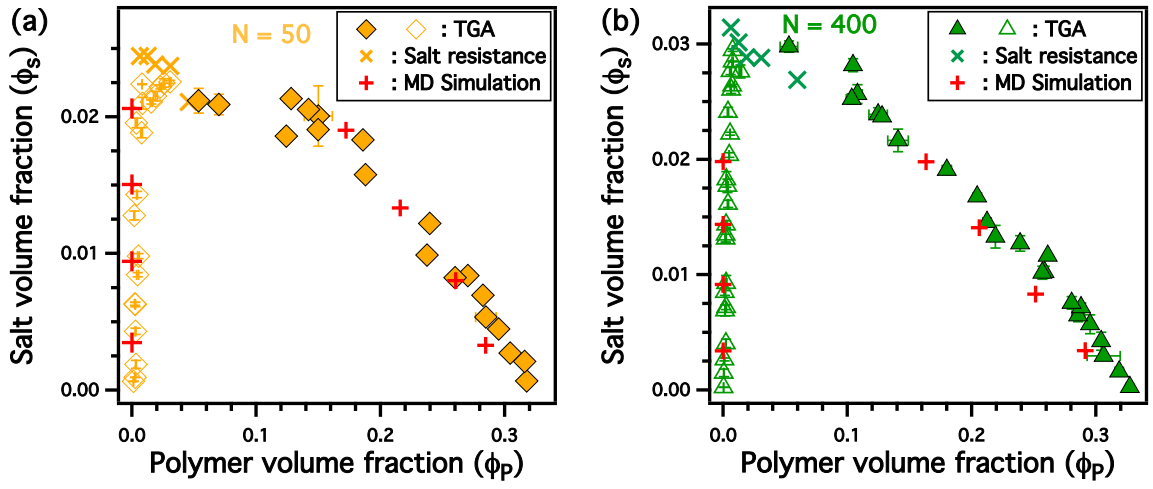

The phase boundaries (yellow and green symbols) were in excellent agreement with the simulation results (red + symbols) for the (a) PLK_{50}+PRE_{50} and (b) PLK_{400}+PRE_{400} systems.

Figure 2-2 that the two-phase region becomes larger and the complexes become more polymer dense as well as more resistant towards salt with increasing polymer chain length while preserving the overall shape of the binodal phase boundary. The maximum in the $\phi_P - \phi_S$ phase boundary also shifts to higher ϕ_S and lower ϕ_P with increasing N, leading to steeper supernatant arms (**Figure 2-3(b)(c)**). These trends are expected, as longer polymer chains are anticipated to have stronger cooperative electrostatic interactions, and at the same time have more stymied entropy, leading to larger relative entropy gains from counterion release and thus a stronger propensity for complexation.

Similar to the $N = 100$ systems, excellent agreement between the experiments and the

Figure 2-5. Salt resistance of polyelectrolyte complexes.

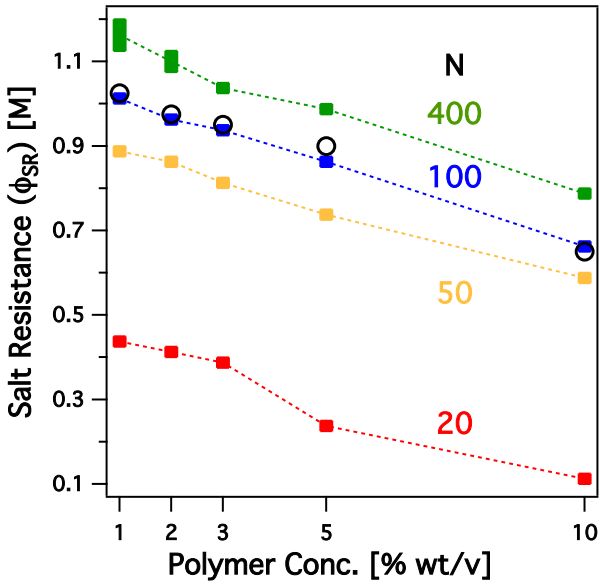

Salt resistances (as defined in Figure 1) at different total polymer concentrations for systems with increasing polymers chain lengths. Solid symbols represent microscopic results and black circles represent turbidimetric analysis for PLK_{100}+PRE_{100}. Heights of the symbols expressed the difference between lowest added salt concentration where no phase separation was observed and the highest added salt concentration where phase separation was observed. Complexes formed at low total polymer concentrations and longer polymer chain length are more resistant towards salt addition.

simulations is demonstrated for the N = 50 and 400 systems (Figure 2-4), thus confirming the ability of the proposed model and the corresponding simulation to describe the experimental results across a range of polymer lengths. It must be noted that the simulation strategy was constructed with the assumption of complete absence of polymer chains in the supernatant, leading to vertical supernatant arms in the phase diagram. This assumption held well for systems with long polymer chains. However, the N = 20 systems had a substantial presence of polymer chains in the supernatant (**Figure 2-3(b)(c)**), thus making the simulation approach inadequate for these systems.

The size of the two-phase region expanded with increasing polymer length but gradually saturated at large polymer chain lengths. The two-phase region for the N = 50 systems was considerably larger than that of the N = 20 system. However, the two-phase regions for the N = 50, 100 and 400 systems nearly overlapped with each other (**Figure 2-2** and **Figure 2-3(b)(c)**). The marginal changes in the entropy of mixing, $\sum_i(\phi_i \ln \phi_i)\,/N_i$ with increasing chains length N_i progressively decrease with increasing chain length, thus leading to a saturation of complex properties, as observed in our experiments. Note, however, that increasing polymer length is still expected to strongly affect the viscoelastic properties of the complexes, owing to the slower relaxation of the chains. These effects will be discussed in a forthcoming manuscript.

2.2.3 Salt Screens Electrostatic Interactions and Inhibits Complexation.

The entropy gain from the release of polyelectrolyte-bound counterions plays a dominant role in driving complexation.[30] Addition of salt leads to a dramatic decrease in the entropy of counterion-release, leading to stronger screening of inter-chain interactions and increasing water content in the complexes (**Figure 2-2**). Sufficiently high salt concentrations completely suppress

phase separation, and lead to homogenous polymer solutions; this transition can be captured via

Figure 2-6. Salient features from phase diagram.

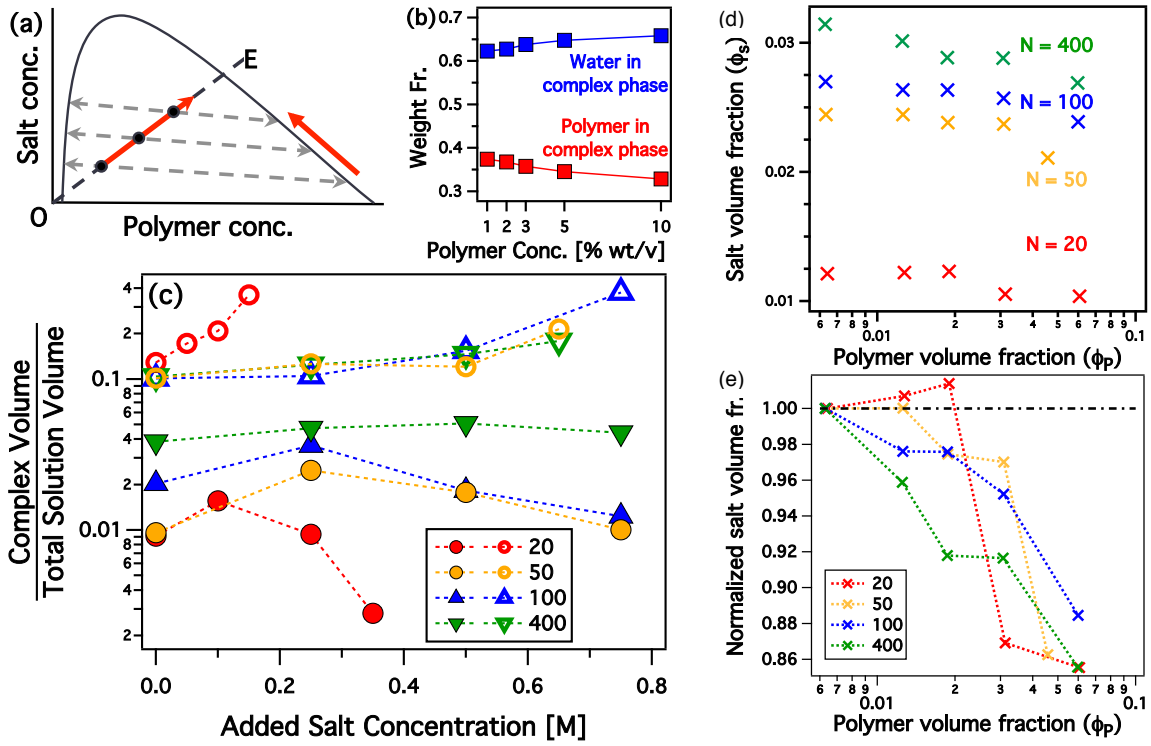

(a) A schematic phase diagram demonstrating self-suppression – suppression of complexation upon increasing total polymer concentration. (b) Compositional changes of water and polymer in the complex phases with increasing total polymer concentration, demonstrating self-suppression. (c) Variations in the volume fraction of complexes upon addition of salt to solutions with 1% wt/v (filled symbols) and 5% wt/v (open symbols) total polymer concentrations for polymers with different chain lengths. (d)(e) The salt volume fraction ϕ_S was obtained by measuring the salt resistances at fixed total polymer concentrations ϕ_P. (d) Boundaries are plotted on logarithm scale for PLK_{20}+PRE_{20} (red), PLK_{50}+PRE_{50} (yellow), PLK_{100}+PRE_{100} (blue), and PLK_{400}+PRE_{400} (green) (e) Salt volume fraction ϕ_S was normalized by ϕ_S values at 1% wt/v total polymer concentration in the respective series. The plot indicates that PLK_{20}+PRE_{20} (red) went through a maximum, PLK_{50}+PRE_{50} (yellow) exhibited a plateau and PLK_{100}+PRE_{100} (blue), and PLK_{400}+PRE_{400} (green) decreased monotonically with increasing ϕ_P. Therefore, the maxima in the binodal phase boundary were at 1% wt/v total polymer concentration for the $N \geq 100$ systems.

optical microscopy or turbidity measurements (**Figure 2-13**). The excess salt concentrations required to unify the complex and the supernatant phases are termed the salt resistance ϕ_{SR} of

the solution (see Figure **1**). As shown in **Figure 2-3**, ϕ_{SR} decreased with increasing total polymer concentration $\phi_{P,0}$. With increasing $\phi_{P,0}$, decreasing available solution volume and increasing concentration of counterions that accompany the polymer chains combine to decrease the entropy gain from counterion release, thereby leading to a weaker driving force for complexation and lower salt resistance.

The results from salt resistance experiments were translated onto the binodal phase boundaries and are depicted by the × symbols in **Figure 2-2** and **Figure 2-3**. Again, very good agreement between the thermogravimetric and salt resistance methods was achieved for all polymer chain lengths. The binodal phase boundary determined via the salt resistance method exhibited a maximum for the N = 20 system, while ϕ_S monotonically decreased with increasing $\phi_{P,0}$ for N = 100 and 400 systems, indicating that the maxima in the binodal phase boundary were at ϕ_P < 1% wt/v for the $N \geq 100$ systems.

2.2.4 Key Features of Complexation

Several key features of polyelectrolyte complexation are elucidated by our results. Suppression of complexation is evident on increasing the added salt concentration, but also occurs upon increasing $\phi_{P,0}$. Increasing $\phi_{P,0}$ translates into traversing along the charge-equivalence line (OE) on the $\phi_P - \phi_S$ map (**Figure 2-4(a)**), resulting from a concomitant increase in the concentration of the salt counterions that accompany the polymer chains $\phi_{S,0}$. Thus, owing to stronger screening, a decrease in polymer content and a corresponding increase in the water content in the complex with increasing $\phi_{P,0}$, termed as *self-suppression*[2,11,14] were observed in our experiments (**Figure 2-4(b)**).

The relative magnitudes of $\phi_{P,0}$ and $\phi_{P,C}$ also determine the variations in the volume of the two phases upon addition of salt. Owing to the general shape of the binodal phase boundary,

Figure 2-7. Excluded volume interactions expel salt ions out of complexes.

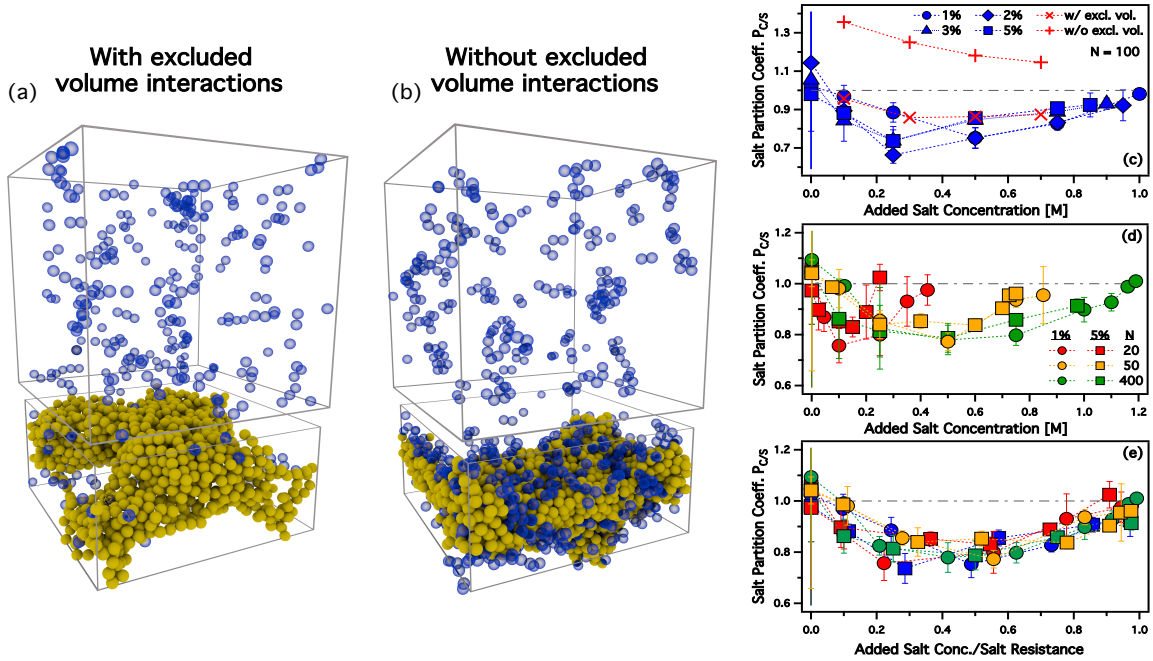

Snapshots from the MD/MC hybrid simulation boxes (a) with and (b) without excluded volume interactions. Yellow beads represent polymer chains and blue beads represent salt ions. The bottom box represents the complex phase, the top box represents the supernatant phase. While the salt ions are strongly concentrated in the complex phase in (b), they are expelled from the complex phase in (a). (c) Salt partition coefficients for PLK_{100}+PRE_{100} at 1% wt/v (circles) and 5% wt/v (squares) total polymer concentrations as a function of concentration of added salt. × and + symbols represent salt partition coefficient predictions from simulation with and without excluded volume interactions, respectively. In the absence of excluded volume interactions, partition coefficients trends in qualitative agreement with Voorn-Overbeek theory were recovered. (d) Salt partition coefficients trends with added salt concentration for systems with $\boldsymbol{N}$ = 20, 50 and 400 at 1% wt/v (circles) and 5% wt/v (squares) total polymer concentrations. The salt partition coefficient follows a universal trend: decreasing initially from ~ 1 to ~ 0.7 and then returning to ~ 1 with increasing concentration of added salt. (e) Salt partition coefficients as a function of scaled added salt concentration. The added salt concentrations were scaled by salt resistance of the respective total polymer concentrations and chain lengths. Owing to the similarity of the two-phase envelope, all the partition coefficient data sets collapsed onto a universal trend.

it has been argued that the complex volume fraction (complex volume/solution volume) must increase to 1 if $\phi_{P,0} > \phi_{P,C}$ and increase slightly before decreasing to 0 if $\phi_{P,0} < \phi_{P,C}$ upon increasing ϕ_S.[13,14] While these trends were predicted in the treatment by Voorn and Overbeek,[13,14] they had not been experimentally elucidated until now. As shown in **Figure 2-6(c)**, the complex volume fraction increased continuously with increasing concentration of added salt, $\phi_{S,added}$, in solutions with $\phi_{P,0}$ = 5% wt/v (open symbols). In solutions with $\phi_{P,0}$ = 1% wt/v, however, the complex volume fraction underwent a maximum before decreasing upon increasing $\phi_{S,added}$ (closed symbols). These trends were observed for all the polymer lengths, indicating that 1% wt/v< $\phi_{P,C}$ < 5% wt/v for all the systems investigated, with $\phi_{P,C}$ being farthest from and closest to 1% wt/v for the systems with shortest and longest chain lengths, respectively. As we discussed earlier, the $\phi_P - \phi_S$ phase boundary has a negative slope in the range of ϕ_P = 1 - 5% wt/v for $N \geq 100$ systems. Thus, the volume measurements again confirm that $\phi_{P,C} > \phi_{P,max}$, at least for the $N \geq 100$ systems.

2.2.5 Salt Partitioning and Excluded Volume Effects

The representative tie-lines in **Figure 2-2** are all negatively sloped, implying an excess of salt ions in the supernatant. These trends were quantified using the salt partition coefficient $P_{C/S}$, defined as the ratio of the salt concentrations in the complex and the supernatant. $P_{C/S}$ exhibited a unique behavior, undergoing a minimum with increasing $\phi_{S,added}$. As shown in **Figure 2-7(c)(d)**, $P_{C/S}$ were all ~ 1 at very low $\phi_{S,added}$, decreased to ~ 0.7 at intermediate $\phi_{S,added}$ and then increased again to values ~1 at $\phi_{S,added} \approx \phi_{SR}$, irrespective of $\phi_{P,0}$ and N. The decrease of $P_{C/S}$ from 1 at low $\phi_{S,added}$ is expected to arise from progressive screening of the electrostatic interactions with increasing $\phi_{S,added}$, allowing excluded volume interactions to dominate in the

complex and expel the counterions out into the supernatant. However, at high $\phi_{S,added}$, the excluded volume interactions become less significant owing to increasing water content in the complex and the two phases becoming compositionally similar, leading to smaller differences in salt partitioning and $P_{C/S}$ returning to values ~1.[19,20] The $\phi_{S,added}$ ranges over which the $P_{C/S}$ variations occur increased significantly with increasing N, ascribed to increasing ϕ_{SR}. However, owing to the similarity of the shapes of the binodal phase boundaries for polymers of different lengths, the $P_{C/S}$ trends were largely unified into a universal behavior upon rescaling $\phi_{S,added}$ by ϕ_{SR}, leading to a collapse of all the $P_{C/S}$ data independent of ϕ_P and N (**Figure 2-7(e)**). Additionally, partition coefficients of the same polymer length but different polymer concentrations (1 and 5% wt/v) reach their minima at slightly different positions on the scaled x-axis.

The $P_{C/S}$ trends were efficiently captured by the simulations as well, represented by the ×

Figure 2-8. Partition coefficients by experiments and simulation for PRE$_{50}$+PLK$_{50}$ and PRE$_{400}$+PLK$_{400}$.

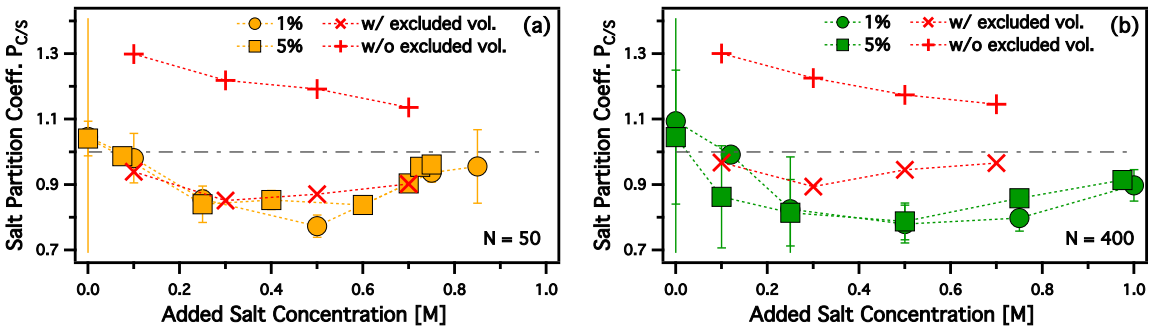

Salt partition coefficients for PLK$_{50}$+PRE$_{50}$ at 1% wt/v (circles) and 5% wt/v (squares) total polymer concentrations as a function of concentration of added salt. × and + symbols represent salt partition coefficient predictions from simulation with and without excluded volume interactions, respectively. In the absence of excluded volume interactions, a qualitative agreement between the partition coefficient trends and the predictions from the Voorn-Overbeek theory were recovered.

symbols in **Figure 2-7(c) and Figure 2-8**, although the magnitude of $P_{C/S}$ was slightly under-predicted by the simulations. A snapshot of the simulation boxes is shown in **Figure 2-7(a)** and depicts an excess of salt ions in the supernatant. The preferential partitioning of salt in the supernatant is in stark contrast to the predictions from the Voorn-Overbeek theory wherein $P_{C/S}$ being always > 1 and continuously decreasing with increasing $\phi_{S,added}$ was postulated.[13,14] The Voorn−Overbeek formalism is particularly inadequate in accounting for the effects from excluded volume interactions, and at the same time treated electrostatic interactions in a mean-field manner by ignoring the effects arising of polymer chain connectedness and architecture on electrostatic interactions.[11,22] These effects have been proposed to have a competing influence, leading to a partial cancellation of their contributions toward the free energy of the system[23] and the apparent ability of the framework to qualitatively predict the complexation phase behavior, though it still fails to provide quantitatively consistent predictions (**Figure 2-3**). Furthermore, due to a lack of the excluded volume interactions in the Voorn-Overbeek framework, salt ions have a greater tendency to reside in the complex, resulting in a lower electrostatic energy of the system and manifesting as preferential partitioning of salt in the complex. In real systems, however, excluded volume interactions will tend to push the salt ions out of the complex, and a preferential segregation of salt in the supernatant is expected.

Our simulations allowed for a systematic investigation of the effects of excluded volume interactions on complexation and the partitioning of the salt ions in the two phases. By employing a very soft-core potential, the excluded volume interactions could be essentially *switched off*. The results in these cases indicated a shrinkage of the complex and an excess of salt ions in the complex, as can be inferred from the comparison of the simulation box snapshots with and without excluded volume interactions in **Figure 2-7(a) and 7(b)**, respectively.

Correspondingly, $P_{C/S}$ was larger than 1 as shown in **Figure 2-7(c)** with + symbols, indicating preferential partitioning of the salt ions in the complex phase. Additionally, the partition coefficient decreased continually with increasing salt concentration, in qualitative agreement with the Voorn-Overbeek theory. It must be noted that agreement between our simulations

Figure 2-9. Turbidity measurements for stability of complexation coacervates against different salts

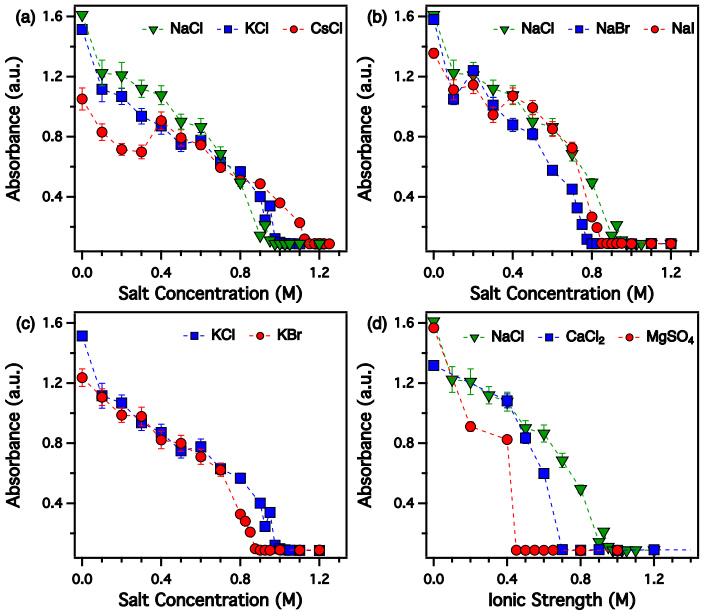

(a) The effect of cationic counterions. (b)(c) The effect anionic counterions for halides. (d) The effect of valency on the coacervates stability.

results and the Voorn-Overbeek theory is not expected, as the theory does not take charge-connectivity into account, leading to an under-prediction of the polymer content in the complex. At the same time, our simulations results do not indicate that the lack of complete description of excluded volume interactions is the only reason for the inability of the Voorn−Overbeek theory to predict the experimentally observed trends of partition coefficients. This inability may also

have contributions from chain connectivity effects on charge correlations,[21] which are not included in the Voorn−Overbeek theory but are implicitly included in our simulations. Furthermore, the salt partition coefficients at extremely low added salt concentrations lie slightly above 1, which is in qualitative agreement with theoretical predictions by Kudlay and Olvera de la Cruz[19,20] as well as Shen and Wang[21,22], and have been ascribed to enhanced electrostatic correlations owing to chain connectivity of charges.

2.2.6 Effect of Salt Identity on Coacervation Stability

At the same time, we have investigated the effect of salt identity on the stability of complex coacervation. The turbidity measurements for PRE_{100}+PLK_{100} system with different cationic, anionic, and divalent counterions were shown in **Figure 2-9**. The drop of the absorbance reading to base line indicate the formation of one homogenous phase and complete dissolution of the coacervate networks. **Figure 2-9(a)** demonstrated the abilities of chloride salt to break the complexes with different alkali metal ions. From the figure, it followed the order of Na>K>Cs, which is understandable due to higher charge density of sodium ions with smaller volume. However, the situation could not be simply explained by charge density for anionic counterions shown in **Figure 2-9(b)(c)**, for which the bromide salt served as the most effective salt for both sodium and potassium salts to interrupt the physical cross-linked complexes. Sadman et al proposed it was attributed to the fact that the thinner hydration layer of bromide salts makes them easier to diffuse into the complex coacervate.[31] Furthermore, salts with different valencies were also examined, and to better comparison, the salt concentrations were converted to ionic strengths. Demonstrated by the figure, divalent salts were generally more effective at suppressing complexation, which agreed with previous experimental results.[4]

2.3 Conclusion

In summary, we have reported a first comprehensive, quantitative description of the phase behavior of polyelectrolyte complexes by combining multiple complementary experimental methodologies on minimally processed complexes and simulations with realistic polymer representation and explicit descriptions of salt ions, solvent molecules and excluded volume interactions. Excellent agreement between the various experimental techniques and the simulations enabled us to characterize the molecular states of the systems under various conditions, and demonstrated various features of complexation, including suppression of complexation upon addition of salt as well as self-suppression of complexation upon increasing total polymer concentration. Importantly, contrary to the contemporary understanding of the complexation phenomena, the salt ions were found to partition preferentially in the polymer-lean supernatant phase, and insights from simulations showed that previously overlooked excluded volume effects play a dominant role in expelling the salt counterions away from the complexes into the supernatant phase. While our results are not the first prediction or demonstration of preferential partitioning of salt in the supernatant,[19,22–24] it is the first instance of concerted experimental and direct simulation efforts wherein the effects of excluded volume interactions, explicit ions, and explicit solvent molecules have been elucidated.

The insights into the complexation phenomenon presented here will contribute towards its better physical description. Improved computer models, such as that presented here, could enable superior predictions of phase behavior for diverse chemical architectures, as well as of partitioning of small molecules into complexes. Such improvements will in turn inspire improved design of polyelectrolyte complex-based materials and facilitate the understanding of biological manifestation of polyelectrolyte complexation. At the same time, the results presented

here can be extended to gain physical insights into the assembly mechanisms and equilibrium properties of a range of complex-based self-assembled structures such as micelles and hydrogels, and thus can significantly enhance their applicability in diverse areas such as gene-delivery, smart bandages and surgical adhesives.

2.4 Methods and Experimental Details

A. Materials and preparation of stock solution. Poly(L-lysine hydrochloride) (PLK, degree of polymerization N = 20, 50, 100, 400, molecular weight = 3300, 8200, 16000, 66000 g/mol) and poly(D,L-glutamic acid sodium salt) (PRE, N = 20, 50, 100, 400, molecular weight = 3000, 7500, 15000, 60000 g/mol) were purchased from Alamanda Polymers and were used without further purification. 10% wt/v stock solutions in MilliQ^{TM} water were prepared, vortexed for 1

Sample	**Molecular weight** (M_n g/mol)	**Polydispersity** (M_w/M_n)	**Degree of Polymerization** (N)
PLK20	3500	1.11	21
PLK50	9000	1.05	55
PLK100	17300	1.07	105
PLK400	60500	1.1	368
PRE20	3000	1.01	20
PRE50	7900	1.01	52
PRE100	14500	1.09	96
PRE400	59000	1.01	391

Table 2-1. Characterization of polypeptides used in the phase behavior study.

minute, and then sonicated for 30 minutes as per manufacturer's instructions to obtain clear solutions. Chemical structures of polypeptides used in this study are listed in the Supplementary Figure 8. Molecular weights, degrees of polymerization and polydispersity values, reported by the vendor, are listed in **Table 2-1**.

B. Preparation of polyelectrolyte complexes. Polyelectrolyte complexes were prepared at 1:1 stoichiometric ratio of charge-matched conditions. Required amounts of PLK stock solutions were added to a solution containing the desired amount of MilliQ^{TM} water and NaCl stock solution (5M) in a 1.5mL Eppendorf^{TM} tube and vortexed for 30 seconds. Then, the required

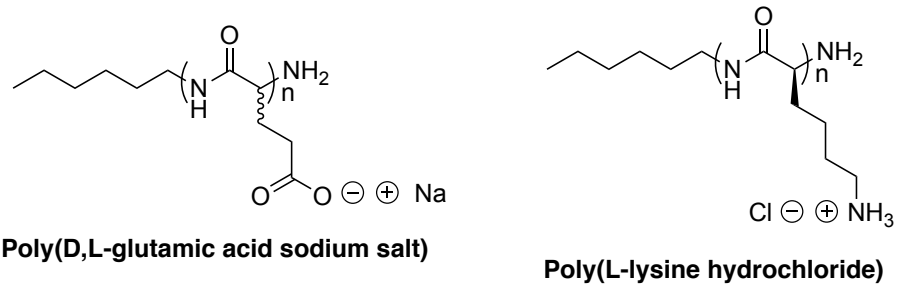

Figure 2-10. Chemical structures of polypeptides. Chemical structures of PLK and PRE

amounts of PRE stock solutions were added and vortexed again for 30 seconds. Upon complexation, solution became turbid. For the turbidity and microscopy experiments, the samples were directly transferred into the sample plates after mixing. For TGA, furnace burning

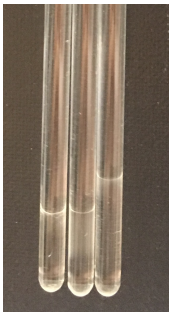

Figure 2-11. Phase-separated polypeptide mixture

400 μl of PLK_{100}+PRE_{100} mixtures at 1% wt/v total polymer concentration and 0, 0.25 and 0.5 M added salt concentration were prepared, centrifuged and equilibrated for one day.

and volume measurements, the samples were centrifuged to achieve distinct separation between the complex and supernatant phases. A representative photograph of PLK100+PRE100 system at 1% wt/v total polymer concentration and 0, 0.25 and 0.5 M added salt concentrations in NMR tubes after centrifugation is shown in **Figure 2-11**.

C. Thermogravimetric analysis. The 1.5mL Eppendorf™ tubes containing the samples were centrifuged at 17000×G for 15 minutes. 20 µl of the supernatant and 5 to 20 µl of the complex was extracted and transferred into separate aluminum pans. The TGA measurement was first conducted on TA Instrument SDT 600 TGA using aluminum pans in air environment. The following protocol was followed: the temperature was ramped up from room temperature to 110 °C at 8 °C /min, held at 110 °C for 90 mins, ramped to 600 °C at 10 °C /min, and then held at 600 °C for 120 mins. The weight of the pan+sample was recorded along the heating procedure to extract the weights of water, polymer and salt contents in each phase.

A similar protocol was followed in furnace burning experiments using Barnstead Thermolyne Furnace 1400. The samples were placed in the furnace at room temperature, and the temperature of the furnace was increased to 110 °C and held there for 2.5 hours. At that point, the samples were cooled to room temperature, the sample weights were measured to estimate the water content, and again placed into the furnace and heated to 600 °C. After heating for 12 hours, the samples were cooled and their weights were measured again to estimate the polymer and salt contents. For each polymer concentration and salt concentration, at least 3 repeating samples were prepared. Weight fractions of water, polymer and salt were recorded and were converted to volume fractions by assuming same density of polymer and salt in bulk and solution state, wherein densities of $\rho_{polymer} = 1.2515$, $\rho_{salt} = 2.16$, and $\rho_{water} = 1$ g/cm^3 were used. Statistical analysis using Dixon's Q test was performed for identification and rejection of

Figure 2-12. Change of weight of the complex and the supernatant upon heating.

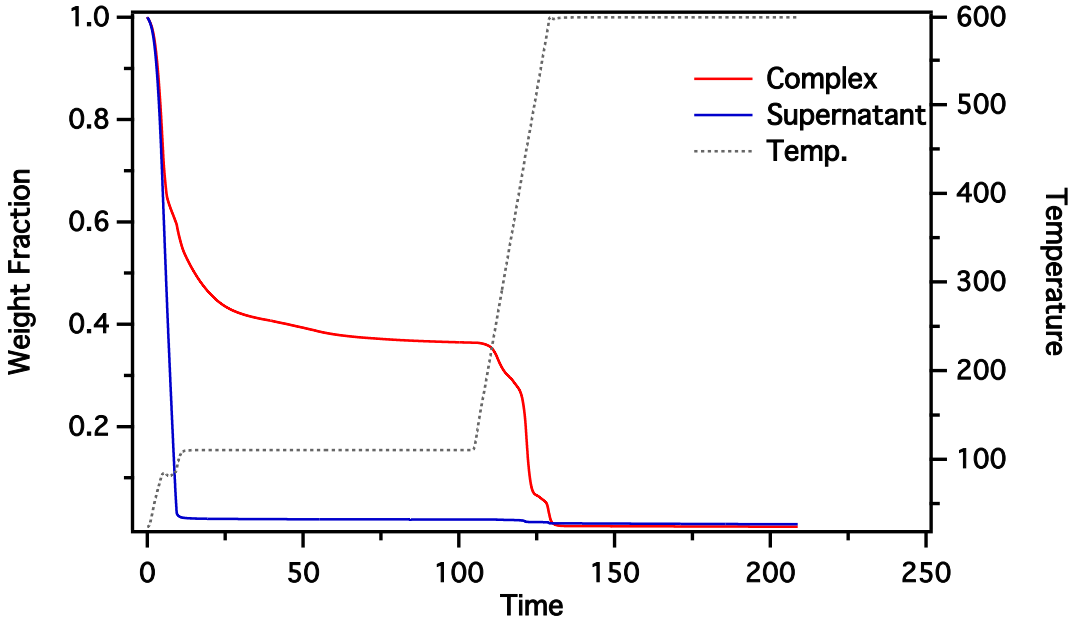

Weight losses of the complex (red line) and the supernatant phase (blue line) during the heating process as a function of time. The corresponding temperature is also shown as a function of time by the grey dotted line.

outliners. TGA measurement was conducted using TA Instrument SDT 600 with aluminum pans following the protocol described in the main text. The heating process was carried out in air environment. **Figure 2-12** showed the changes of weight fraction with respective to time of both the complex and the supernatant from the PLK100+PRE100 system at 1% wt/v total polymer concentrations and 0.5 M added salt concentration.

During the experiments, the samples lost weight in two steps. The first step, corresponding to temperature range from room temperature to 110 °C, corresponded to evaporation of water in the samples. The second step, from ~ 240 °C to 600 °C, corresponded to the oxidation of the organic matter. The supernatant lost more than 90% of the weight in the first phase, signifying that supernatant phases were composed of mostly water and small fractions of

polymer or salt. Upon completion of the heating process, salt would be the only component remained in the pan.

We adopted the knowledge from TGA experiments and developed a similar protocol to conduct furnace burning experiments, which could be used for measuring multiple samples at the same time and consequently were more efficient for gaining better statistics.

Figure 2-13. Salt stability of polypeptide complexes.

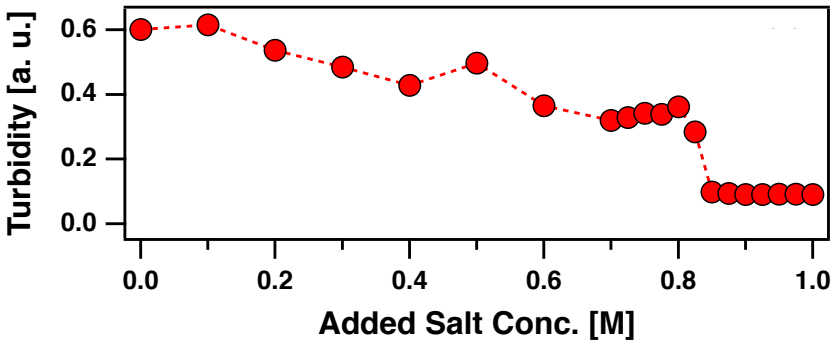

Turbidity measurements as a function of added salt concentration for the PLK_{100}+PRE_{100} system at a total polymer concentration of 2% wt/v.

D. Salt resistance measurements. Turbidity for as-mixed solutions was measured by UV spectrophotometer on Tecan, Infinite M200 plate reader at the wavelength of 500nm and at 25°C. The turbidity (T) is defined as $T = -\ln I/I_0$, with I_0 being the incident light intensity and I being the intensity of light transmitted through the sample. Three measurements with plate

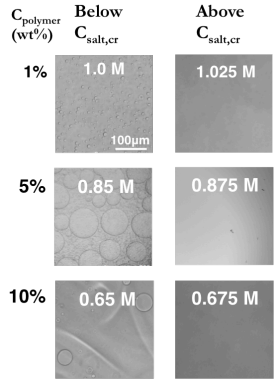

Figure 2-14. Micrographs depicting suppression of complexation.

Representative micrographs of the PLK_{100}+PRE_{100} systems at 1%, 5% and 10% wt/v total polymer concentrations and added salt concentrations just below and above the salt resistance values. The disappearance of the liquid droplets upon increasing the added salt concentration by 0.025M close to the phase boundary is evident.

shaking for 1 second followed by measurements at four points in each sample were conducted. 12 repeats for each sample condition were carried out. The phase separated complexes were also observed by phase contrast optical microscopy (Leica DMI 6000B). 200 µl of sample solution was injected in to the ultra-low attachment 96-well plates (Costar, Corning Inc.) for observation. Results from the turbidity measurements of PLK100+PRE100 system with 2 wt/v% total polymer concentration and added salt concentrations ranging between 0 to 1.0 M is shown as **Figure 2-13**. Absorbance values below 0.01 were deemed as an indication of a homogenous phase. Turbidity measurements served the same purposes as the optical microscopy examinations, with the latter being more accurate in detecting small droplets. Therefore, only one set of turbidity measurements of PLK100+PRE100 were carried out to test the agreement between the two techniques. The complex droplets formed upon complexation were observed by

Figure 2-15. Conductivity measurements for salt concentrations.

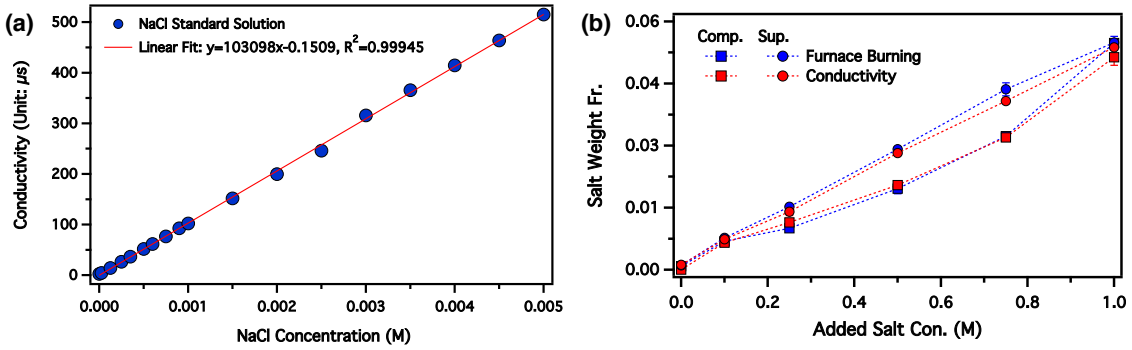

(a) The correlation between salt concentration and conductivities of salt solution was calibrated using a series of standard NaCl solutions. (b) Salt weight fractions measured from furnace burning method (blue symbols) and conductivity measurements (red symbols) were nearly identical for both complex and supernatant phases.

phase contrast optical microscopy. As the salt concentration in the solution was increased, the tendency for complexation diminished and was eventually completely suppressed. No complex

droplets were observed when added salt concentrations exceeded the salt resistance values. Representative micrographs of PLK100+PRE100 at 1, 5 and 10% wt/v total polymer concentration and at two added salt concentrations just below and above the salt resistance values are presented in **Figure 2-14**.

E. Conductivity measurement. Conductivity test was performed to ensure the accuracy of the salt measurements from TGA. In order to determine the absolute amounts of salt in the samples, a standard calibration curve based on NaCl solutions was prepared by measuring conductivities of 18 standard solutions ranging from 0 to 5×10^{-3}M. For each sample, three independent measurements were taken. The remaining materials in the aluminum pan following a furnace experiment was transferred into a 15 mL Eppendorf Tube and mixed with 5 mL of Milli-Q water. The mixture was sonicated for 30 seconds before taking the conductivity measurements. Conductivity measurements were performed to ensure the accuracy of the measurements of salt concentration in both the complex and the supernatant phases. In order to determine the absolute amount of salt in a sample, a standard calibration curve was prepared based on NaCl solutions of known concentrations. The conductivity probe used in the experiments was Traceable ® probe from Fisher Scientific, and for each sample, three independent measurements were taken. 18 standard solutions ranging from 0 to 5×10^{3}M NaCl concentrations were prepared and their respective conductivities were measured. The conductivities of the solutions were found to be linearly dependent on the salt concentration in the solution, as shown in **Figure 2-15(a)**. Comparison of salt weight fraction in complex and supernatant phases measured by furnace burning and conductivity measurements are shown as an example in **Figure 2-15(b)** for PLK100+PRE100 systems with 1% wt/v total polymer concentration and 0, 0.1, 0.25, 0.5, 0.75

and 1.0 M added salt concentrations. The two sets of data showed excellent match with each other.

F. Volume measurement. Bruker MatchTM System NMR sample Tubes with inner diameter 2.41±0.010 mm and length 100mm were used for accurate volume evaluation. Required amounts of water, 5M NaCl stock solutions, 10% wt/v polycation stock solutions and 10% wt/v polyanion stock solutions were added by pipette into the tube. The NMR tubes were centrifuged at 5000 rpm for 1 hour and then capped and left to equilibrate for 1 day before measurements. Total height of the sample tube, height of the total solution and height of the complex phase were measured, and volume of the complex phase was calculated based on a calibration curve. In

Figure 2-16. Photographs of the PLK_{400}+PRE_{400} complexes & Calibration of the volume-solution height correlation in NMR tubes.

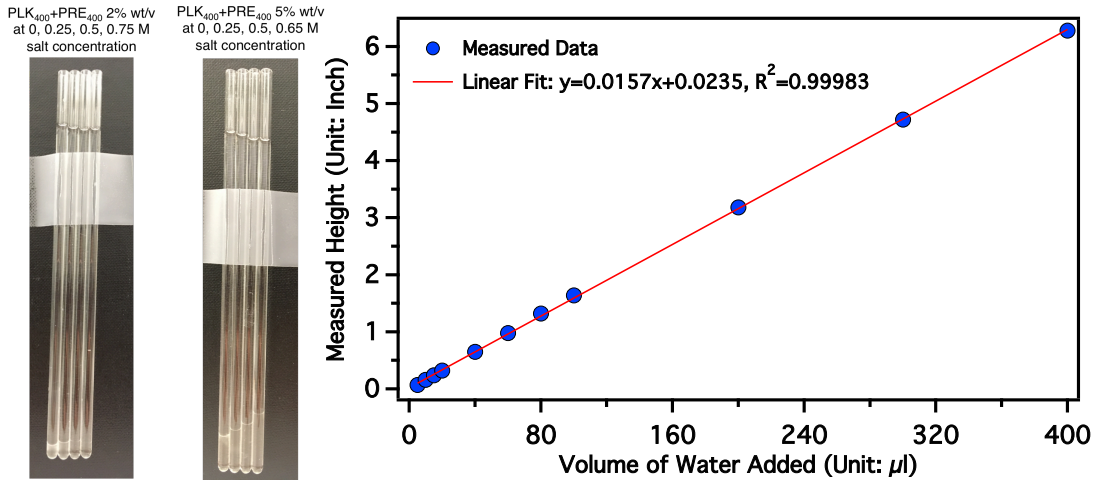

The photographs were obtained for complexing systems at different total polymer concentrations and added salt concentrations, and were analyzed for estimation of volume of the two phases. The measurement was conducted for range of 0~400 μl. The liquid used in calibration process was MilliQ^{TM} water.

order to accurately quantify the volume fractions of complex phases, NMR tubes with consistent inner diameter were chosen. Bruker MatchTM System NMR sample Tubes of 3-3.0-500-1 with outer diameter of 2.99+0.010-0.025 mm, inner diameter of 2.41±0.010 mm, length of 100mm from Norell Inc. were used. Since the variation of inner diameter among different tubes was within 0.5%, we assumed cylindrical shape with identical inner diameter for the tubes used and linear relationship between volume and measured length from bottom of the tube to the height of 400 µl. Known amounts of water were used to calibrate the tube. The calibration curve is shown as **Figure 2-16**.

Photographs of the complexes and supernatants of PLK+PRE systems with N = 20, 50, 100, and 400 at 1% and 5% wt/v total polymer concentrations and 4 different added salt conditions were analyzed to measure the height of the respective phases in the tubes, and thus estimate the volumes of each of the phases. Selective photos for 1% and 5% wt/v total polymer concentrations and 4 added salt conditions for PLK400+PRE400 systems are shown in **Figure 2-16**.

G. MD/MC hybrid Simulation. MD/MC calculations were used to generate the phase behavior of model polyelectrolyte solutions and complexes in which a modified Lennard-Jones (LJ) potential was used to describe interactions between polymer sites, ions and solvent. Chemical monomers in the polymer chains was represented by beads, which were connected by FENE springs along with a bending potential. Ion and polymer beads both carried an elementary charge. The systems considered here comprised 8200 beads in a periodic cubic box of size $L = 22\sigma$. Equal numbers of positively and negatively charged beads were present, and the total number of charged beads ranged from 1000 to 3000.

The radius of the LJ beads, described by the interaction range parameter σ, was taken to be same for all species. The interaction strength parameter ϵ of the LJ potential for interactions of ions and water with themselves was fixed and the cut-off was set to 3σ. More specifically, LJ parameters for self-interactions were taken to be: $\varepsilon = 1.0k_{\mathrm{B}}T$ and $\sigma = 1$, values chosen in previous modeling of polyelectrolyte solutions. For solvent-charge interactions, we used $\varepsilon = 1.5k_{\mathrm{B}}T$. We assumed $\sigma = 0.53\mathrm{nm}$. In addition to LJ interactions, the charged beads were subject to Coulomb potential.

The phase behavior of the model adopted here was determined from simulations in the Gibbs ensemble. A soft-core modification (**Figure 2-17**) was introduced that had a finite potential value at contact (zero distance), which allowed for a higher acceptance probability in Gibbs ensemble exchange moves, while still preventing significant bead overlap after MD relaxation. Note that polymer molecules were constrained to remain in the complex coacervate phase. Overall, Gibbs simulations were performed for 625τ after 1000τ equilibration, where $\tau = \sigma(m/\epsilon)^{1/2}$ and the basic timestep equaled 0.005τ. The total number of MC exchange

Figure 2-17. Soft-core potentials used in Gibbs ensemble calculations.

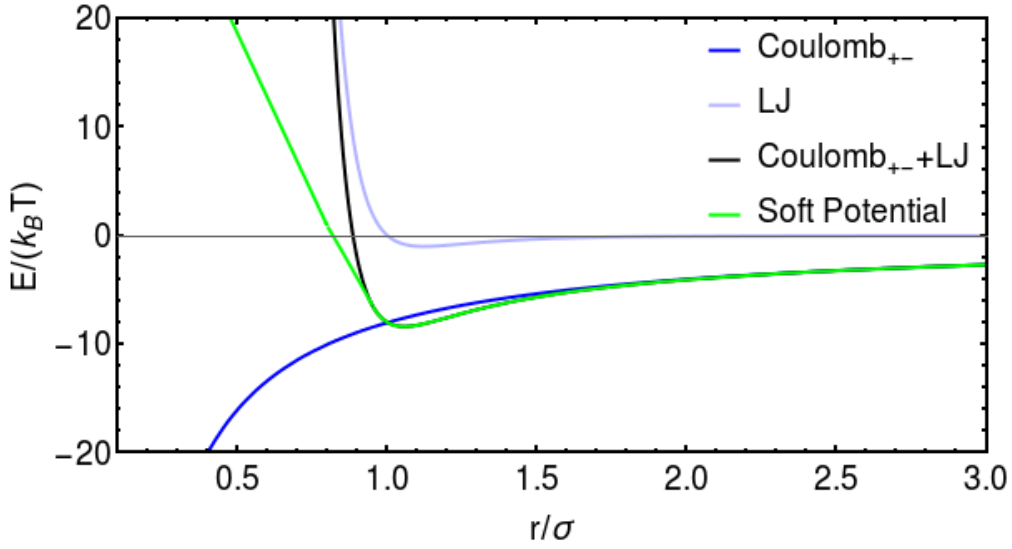

moves was 25000. To match the experimental phase diagram, the Coulomb potential strength l_B was set to $\sqrt{13}\sigma$. A short-range attraction between charged and solvent beads was modified to represent solvation effects that are particularly important for description of rheological properties.[32]

All simulations were performed at $T = 1.0, P = 0.4$. The simulation box was coupled to a MTK barostat-thermostat with time constants $\tau_T = 1.0$, and $\tau_P = 10.0\tau$, respectively. Calculations were performed with HOOMD, a GPU-optimized molecular dynamics software package,[33,34] with Coulomb interactions calculated by the PPPM Ewald summation method.

2.5 References.

1. Arthur Veis, C. A. Phase separation in polyelectrolyte systems. I. complex coacervates of gelatin. *J. Phys. Chem.* **64**, 1203–1210 (1960).

2. Arthur, V., Edward, B. & Shirley, M. Molecular weight fractionation and the self-suppression of complex coacervation. *Biopolymers* **5**, 37–59 (1967).

3. Veis, A. A review of the early development of the thermodynamics of the complex coacervation phase separation. *Adv. Colloid Interface Sci.* **167**, 2–11 (2011).

4. Perry, S. L., Li, Y., Priftis, D., Leon, L. & Tirrell, M. The effect of salt on the complex coacervation of vinyl polyelectrolytes. *Polymers (Basel).* (2014). doi:10.3390/polym6061756

5. Chollakup, R., Beck, J. B., Dirnberger, K., Tirrell, M. & Eisenbach, C. D. Polyelectrolyte molecular weight and salt effects on the phase behavior and coacervation of aqueous solutions of poly(acrylic acid) sodium salt and poly(allylamine) hydrochloride hydrochloride. *Macromolecules* **46**, 2376–2390 (2013).

6. Priftis, D. *et al.* Ternary, tunable polyelectrolyte complex fluids driven by complex coacervation. *Macromolecules* (2014). doi:10.1021/ma500245j

7. Priftis, D. & Tirrell, M. Phase behaviour and complex coacervation of aqueous polypeptide solutions. *Soft Matter* **8**, 9396–9405 (2012).

8. Zhang, Y., Li, F., Valenzuela, L. D., Sammalkorpi, M. & Lutkenhaus, J. L. Effect of water on the thermal transition observed in poly(allylamine hydrochloride)-poly(acrylic acid) complexes. *Macromolecules* (2016). doi:10.1021/acs.macromol.6b00742

9. Wang, Q. & Schlenoff, J. B. The polyelectrolyte complex/coacervate continuum. *Macromolecules* (2014). doi:10.1021/ma500500q

10. Fu, J., Fares, H. M. & Schlenoff, J. B. Ion-Pairing Strength in Polyelectrolyte Complexes. *Macromolecules* (2017). doi:10.1021/acs.macromol.6b02445

11. Samanvaya, S. & V., T. M. Polyelectrolyte Complexation. *Adv. Chem. Phys.* 499–544 (2016). doi:10.1002/9781119290971.ch7

12. Spruijt, E., Westphal, A. H., Borst, J. W., Cohen Stuart, M. A. & Van Der Gucht, J. Binodal compositions of polyelectrolyte complexes. *Macromolecules* **43**, 6476–6484 (2010).

13. Voorn, M. J. *Complex Coacervation.* (Wiley-VCH Verlag GmbH Co., 1956).

14. Overbeek, J. T. G. & Voorn, M. J. Phase separation in polyelectrolyte solutions. Theory of complex coacervation. *J. Cell. Comp. Physiol.* **49**, 7–26 (1957).

15. Bungenberg De Jong, H. G. & Kruyt, H. R. Coacervation. (Partial miscibility in colloid systems). (Preliminary Communication). *Chemistry (Easton)*. (1929).

16. Nakajima, A. & Sato, H. Phase relationships of an equivalent mixture of sulfated polyvinyl alcohol and aminoacetalyzed polyvinyl alcohol in microsalt aqueous solution. *Biopolymers* **11**, 1345–1355 (1972).

17. Sato, H. & Nakajima, A. Complex coacervation in sulfated polyvinyl alcohol-aminoacetalyzed polyvinyl alcohol system. *Colloid Polym. Sci.* **252**, 944–948 (1974).

18. Ermoshkin, A. V. & Olvera De La Cruz, M. A modified random phase approximation of polyelectrolyte solutions. *Macromolecules* **36**, 7824–7832 (2003).

19. Kudlay, A. & De la Cruz, M. O. Precipitation of oppositely charged polyelectrolytes in salt solutions. *J. Chem. Phys.* **120**, 404–412 (2004).

20. Kudlay, A., Ermoshkin, A. V. & De La Cruz, M. O. Complexation of oppositely charged polyelectrolytes: Effect of ion pair formation. *Macromolecules* **37**, 9231–9241 (2004).

21. Shen, K. & Wang, Z. G. Polyelectrolyte chain structure and solution phase behavior. *Macromolecules* (2018). doi:10.1021/acs.macromol.7b02685

22. Zhang, P., Shen, K., Alsaifi, N. M. & Wang, Z. G. Salt Partitioning in Complex Coacervation of Symmetric Polyelectrolytes. *Macromolecules* **51**, 5586–5593 (2018).

23. Perry, S. L. & Sing, C. E. PRISM-Based Theory of Complex Coacervation: Excluded Volume versus Chain Correlation. *Macromolecules* (2015). doi:10.1021/acs.macromol.5b01027

24. Radhakrishna, M. *et al.* Molecular Connectivity and Correlation Effects on Polymer Coacervation. *Macromolecules* (2017). doi:10.1021/acs.macromol.6b02582

25. Qin, J. & De Pablo, J. J. Criticality and connectivity in macromolecular charge complexation. *Macromolecules* (2016). doi:10.1021/acs.macromol.6b02113

26. Salehi, A. & Larson, R. G. A Molecular Thermodynamic Model of Complexation in Mixtures of Oppositely Charged Polyelectrolytes with Explicit Account of Charge Association/Dissociation. *Macromolecules* (2016). doi:10.1021/acs.macromol.6b01464

27. Zhang, P., Alsaifi, N. M., Wu, J. & Wang, Z. G. Salting-Out and Salting-In of Polyelectrolyte Solutions: A Liquid-State Theory Study. *Macromolecules* (2016). doi:10.1021/acs.macromol.6b02160

28. Delaney, K. T. & Fredrickson, G. H. Theory of polyelectrolyte complexation - Complex coacervates are self-coacervates. *J. Chem. Phys.* **146**, (2017).

29. Perry, S. L. *et al.* Chirality-selected phase behaviour in ionic polypeptide complexes. *Nat. Commun.* (2015). doi:10.1038/ncomms7052

30. Ou, Z. & Muthukumar, M. Entropy and enthalpy of polyelectrolyte complexation: Langevin dynamics simulations. *J. Chem. Phys.* **124**, (2006).

31. Sadman, K. *et al.* Influence of Hydrophobicity on Polyelectrolyte Complexation. *Macromolecules* **50**, 9417–9426 (2017).

32. Andreev, M., Chremos, A., De Pablo, J. & Douglas, J. F. Coarse-Grained Model of the Dynamics of Electrolyte Solutions. *J. Phys. Chem. B* **121**, 8195–8202 (2017).

33. Anderson, J. A., Lorenz, C. D. & Travesset, A. General purpose molecular dynamics simulations fully implemented on graphics processing units. *J. Comput. Phys.* **227**, 5342–5359 (2008).

34. Lebard, D. N. *et al.* Self-assembly of coarse-grained ionic surfactants accelerated by graphics processing units. *Soft Matter* **8**, 2385–2397 (2012).

CHAPTER 3. Phase Behavior in Hydrophobic System: Electrostatic Complexation and Physical Interactions Beyond

3.1 Introduction

The associative phase separation resulted from polyelectrolyte complexation (PEC) differs from segregative phase separation caused by repulsive forces between solvent and polymers in the fact that the complex phase contains both of the oppositely charged polyelectrolytes.[1–5] With increasing awareness of striking parallels in biology (e.g., the resemblance of PEC with membraneless organelles based on spontaneous liquid-liquid phase separation[6,7]) and materials science as exceptionally tunable self-assembled structures, PEC-based materials have become increasingly popular candidates in producing desirable macroscopic properties and targeting functionalities across multiple industries. For instance, they have been employed as prototypes in reversible morphological phase transition[8,9], fabricated into hollow microcapsules and intertwined membranes by injection suspension or electron spinning[10–12], and formulated into therapeutic delivery micelles[13–15] as well as biocompatible hydrogels[16].

Continued studies have been carried out to understand the thermodynamics[17–19] and kinetics[20,21] of PEC formation both experimentally[22–29] and theoretically[30–33]. We have investigated the phase behaviors for the "clean" systems of polypeptides with hydrophilic backbones in the previous chapter. However, some key aspects in this polymeric system, such as (1) unique chemical attributes of the individual polymers, and (2) solvent effects, quantitatively expressed by χ in classic polymer physics framework, have not been fully explored. Fortunately, more researchers in the community are actively pursuing these open questions[34–36]. Sadman et al. have demonstrated how higher mechanical and rheological strengths can be achieved for PEC of

poly(styrene sulfonate) and poly(4-vinyl pyridine) containing more hydrophobic alkyne substitutions[35]. A recent theoretical study by Rumyantsev et al. outlined a salt concentration-solvent quality diagram of polyelectrolyte complexes based on scaling laws[34]. Unfortunately, there is still little to no complete datasets accompanied by a proper theory/model that can describe the thermodynamic phase behaviors quantitatively to illustrate the effect of hydrophobicity and other prevailing physical noncovalent interactions. These more realistic aspects of PEC are essential to advance our current understanding of selecting polyelectrolyte pairs and to harness such materials into products and end-use technologies.

The two model polymers chosen for this study were poly(acrylic acid) (PAA) and poly(allylamine hydrochloride) (PAH) due to their facile synthetic preparation routes, commercial availability, and widespread application in both academia and industry[25,37–41]. However, the interplay between electrostatic and other physical contributions to complexation for this system remains unclear, which have resulted in inconsistent agreement from different works. The morphological phase behaviors have been explored in Chollakup and coworkers' reports[24,25], where they found the maximum amount of complexation with highest salt resistance occur around neutral conditions. Fu et al. ranked PAA as the weakest polyanion in the ion-pairing strength[42], supporting these findings. However, several contradictory studies have shown that instead of yielding less and weaker complexes when PAA-PAH or PAA related complexes were set in acidic conditions, they actually exhibited at least comparable high salt resistance[36,43]. By measuring the segmental mobility of PAA in complexes, Lappan et al. found the dynamics of individual polymer were slower for PAA in acidic conditions[44]. On the other hand, theoretical and simulation work proposed polymer-solvent interaction would make the phase behavior of complexation system fundamentally different from expectation[34,36]. Thus, a comprehensive study

of the phase behavior of PAA-PAH at various pH levels is needed to clarify these issues. Additionally, since we have previously studied the phase behavior of a "simpler" hydrophilic polypeptide system[23], we believed that this more sophisticated system can enable a more comprehensive understanding of PEC formation and partitioning of individual components.

3.2 Results and Discussion

3.2.1 Binodal Phase Diagrams of PAA-PAH System Under Neutral and Basic Conditions

Upon mixing of PAA (PAANa) and PAH with similar chain lengths at controlled polymer as well as added salt concentrations, $\phi_{P,0}$ and $\phi_{S,added}$ respectively, complexation was observed instantly and the mixture became turbid with feature-like white precipitates[24,39] suspended in the solution (shown by **Figure 3-8**). When investigating the morphology of the complexes, the vast majority of investigators (including our group) have relied on turbidity

Figure 3-1. Turbidimetric measurement of PAA-PAH complexes under neutral condition.

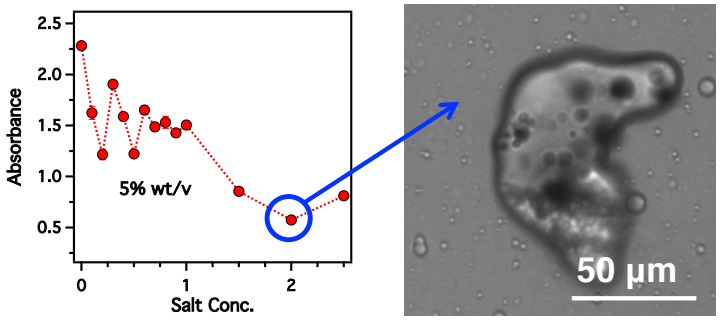

Turbidity measurement of PAA-PAH complexes at 5% wt/v under neutral conditions (pH = 6.5).

measurement as a semi-quantitative indication for transition from two phase region into one homogenous phase[22,24,45,46]. As shown by **Figure 3-1** for PAANa-PAH complexes mixed at 5% *wt/v* in pH = 6.5 solution, the turbidity decreased after addition of salt and reached a minimum

around 2 M. However, this decline did not guarantee complete dissolution of the precipitates, and the structures shown in the microscopic image on the right indicated complexes still persisted in the system at this salt concentration and above. We believe that the main reason for this inconsistent result with previous literature is that the complexes were solid precipitates in nature. The precipitates would tend to sediment to the bottom of the vial due to the density difference, making the light transmission from supernatant phase decrease by time. This observation was similar for other polymer concentrations, shown in the **Figure 3-10**. For future experimental investigations of PEC phase behavior, simply relying on turbidity can be sometimes misleading – we strongly recommend combining these datasets with other visual characterization techniques like light microscopy to unambiguously identify the morphological transition in solution and avoid reproducibility issues, especially for the polyelectrolyte pairings

Figure 3-2. Binodal phase diagram of PAA-PAH system under neutral conditions.

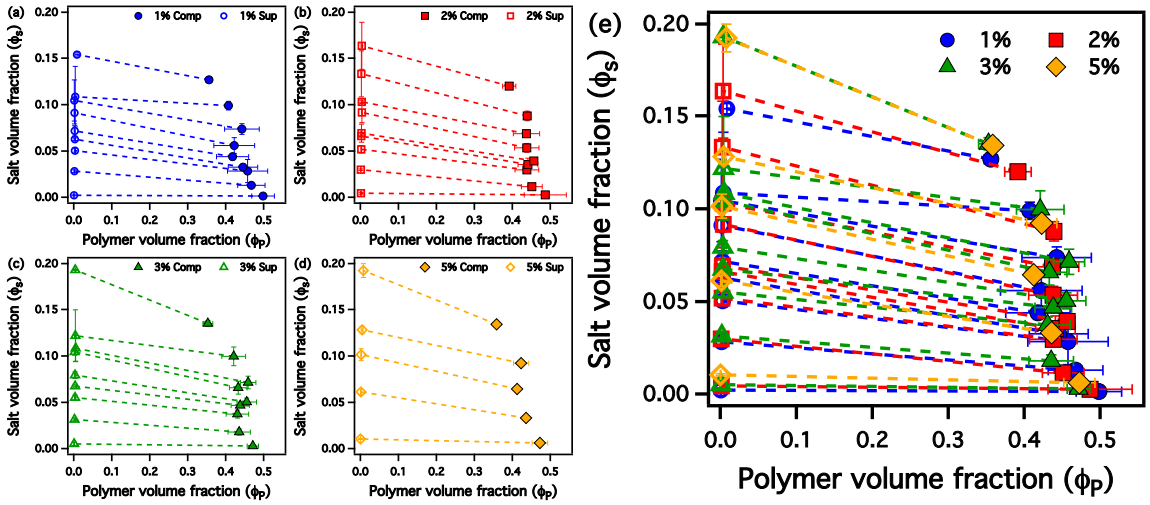

Phase diagrams comprising PAA_{100} (sodium salt), PAH_{100} and NaCl were measured by TGA at a $\phi_{P,0}$ = (b) 1 *wt/v* %, (c) 2 *wt/v* %, (d) 3 *wt/v* %, and (e) 5 *wt/v* %. The filled circles (complex phase) and unfilled circles (supernatant phase) are connected by dotted tie-lines with negative slopes. Error bars denote the standard deviation. (f) Overlay summary of all TGA results.

that can form solid complexes.

Consequently, we adopted the protocol developed in our previous report[23], utilizing thermogravimetric analysis (TGA) to determine the water, polymer, and salt contents of both the complex and supernatant phases (see Methods and experimental details for full explanation), thereby investigating the exact salt-polymer phase behavior state space. To ensure that the polyelectrolytes were fully charged prior to mixing, both of the polyanion and polycation stock solutions were neutralized in their salt forms. After mixing, the pH of the resultant mixture was measured to be 6.5, which we assigned as the neutral condition. **Figure 3-2a~d** show the binodal phase boundaries for PAANa-PAH complexes at 1, 2, 3 and 5% *wt*/*v* total polymer concentrations ($\phi_{P,0}$) under neutral pH conditions on the polymer concentration (ϕ_P)-salt concentration (ϕ_S) map. The added salt concentration ($\phi_{S,added}$) range was 0 to 4 M of NaCl. Each one of the phase-separated samples yielded two phases: the measured compositions of the complex and supernatant phases were represented by filled and unfilled symbols, respectively, on the diagram, which are connected by a negatively sloped tie-line. The polymer content (ϕ_P) of the complex phases generally decreased with increasing $\phi_{P,0}$ and $\phi_{S,added}$, attributed to the self-suppression and screening effect of added salt in accordance with the Voorn-Overbeek (V-O) theory[3] and previous studies[26,31,47].

Noticeably, the merging of the complex branch with the supernatant branch, an indication of the transition from two-phase region into one homogenous phase, was not observed even up to 4 M of added NaCl. This unusually high salt resistance has been reported by others[48] and is unexpected considering the conventional nature of weak polyelectrolytes bearing simple ionizable moieties without structurally steric components. Additionally, in the intermediate

$\phi_{S,added}$ range of 0.5 to 1.5 M in **Figure 1b~e**, the data points deviated slightly from the general trend of decreasing ϕ_P with $\phi_{S,added}$ on the right branches for all phase diagrams.

Figure 3-2e shows the superposition of a~d, where the deviation from the decreasing trend of ϕ_P became more pronounced. Compared to our previous work involving poly(glutamic acid) (PRE) and poly(lysine) (PLK), polypeptides comprising completely hydrophilic backbones[23], the pairing of PAANa and PAH exhibited much higher resistance to both NaCl and

Figure 3-3. PAANa-PAH complexation phase diagrams under basic conditions (pH = 9).

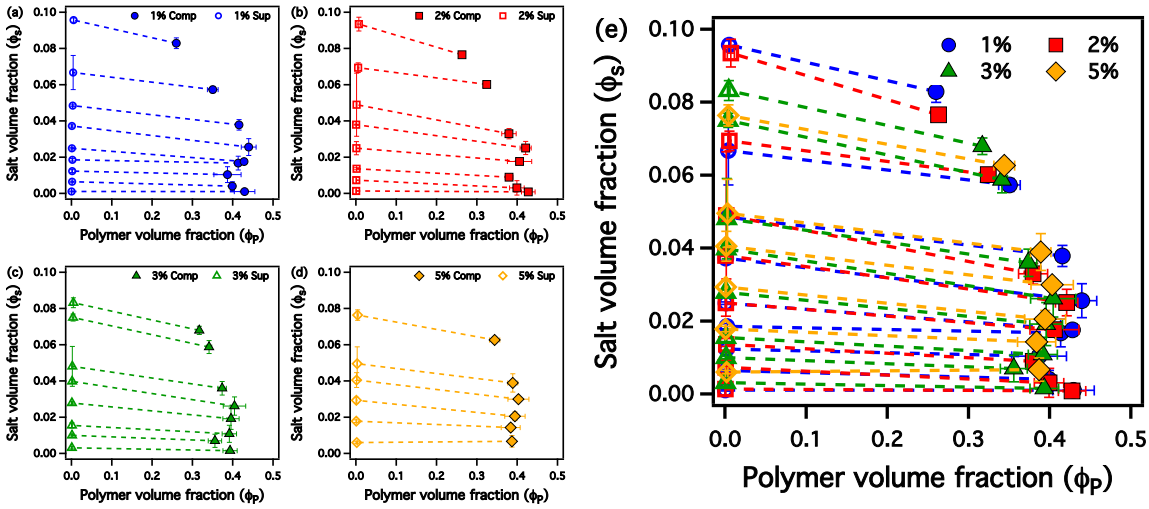

Phase diagrams comprising PAANa158 (sodium salt), PAH160 and NaCl were measured by TGA at φ_(P,0) = (a) 1% wt/v, (b) 2% wt/v, (c) 3% wt/v, and (d) 5% wt/v. The filled circles (complex phase) and unfilled circles (supernatant phase) are connected by dotted tie-lines with negative slopes. Error bars denote the standard deviation. (e) Overlay summary of all TGA results.

KBr (shown in **Figure 3-15**). We hypothesize that the hydrophobicity of the backbone is likely one of the major contributing factors to the discrepancy of decreasing ϕ_P with increasing $\phi_{S,added}$ on the binodal phase diagrams. This will be discussed in greater details toward the end of this text. As for similarities, the tie-lines in this phase diagram were negatively-sloped, which resembled the phase behavior of PRE-PLK and, consequently, indicated preferential partitioning

of salt into the supernatant phases. The universal structure-property relationship of salt partitioning across both the hydrophobic and hydrophilic systems is clear. Nevertheless, imposing preferential partitioning of salt into the complex phase may be possible by manipulating polymer and counterion identity by molecular engineering of different chemical structures, valency, and physical features[49,50].

Next, the phase behaviors of PAANa and PAH under basic conditions were explored. The pHs of stock solutions and complexation mixture were all adjusted to 9. Similar to **Figure 3-2**, small deviations were observed for $\phi_{S,added}$ of 0.5 to 1.5 M for different $\phi_{P,0}$. Notably, ϕ_P increased with increasing $\phi_{S,added}$ under low ϕ_S region for the 5% *wt/v* samples compared to the

Figure 3-4. PAA-PAH complexation phase diagrams under acidic conditions (pH = 3).

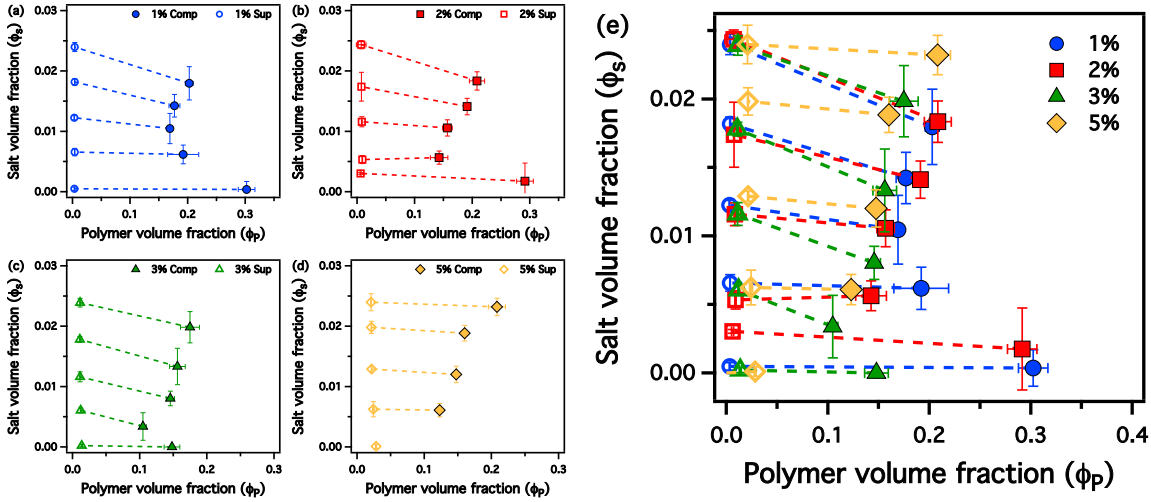

Phase diagrams comprising PAANa138 (sodium salt), PAH160 and NaCl were measured by TGA at ϕ_(P,0) = (a) 1% wt/v, (b) 2% wt/v, (c) 3% wt/v, and (d) 5% wt/v. The filled circles (complex phase) and unfilled circles (supernatant phase) are connected by dotted tie-lines with negative slopes. Error bars denote the standard deviation. (e) Overlay summary of all TGA results.

1% *wt*/*v* counterparts. We believe that this might be attributed to the higher effective counterions with higher $\phi_{P,0}$, consequently increasing the overall ϕ_S in the solution and enhancing hydrophobic effects. **Figure 3-3e** summarized the overall binodal phase boundaries under basic conditions. Excellent overlap of the data preserves the expected shape of the phase envelope, with increased uncertainties in the low salt concentration regime. By comparison to the two overall phases in the neutral pH conditions, the ϕ_P in the complex phase under the same $\phi_{P,0}$ and $\phi_{S,added}$ was systematically lower. For instance, at $\phi_{S,added}$ of 4 M (the highest point on the diagrams denoted in blue symbols due to largest concentration of added salt) and $\phi_{P,0}$ of 1% *wt*/*v*, the ϕ_P was determined to be 35% under neutral conditions and 30% under basic environments. Since both PAANa and PAH are weak polyelectrolytes, their ionization is strongly affected by the pH of the surrounding environment. Accordingly, the dissociation of PAH is less under basic condition, leading to the formation of less complex materials.

3.2.2 Binodal Phase Behaviors Under Acidic Conditions

Finally, the phase behaviors of PAA-PAH complexes were investigated under acidic conditions. When we tried to adjust the pH of stock solutions, PAANa was found to precipitate upon addition of HCl. Hence, for this set of experiments the acidic form of the PAA was used directly with PAH at the same monomer concentration to ensure charge matching. The pHs of stock solutions and complexation mixture were adjusted to 3. **Figure 3-4a~d** contain the representative phase diagrams at $\phi_{P,0}$ = 1, 2, 3, and 5% *wt*/*v* along with $\phi_{S,added}$ = 0 to 1 M. Qualitatively at first glance, the general binodal shapes of the phase diagrams are distinctively different compared to the previously obtained diagrams under the basic and neutral conditions. Specifically, the complex branch extended right towards higher ϕ_P with increasing $\phi_{S,added}$, which exhibits the opposite trend compared to the neutral and basic conditions. This abnormality

was hypothesized to arise from the effects of hydrophobicity of the connected hydrocarbon backbone and the hydrogen bonding propensity of unionized acrylic acid moieties at low pH, which have literature precedence in older investigations of the individual polymers[51,52].

To further investigate the aforementioned physical arguments for the unexpected phase behavior under acidic conditions compared with neutral and basic ones, turbidimetric analysis and microscopic study were conducted together for the two individual PAANa and PAH polymers. **Figure 3-5a** shows the turbidimetry behavior of PAA at 5% *w/v* as a function of total salt concentration. From the plot, the absorbance steadily increased starting at 0.15 M NaCl, indicating the formation of a secondary phase in the solution. Aggregates at this salt concentration were identified upon visual inspection and by microscopy. As the salt concentration continued to increase, more precipitates formed, agglomerated, and eventually settled down out of solution, as demonstrated in the absorbance returning to baseline upon sedimentation (instead of complete dissolution as discussed before). **Figure 3-5b** shows

Figure 3-5. Examining the hydrophobic natures of individual polymers.

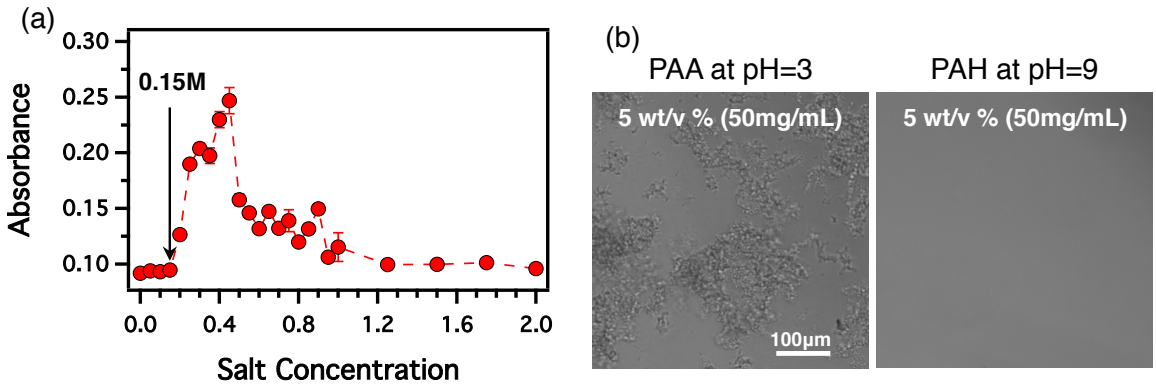

(a) Turbidity measurement as a function of added salt concentration at a PAA concentration of 1% *wt/v*. The peak in absorbance, starting from the marked point of 0.15 M, corresponds to PAA precipitation; the following decrease results from sedimentation of the as-formed precipitates. (b) Representative micrography images of pure PAA (pH =3) and PAH (pH = 9) at 5% *wt/v* in 2 M NaCl. Precipitation was observed in PAA solutions, while PAH solution remained a homogeneous phase. The scale bars were the same for both images.

representative micrography images of individual PAA (pH = 3) and PAH (pH = 9) polymers in 2 M NaCl solution at 5% *wt/v* ϕ_P. At these chosen pH conditions, PAA precipitated considerably in salt environment, while PAH remained stable in solution. This result also accounts for the formation of precipitates when we tried to lower the pH of the stock PAANa solution to 3, due to

Figure 3-6. Study of hydrogen bonding effects in PAA-PAH complexes.

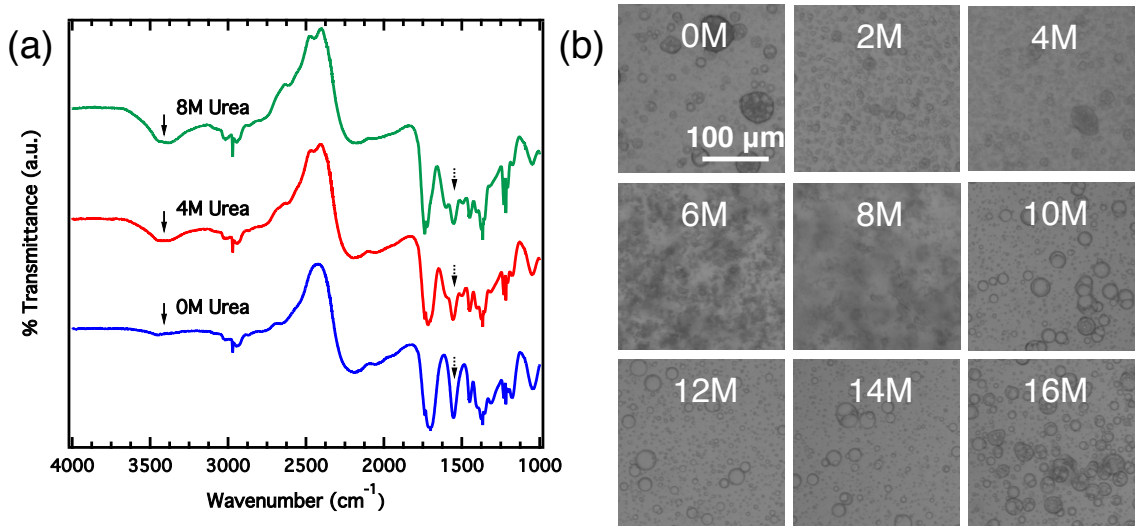

(a) FTIR spectra of PAA-PAH complexes obtained in 0, 4, and 8 M of urea under acidic condition. The solid arrows at ~3450 cm-1 indicate free O-H stretching vibrations. The dashed arrows at ~1560 cm-1 denote deprotonated carboxylic acids. (b) Microscopy gallery of the complexes with 2 M NaCl at polymer concentration= 1% wt/v under acidic condition as a

the released salt ions in the aqueous media.

3.2.3 Interactions Beyond Electrostatic Interactions: Hydrophobicity and Hydrogen Bonding

For polyelectrolytes with aliphatic backbone, one of the main driving forces to form homogenous aqueous solution is the tendency for water molecules to hydrate the charged functional groups. When salt is added to the solution, the screening effect of sodium and chloride

ions via electrostatic interactions interrupts the active physical links between water and ionized moieties, undermining the solvation of the otherwise insoluble polymers. For PAA, categorically labeled as a weak acid due to the labile carboxyl groups, low pH solutions result in a majority of the carboxyl groups to be protonated. If this intermolecular attraction is shielded by the large excess of NaCl in the acidic solution environment, the electrostatic interactions are screened, consequently lowering the compatibility between polymer and water as the solvent. The unionized functional groups in PAA can serve as hydrogen bond donors and/or acceptors; Buscall and Corner have proposed that hydrogen bonding can be facilitated under acidic conditions for PAA[52]. This precipitation of pure PAA induced by poor solvent condition was confirmed by H^1 NMR (shown in **Figure 3-10**), wherein the molar ratio of PAA to PAH was 67% in acidic samples, as compared to 43% and 40% in neutral and basic samples, respectively, in good agreement with previous literature.[8,36]

The work from R.G. Larson's group has provided similar theoretical and experimental observations of unusually high salt resistance and polymer content in the complex phase under low pH conditions for PAA-PDMAEMA system.[53] After introducing a Flory-Huggins parameter of $\chi = 0.75$ representing the interactions between PAA and water as solvent into the V-O model, they found when no hydrophobicity was assumed for PAA with $\chi = 0$, the salt resistance concentration was calculated to be symmetric around the midpoint between the pKas of PAA and PDMAEMA with the highest salt resistance concentration lying around pH=6.5, which is contrary to the experimental fact that the salt resistance is the highest at pH=4. However, qualitative agreement was achieved when χ was set to 0.75. Furthermore, from atomistic simulation, each neutral PAA monomers formed 2.5 hydrogen bondings with water, while each charged PAA monomer could form 6 hydrogen bondings with water, verifying the assumption

that neutral PAA monomers with $\chi = 0.75$ at acidic pH are much more hydrophobic than charged PAA at neutral or basic conditions with $\chi = 0$. At the same time, both neutral and charged PDMAEMA monomers formed 2 hydrogen bondings with water, identifying the fact that it is mainly the properties of PAA influencing the phase behavior of system investigated.

On the other hand, the χ value of charged PAA was reported to be 0.5.[54,55] Accordingly to the equation of $\chi_{eff} = \chi_0 - \frac{w_c}{\kappa^2}$, where w_c is the strength of the screened Coulombic

Figure 3-7. Comparison of the composition partitioning at different pH values.

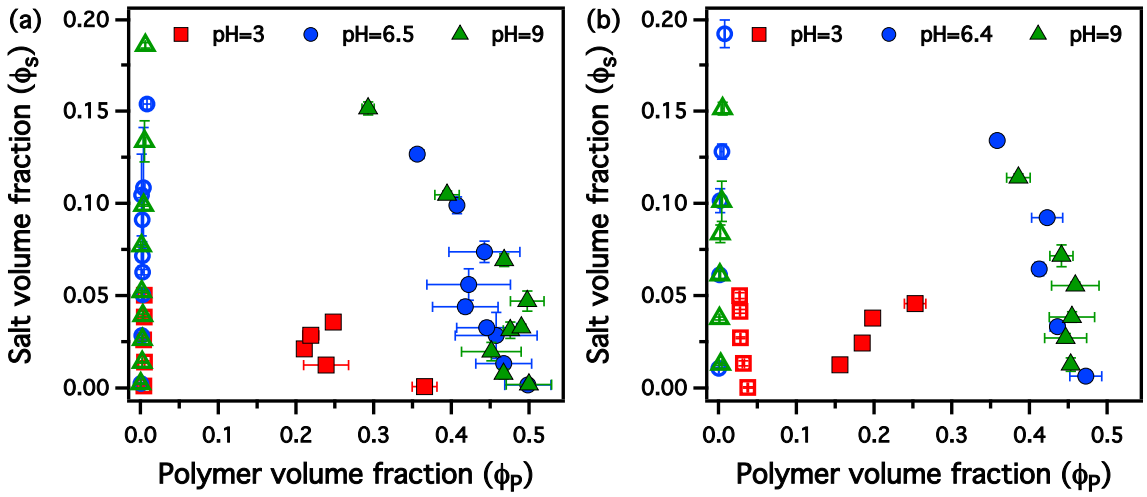

A comprehensive comparison of the phase diagrams for PAA(PAANa)-PAH complexes at three different pH values with $\phi_{P,0}$ of (a) 1% *wt/v* and (b) 5% *wt/v*. While large portions of the phase diagrams at neutral and basic pH conditions overlap, the phase diagrams at acidic pH conditions exhibit non-trivial deviations due to hydrophobic effects and hydrogen bonding of PAA. The polymer content of the complex phase at acidic condition is roughly the half of those in neutral and basic pH conditions, which is the reverse for the supernatant phase.

interaction among monomers, and κ^2 is the inverse-square Debye screening length, proportional to salt concentration,[4,56] χ_{eff} will increase with increasing salt concentration. The χ_{eff} value for charged PAA is 0.5 without salt; consequently, the χ_{eff} will be higher than 0.5 for uncharged

PAA under acidic conditions and increase further by addition of salt, meaning assigning $\chi = 0.75$ is experimental practical. Besides different phase behavior under various pHs, here we also have shown detailed compositional binodal phase diagrams delineating the unusual PAA accumulation in the complex phase under acidic conditions with associative and segregative phase separation working simultaneously. In this sense, the phase behavior of PAA and PAH system, instead of being thought of as a simple polyelectrolyte complexation phenomenon, can be regarded as an association driven by a complication of various factors, from electrostatics, hydrophobicity, and hydrogen bonding. The experimentally measured phase diagram data is reflecting the final result of interconnected competition among all these parameters as a function of polymer concentration, salt concentration, and pH.

At the same time, in order to examine hydrogen bonding effects under acidic condition, urea was used as a hydrogen bonding disruptor for the PAA-PAH network. The strong intermolecular interactions between the urea nitrogen and oxygen atom (N–H · · · O) are known to drive biological phenomena in water, e.g., protein denaturation. Fourier transform infrared (FTIR) spectroscopy was used to examine the effect of urea on the hydrogen bonding formed between the acrylic acid monomer units in the complexes, shown in **Figure 3-6a**. To avoid overlap with water on the FTIR spectrum, the stock solutions of PAA, PAH, NaCl, and urea were all prepared in D_2O. The select spectra of PAA-PAH solid precipitate complexes at 0, 4, and 8 M urea show clear evidence of weakened intermolecular hydrogen bonding between PAA chains. Specificcally, the solid arrows at ~3450 cm^{-1} indicate band sharpening of free O-H stretching vibrations as urea concentration increased. Furthermore, the dashed arrows at ~1560 cm^{-1} correspond to deprotonated carboxylic acids, which broadens from a sharp single peak into a bimodal peak as urea molecules hydrogen bond with –COOH moieties. **Figure 3-6b** displays a

representative collection of microscopy images for the PAA-PAH complexes prepared at 1% *wt*/*v* $\phi_{P,0}$ and 2 M of NaCl, with the addition of increasing urea concentration from 0 to 16 M (the maximum achievable concentration at 20 ^{o}C) under acidic conditions. Despite the morphological changes by addition of urea, the complexes still persisted under exceptionally high urea content. This indicates that while hydrogen-bonding indeed partitially facilitate the precipitation process of PAA, hydrogen bonding is not the sole reason for the unusual high salt tolerance. We acknowledge that it is unclear why uncharged PAA precipitates out of solution while uncharged PAH does not, but the strength of PAA as a hydrogen bond donor and acceptor might be one possible explanation. From this indirect evidence, we reason that hydrophobic effects of the chain backbone, coupled with intermolecular hydrogen bonding, allow PAA(PAANa)-PAH complexes to be highly resistant towards salt. Additional details on morphological changes of the PAANa-PAH complexes in different concentration of urea could be found in the Supporting Information.

In context of the previous phase diagram in **Figure 3-4a**, for complexes at $\phi_{P,0}$ = 1% *wt*/*v*, the ϕ_P of the complex phase decreased slightly upon addition of salt at low salt concentration region. However, the trend reversed when additional salt was further increased. This trend became more pronounced when higher $\phi_{P,0}$ was used, e.g., 5% *wt*/*v* in **Figure 3-4d**, in which the ϕ_P experienced monotonic increase upon addition of salt. The abnormal behavior of increasing the ϕ_P with $\phi_{S,added}$ in the complex phase is more prominent from Figures 3-4a to d, which is rationalized by the higher PAA content in the solution with amplified hydrophobicity and hydrogen bonding effects.

3.3 Conclusion

From the results presented above, we collectively compared the phase behaviors of PAA(PAANa)-PAH complexes as a function of pH solvent effects. **Figure 3-7** showed the polymer-salt compositions for samples at a $\phi_{P,0}$ of 1% *wt*/*v* in (a) and 5% *wt*/*v* in (b) under three pH conditions. As seen in these plots, the compositional difference of the two phases under basic and neutral conditions is negligible and within experimental error. However, the acidic series shows an utterly different behavior. At the neutral pH conditions, both polymers were fully-charged, given the pKa of PAA is reported to be around 4.5 and PAH 8.5[57]. Under the basic pH conditions, PAH was predominately uncharged, while PAA was fully-charged, but the complexation behavior was not significantly affected. Even though PAH was unionized, it still possessed the potential to interact with the carboxyl groups on PAA. The association of amino groups in PAH with carboxyl groups in PAA, facilitated by hydroxide ions in the aqueous solutions, resulted in the formation of stable complexes. However, if the environment were adjusted to acidic pH conditions, a fraction of the PAA polyelectrolyte precipitated under high salt conditions, rendering it unable to participate in complexation with PAH. The solid precipitate formed under low pH comprised both pure PAA precipitates (due to hydrophobic effects and hydrogen bonding) and PAA-PAH complexes. Greater quantities of PAA precipitate formed at $\phi_{P,0}$ = 5% *wt*/*v* over 1% *wt*/*v*. Noticeably, the ϕ_P of the complex phase under acidic conditions was roughly the half of its counterparts under basic and neutral conditions. Additionally, with the same amount of total polymer used in the system, the ϕ_P in the supernatant phase was apparently higher under acidic conditions by the mass balance.

Altogether, this investigations brings attention to the fact that the polyelectrolyte complexation is a fairly complicated system driven by not only electrostatic forces among the

oppositely charged polymers and entropic gains from counterion release[58,59], but also solvent effect and unavoidable intermolecular interactions. Oftentimes, such factors in realistic materials like PAA and PAH are overlooked or assumed to be inconsequential compared to charge-driven complexation mechanisms. To incorporate more of these advanced features into a wider materials infrastructure, we anticipate that theory and simulations can more easily interrogate the interplay of such variables. This experimental work provides elucidates molecular level insight of various complexation effects for the model polymer pairing of PAA(PAANa) and PAH, which can enable greater comprehension and control over the structure-property relationship of synthetic polymeric systems in micellar and gel-like architectures[60,61].

Sample	**Molecular Weight** (M_n g/mol)	**Polydispersity** (M_w/M_n)	**Degree of Polymerization** (N)
PAA	10,000	1.04	138
PAANa	14,800	1.04	158
PAH	15,000	1.18	160

Table 3-1. Characterization of aliphatic polymers used in the study.

3.4 Methods and Experimental Details

A. Materials and preparation of stock solution. Poly(acrylic acid) (PAA) and poly(acrylic acid sodium salt) (PAANa) were purchased from Polymer Source Inc.(Dorval, Canada) Poly(allylamine hydrochloride) (PAH) were purchased from AK Scientific Inc.(Union City, CA USA) Sodium Chloride (NaCl, ACS grade) was purchased from Sigma (St. Louis, MO). The chemical reagents were used as received. The molecular weight, degree of polymerization, and

dispersity values from the vendors are listed in **Table 3-1**. PAA or PAANa and PAH formed white solid or semi-solid precipitate when mixed together due to complexation. 10% *wt*/*v* PAA

Figure 3-8. Phase-separated PAA-PAH mixture.

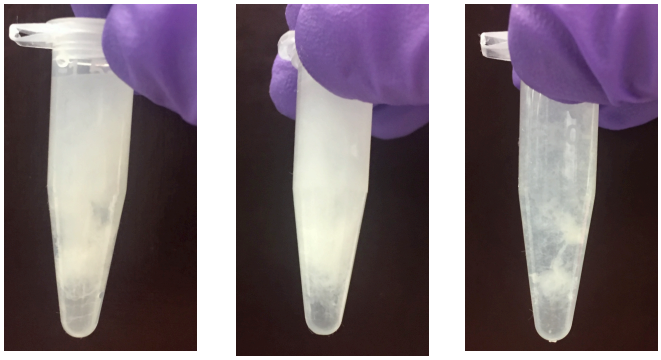

1500 μL PAA(PAANa)+PAH mixtures at 1% *wt*/*v* total polymer concentration without added salt under neutral (left), basic (middle) and acidic (right) conditions. The photos were taken after mixing and vortexing for 30 s.

Figure 3-9. Conductivity measurements for salt concentrations

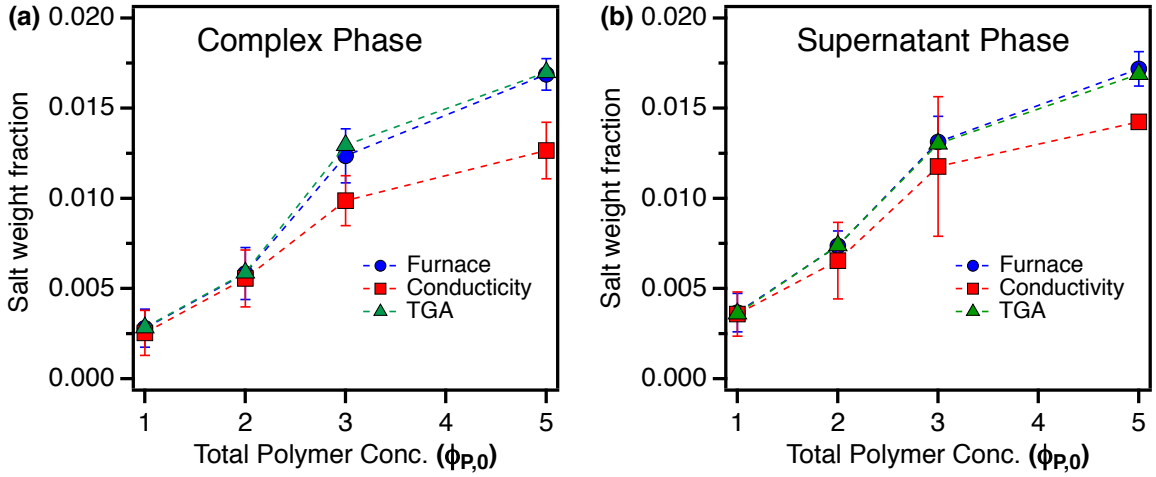

Salt weight fractions measured from furnace burning method (blue symbols), TGA methods using the protocol from our previous publication (green symbols), and conductivity measurements (red symbols) were nearly identical for both complex (a) and supernatant phases (b). Dashed lines are drawn to guide the eye.

Figure 3-10. Turbidimetric analysis of PAANa-PAH complexes at $\phi_{P,0}$ 0.05 to 1% *wt*/*v* under neutral pH conditions (pH = 6.5).

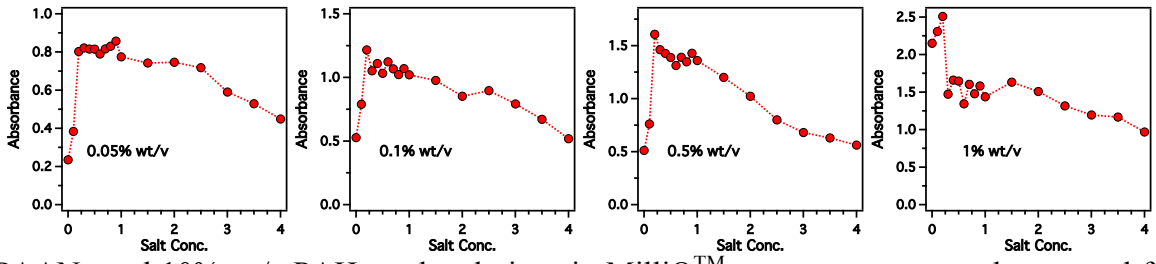

or PAANa and 10% *wt*/*v* PAH stock solutions in MilliQ^{TM} water were prepared, vortexed for 1 min, and sonicated for 6 h to fully dissolve the polymers and obtain clear stock solutions. 5.0 M of NaCl stock solutions were prepared for future sample preparation.

B. Preparation of polyelectrolyte complexes. olyelectrolyte complexes were prepared at 1:1 stoichiometric ratio of charge-matched conditions. The required amounts of PAH stock solutions were added to a solution containing the desired amounts of MilliQ water and NaCl stock solution (5 M) in a 1.5 mL Eppendorf tube and vortexed for 30 sec. Next, the required amounts of PAA or

Figure 3-11. ^{1}H NMR spectrum of the PAANa-PAH complexes prepared under neutral pH conditions.

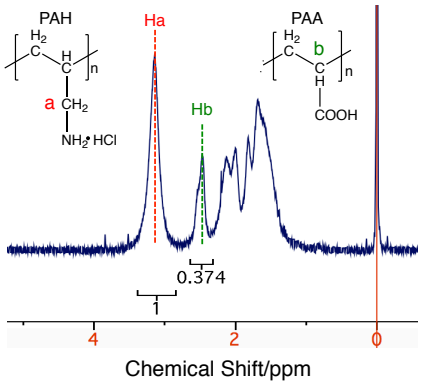

All the precipitate phases were collected and lyophilized before dissolving in the $CDCl_3$ solvent for NMR measurements. The protocol was same for the samples under acidic, neutral, and basic pH conditions.

PAANa stock solutions were added, and the solution mixtures were vortexed again for 30 sec. **Figure 3-8** showed the complexation mixture of PAA (or PAANa) and PAH under acidic, neutral, and basic conditions, for which the resultant white, feather-like precipitate suspended in the solution.

C. Thermogravimetric analysis (TGA). The 1.5 mL Eppendorf tubes containing the samples were centrifuged at 17000×G for 15 min. 30 μL of the supernatant and the whole complex phase were extracted, transferred into separate aluminum pans, and put into Barnstead Thermolyne Furnace 1400 for heating processing. The operating atmosphere in the furnace was air. The

Figure 3-12. Representative microscopy images of PAANa-PAH complexes in NaCl solution under neutral condition

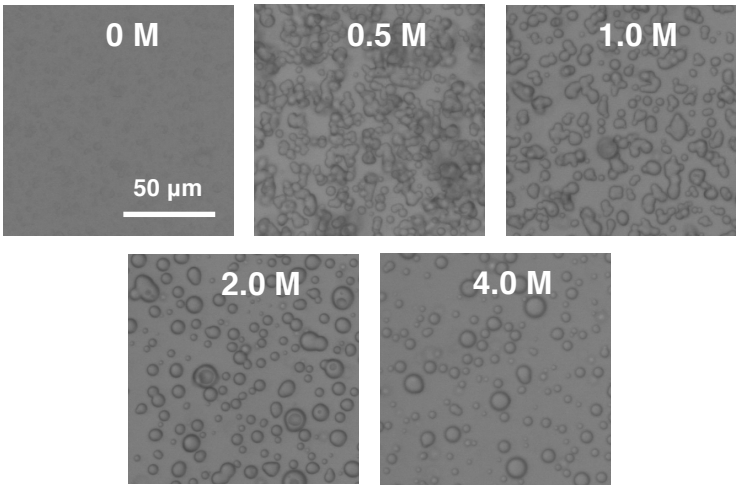

PAANa-PAH complexes prepared at $\phi_{P,0}$ of 1% *wt*/*v* and $\phi_{S,\,added}$ = 0, 0.5, 1.0, 2.0, and 4.0 M NaCl under pH = 6.5. The morphology of the complexes changed from flake-like precipitates to semi-solid droplets with addition of salt due to the screening effect. The scale bars were the same for all images.

following protocol was used: samples were placed in the furnace at room temperature, and the temperature of the furnace was increased to 110 °C and held there for 2.5 h. At that point, the samples were cooled to room temperature, sample weights were measured to estimate the water content, and again returned to the furnace and heated to 600 °C. After heating for 12 h, the

samples were cooled to room temperature, and their weights were measured again to estimate the polymer and salt contents. For each total polymer concentration and salt concentration, at least 3 repeating samples were prepared. The weight fractions of water, polymer, and salt were recorded and converted to volume fractions by assuming same density of polymer and salt in bulk and solution state, wherein densities $\rho_{polymer}$= 1.3308 g/mL, ρ_{salt}= 2.16 g/mL, and ρ_{water}= 1.00 g/mL at 20 °C were used. Statistical analysis using Dixon's Q test was performed for the identification and rejection of outliers.

Figure 3-13. Representative microscopy images of PAA-PAH complexes in NaCl solution under basic condition

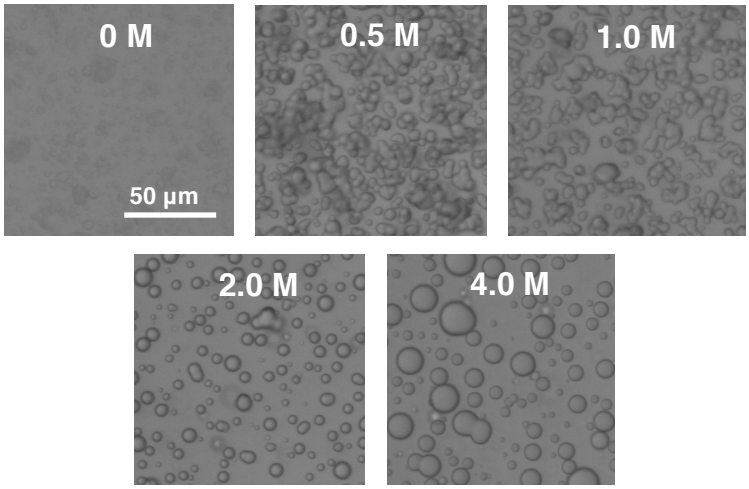

PAA-PAH complexes prepared at $\phi_{P,0}$ of 1% *wt*/*v* and $\phi_{S,\ added}$ = 0, 0.5, 1.0, 2.0 and 4.0 M NaCl under pH = 9. The morphology of the complexes changes were similar to the neutral pH condition. The scale bars were the same for all images.

D. Conductivity measurement: Conductivity tests were conducted to ensure the accuracy of the salt measurements on the microbalance for TGA measurements. To determine the absolute amounts of salt in the samples, a standard calibration curve based on NaCl solutions was prepared by measuring conductivities of 18 standard solutions ranging from 0 to 5×10^{-3} M. For

each sample, three independent measurements were taken. The remaining materials in the aluminum pan following a furnace experiment were each transferred into 15 mL Eppendorf tubes and mixed with 5 mL of MilliQ water. The mixture was sonicated for 30 s before taking the conductivity measurements. **Figure 3-9** demonstrates that the measured quantities of salt in the two respective phases were statistically identical for these three kinds of methods, verifying the

Figure 3-14. Representative microscopy images of PAA-PAH complexes in NaCl solution under acidic condition

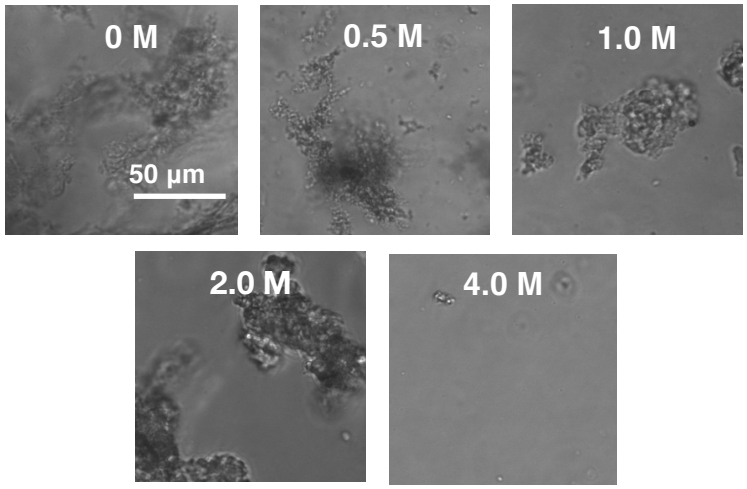

PAA-PAH complexes prepared at $\phi_{P,0}$ of 1% wt/v and $\phi_{S,\,added}$ = 0, 0.5, 1.0, 2.0 and 4.0 M NaCl under pH = 3. Notably, the amount of precipitates might seem very limited at 4 M, but appreciable amount of precipitates could be identified and isolated after centrifugation. The scale bars were the same for all photos.

accuracy of the furnace burning method.

E. Turbidity, 1H NMR, and microscopic studies. Turbidity was measured using a UV spectrophotometer on a Tecan Infinite M200 plate reader at the wavelength of 500 nm and at 20 °C. None of the polymers absorb light at this wavelength. The turbidity (T) is defined as $T = -\ln I/I_0$, with I_0 as the incident light intensity, and I as the intensity of light transmitted through the sample. Three measurements were collected with plate shaking for 1 s, followed by

measurements at four points per sample. Twelve repeats for each sample condition were carried out. **Figure 3-10** shows the turbidity measurements at different total polymer concentrations for PAANa and PAH under neutral pH conditions.

The ^{1}H NMR spectrum of PAA-PAH complexes prepared at neutral conditions in **Figure 3-11** is shown below as an example. The measuring protocol was adopted from Reference 36 in the main text. We note here that the solubility of the acidic samples in water was not ideal, so measurement uncertainties for the acidic samples was encountered. The mole fractions of PAA in the complexes obtained under three kinds of conditions are 67% for acidic condition, 43% for neutral condition and 40% for basic condition, which were in good overall agreement with previously reported values of References 8 and 36 in the main text. From these values, the precipitates that formed under acidic conditions likely contained a large amount of pure PAA

Figure 3-15. Representative microscopy images of PAA-PAH complexes in KBr solutions under neutral condition.

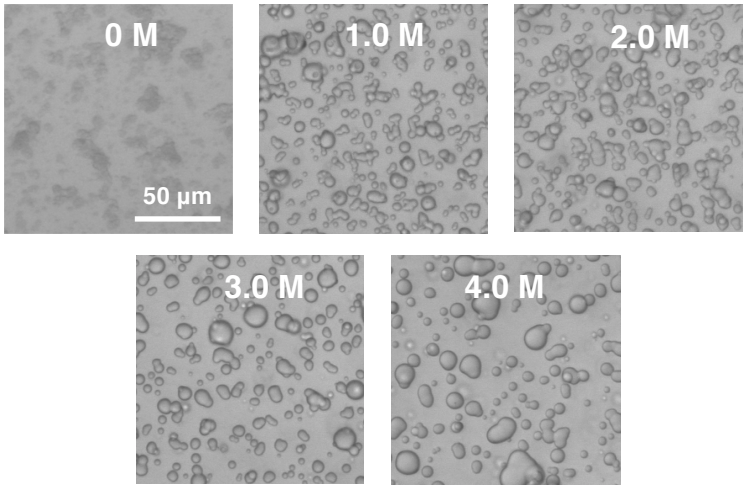

PAA-PAH complexes prepared at $\phi_{P,0}$ of 1% *wt*/*v* and $\phi_{S,\,added}$ = 0, 1.0, 2.0, 3.0 and 4.0 M KBr under pH = 6.5. The morphological changes of the complex phase upon the addition of KBr is similar to that of NaCl, and no one homogenous phase has been observed to form within the concentration added. The scale bars were the same for all photos.

aggregates, compared to the samples measured under neutral and basic pH conditions.

The phase-separated complexes and PAA precipitate were observed using phase contrast optical microscopy (Leica DMI 6000B). 200 μL of sample solution mixture was injected in to the ultralow attachment 96-well plates (Costar, Corning Inc.) for observation and image capturing **Figure 3-12** shows the images taken for PAA-PAH complexes under neutral pH, and the morphological changes could be identified by the screening effect of added NaCl.

Figure 3-13 shows the images taken for PAA-PAH complexes under basic pH conditions, and the morphological changes were similar to those under neutral conditions. **Figure 3-14** shows the images taken for PAA-PAH complexes under acidic pH conditions. Even though there seemed to be limited amounts of precipitates at 4 M of NaCl, appreciable precipitates can be identified and isolated from the upper supernatant phase after centrifugation.

F. Salt resistance of KBr. KBr is known as one of the most effective salts to explore the polyelectrolyte coacervate/complex continuum. To check the universality of the usually high salt resistance of the PAANa-PAH complexes, we also looked at morphological changes of PAANa-PAH by addition of KBr. **Figure 3-15** shows representative micrographs of PAANa-PAH obtained from 0 to 4 M of KBr. Bulk complexes persisted even in 4 M KBr solution, demonstrating the usually high salt resistance of this polymer pairing.

3.5 References

1. Jong, B. de, Kruyt, H. G. & R, H. Koazervation. *Proc. K. Ned. Akad. Wet.* **32**, 849–856 (1929).

2. Voorn, M. J. *Complex Coacervation.* (Wiley-VCH Verlag GmbH Co., 1956).

3. Overbeek, J. T. G. & Voorn, M. J. Phase separation in polyelectrolyte solutions. Theory of complex coacervation. *J. Cell. Comp. Physiol.* **49**, 7–26 (1957).

4. Muthukumar, M. 50th Anniversary Perspective: A Perspective on Polyelectrolyte Solutions. *Macromolecules* (2017). doi:10.1021/acs.macromol.7b01929

5. Samanvaya, S. & V., T. M. Polyelectrolyte Complexation. *Adv. Chem. Phys.* 499–544 (2016). doi:10.1002/9781119290971.ch7

6. Brangwynne, C. P., Tompa, P. & Pappu, R. V. Polymer physics of intracellular phase transitions. *Nat. Phys.* (2015). doi:10.1038/nphys3532

7. Strom, A. R. *et al.* Phase separation drives heterochromatin domain formation. *Nature* **547**, 241–245 (2017).

8. Aumiller, W. M., Pir Cakmak, F., Davis, B. W. & Keating, C. D. RNA-Based Coacervates as a Model for Membraneless Organelles: Formation, Properties, and Interfacial Liposome Assembly. *Langmuir* **32**, 10042–10053 (2016).

9. Aumiller, W. M. & Keating, C. D. Phosphorylation-mediated RNA/peptide complex coacervation as a model for intracellular liquid organelles. *Nat. Chem.* (2016). doi:10.1038/nchem.2414

10. Wang, Q. & Schlenoff, J. B. Single- and multicompartment hollow polyelectrolyte complex microcapsules by one-step spraying. *Adv. Mater.* **27**, 2077–2082 (2015).

11. Meng, X., Schiffman, J. D. & Perry, S. L. Electrospinning Cargo-Containing Polyelectrolyte Complex Fibers: Correlating Molecular Interactions to Complex Coacervate Phase Behavior and Fiber Formation. *Macromolecules* **51**, 8821–8832 (2018).

12. Meng, X., Perry, S. L. & Schiffman, J. D. Complex Coacervation: Chemically Stable Fibers Electrospun from Aqueous Polyelectrolyte Solutions. *ACS Macro Lett.* **6**, 505–511 (2017).

13. Kuo, C. H. *et al.* Inhibition of atherosclerosis-promoting microRNAs via targeted polyelectrolyte complex micelles. *J. Mater. Chem. B* **2**, 8142–8153 (2014).

14. Black, K. A. *et al.* Protein encapsulation via polypeptide complex coacervation. *ACS*

Macro Lett. **3**, 1088–1091 (2014).

15. Krogstad, D. V. *et al.* Structural evolution of polyelectrolyte complex core micelles and ordered-phase bulk materials. *Macromolecules* **47**, 8026–8032 (2014).

16. Srivastava, S. *et al.* Gel phase formation in dilute triblock copolyelectrolyte complexes. *Nat. Commun.* **8**, 1–9 (2017).

17. Priftis, D., Laugel, N. & Tirrell, M. Thermodynamic Characterization of Polypeptide Complex Coacervation. *Langmuir* **28**, 15947–15957 (2012).
18. Vitorazi, L. *et al.* Evidence of a two-step process and pathway dependency in the thermodynamics of poly(diallyldimethylammonium chloride)/poly(sodium acrylate) complexation. *Soft Matter* **10**, 9496–9505 (2014).

19. Fu, J. & Schlenoff, J. B. Driving Forces for Oppositely Charged Polyion Association in Aqueous Solutions: Enthalpic, Entropic, but Not Electrostatic. *J. Am. Chem. Soc.* **138**, 980–990 (2016).

20. Wu, H., Ting, J. M., Werba, O., Meng, S. & Tirrell, M. V. Non-equilibrium phenomena and kinetic pathways in self-assembled polyelectrolyte complexes. *J. Chem. Phys.* **149**, (2018).

21. Takahashi, R., Narayanan, T. & Sato, T. Growth Kinetics of Polyelectrolyte Complexes Formed from Oppositely-Charged Homopolymers Studied by Time-Resolved Ultra-Small-Angle X-ray Scattering. *J. Phys. Chem. Lett.* **8**, 737–741 (2017).

22. Priftis, D. & Tirrell, M. Phase behaviour and complex coacervation of aqueous polypeptide solutions. *Soft Matter* **8**, 9396–9405 (2012).

23. Li, L. *et al.* Phase Behavior and Salt Partitioning in Polyelectrolyte Complex Coacervates. *Macromolecules* (2018). doi:10.1021/acs.macromol.8b00238

24. Chollakup, R., Smitthipong, W., Eisenbach, C. D. & Tirrell, M. Phase behavior and coacervation of aqueous poly(acrylic acid)-poly(allylamine) solutions. *Macromolecules* **43**, 2518–2528 (2010).

25. Chollakup, R., Beck, J. B., Dirnberger, K., Tirrell, M. & Eisenbach, C. D. Polyelectrolyte molecular weight and salt effects on the phase behavior and coacervation of aqueous solutions of poly(acrylic acid) sodium salt and poly(allylamine) hydrochloride hydrochloride. *Macromolecules* **46**, 2376–2390 (2013).

26. Spruijt, E., Westphal, A. H., Borst, J. W., Cohen Stuart, M. A. & Van Der Gucht, J. Binodal compositions of polyelectrolyte complexes. *Macromolecules* **43**, 6476–6484 (2010).

27. Gucht, J. van der, Spruijt, E., Lemmers, M. & Cohen Stuart, M. A. Polyelectrolyte complexes: Bulk phases and colloidal systems. *J. Colloid Interface Sci.* **361**, 407–422 (2011).

28. Veis, A. A review of the early development of the thermodynamics of the complex coacervation phase separation. *Adv. Colloid Interface Sci.* **167**, 2–11 (2011).

29. Perry, S. L. *et al.* Chirality-selected phase behaviour in ionic polypeptide complexes. *Nat. Commun.* (2015). doi:10.1038/ncomms7052

30. Qin, J. & De Pablo, J. J. Criticality and connectivity in macromolecular charge complexation. *Macromolecules* (2016). doi:10.1021/acs.macromol.6b02113

31. Kudlay, A., Ermoshkin, A. V. & De La Cruz, M. O. Complexation of oppositely charged polyelectrolytes: Effect of ion pair formation. *Macromolecules* **37**, 9231–9241 (2004).

32. Kudlay, A. & De la Cruz, M. O. Precipitation of oppositely charged polyelectrolytes in salt solutions. *J. Chem. Phys.* **120**, 404–412 (2004).

33. Perry, S. L. & Sing, C. E. PRISM-Based Theory of Complex Coacervation: Excluded Volume versus Chain Correlation. *Macromolecules* (2015). doi:10.1021/acs.macromol.5b01027

34. Rumyantsev, A. M., Zhulina, E. B. & Borisov, O. V. Complex Coacervate of Weakly Charged Polyelectrolytes: Diagram of States. *Macromolecules* (2018). doi:10.1021/acs.macromol.8b00342

35. Sadman, K. *et al.* Influence of Hydrophobicity on Polyelectrolyte Complexation. *Macromolecules* **50**, 9417–9426 (2017).

36. Jha, P. K., Desai, P. S., Li, J. & Larson, R. G. pH and salt effects on the associative phase separation of oppositely charged polyelectrolytes. *Polymers (Basel).* (2014). doi:10.3390/polym6051414

37. Wang, Q. & Schlenoff, J. B. Single- and multicompartment hollow polyelectrolyte complex microcapsules by one-step spraying. *Adv. Mater.* (2015). doi:10.1002/adma.201405376

38. Boas, M., Burman, M., Yarin, A. L. & Zussman, E. Electrically-responsive deformation of polyelectrolyte complex (PEC) fibrous membrane. *Polymer (Guildf).* (2018). doi:10.1016/j.polymer.2018.10.064

39. Zhang, Y., Li, F., Valenzuela, L. D., Sammalkorpi, M. & Lutkenhaus, J. L. Effect of water on the thermal transition observed in poly(allylamine hydrochloride)-poly(acrylic acid) complexes. *Macromolecules* (2016). doi:10.1021/acs.macromol.6b00742

40. Reisch, A. *et al.* On the benefits of rubbing salt in the cut: Self-healing of saloplastic PAA/PAH compact polyelectrolyte complexes. *Adv. Mater.* (2014). doi:10.1002/adma.201304991

41. Zhao, M. *et al.* Composition and property tunable ternary coacervate: branched polyethylenimine and a binary mixture of a strong and weak polyelectrolyte. *Mol. Syst. Des. Eng.* **4**, 110–121 (2019).

42. Fu, J., Fares, H. M. & Schlenoff, J. B. Ion-Pairing Strength in Polyelectrolyte Complexes. *Macromolecules* (2017). doi:10.1021/acs.macromol.6b02445

43. Weidman, J. L., Mulvenna, R. A., Boudouris, B. W. & Phillip, W. A. Unusually Stable Hysteresis in the pH-Response of Poly(Acrylic Acid) Brushes Confined within Nanoporous Block Polymer Thin Films. *J. Am. Chem. Soc.* (2016). doi:10.1021/jacs.6b01618

44. Lappan, U., Wiesner, B. & Scheler, U. Segmental dynamics of poly(acrylic acid) in polyelectrolyte complex coacervates studied by spin-label EPR spectroscopy. *Macromolecules* **49**, 8616–8621 (2016).

45. Huang, S. *et al.* Effect of small molecules on the phase behavior and coacervation of aqueous solutions of poly(diallyldimethylammonium chloride) and poly(sodium 4-styrene sulfonate). *J. Colloid Interface Sci.* (2018). doi:10.1016/j.jcis.2018.02.029

46. Aberkane, L., Jasniewski, J., Gaiani, C., Scher, J. & Sanchez, C. Thermodynamic characterization of acacia gum-β-Lactoglobulin Complex Coacervation. *Langmuir* **26**, 12523–12533 (2010).

47. Arthur, V., Edward, B. & Shirley, M. Molecular weight fractionation and the self-suppression of complex coacervation. *Biopolymers* **5**, 37–59 (1967).

48. Perry, S. L., Li, Y., Priftis, D., Leon, L. & Tirrell, M. The effect of salt on the complex coacervation of vinyl polyelectrolytes. *Polymers (Basel).* (2014). doi:10.3390/polym6061756

49. Zhang, P., Shen, K., Alsaifi, N. M. & Wang, Z. G. Salt Partitioning in Complex Coacervation of Symmetric Polyelectrolytes. *Macromolecules* (2018). doi:10.1021/acs.macromol.8b00726

50. Lytle, T. K. & Sing, C. E. Tuning chain interaction entropy in complex coacervation using polymer stiffness, architecture, and salt valency. *Mol. Syst. Des. Eng.* (2018). doi:10.1039/c7me00108h

51. Flory, P. J. & Osterheld, J. E. Intrinsic viscosities of polyelectrolytes. Poly-(acrylic acid).

J. Phys. Chem. **58**, 653–661 (1954).

52. Buscall, R. & Corner, T. The phase separation behaviour of aqueous solutions of polyacrylic acid and its partial sodium salts in the presence of sodium chloride. *Eur. Polym. J.* **18**, 967–974 (1982).

53. Jha, P. K., Desai, P. S., Li, J. & Larson, R. G. pH and salt effects on the associative phase separation of oppositely charged polyelectrolytes. *Polymers (Basel).* **6**, 1414–1436 (2014).

54. Thakur, A., Wanchoo, R. K. & Singh, P. Structural Parameters and Swelling Behavior of pH Sensitive Poly(acrylamide-co-acrylic acid) Hydrogels. *Chem. Biochem. Eng. Q.* **25**, 181–194 (2011).

55. Eustace, D. J., Siano, D. B. & Drake, E. N. Polymer compatibility and interpolymer association in the poly(acrylic acid)–polyacrylamide–water ternary system. *J. Appl. Polym. Sci.* **35**, 707–716 (1988).

56. Prabhu, V. M., Muthukumar, M., Wignall, G. D. & Melnichenko, Y. B. Polyelectrolyte chain dimensions and concentration fluctuations near phase boundaries. *J. Chem. Phys.* **119**, 4085–4098 (2003).

57. Bhatia, S. R., Khattak, S. F. & Roberts, S. C. Polyelectrolytes for cell encapsulation. *Curr. Opin. Colloid Interface Sci.* **10**, 45–51 (2005).

58. Borue, V. Y. & Erukhimovich, I. Y. A Statistical Theory of Weakly Charged Polyelectrolytes: Fluctuations, Equation of State and Microphase Separation. *Macromolecules* **21**, 3240–3249 (1988).

59. Ou, Z. & Muthukumar, M. Entropy and enthalpy of polyelectrolyte complexation: Langevin dynamics simulations. *J. Chem. Phys.* **124**, (2006).

60. Ting, J. M., Wu, H., Herzog-Arbeitman, A., Srivastava, S. & Tirrell, M. V. Synthesis and Assembly of Designer Styrenic Diblock Polyelectrolytes. *ACS Macro Lett.* (2018). doi:10.1021/acsmacrolett.8b00346

61. Hunt, J. N. *et al.* Tunable, high modulus hydrogels driven by ionic coacervation. *Adv. Mater.* **23**, 2327–2331 (2011).

CHAPTER 4. Effect of Solvent Quality and Chain Length on the Complexation Stability

4.1 Introduction

Since the resurgence of the interests for polyelectrolyte complexation, there have been a lot of in-depth studies to demonstrate the effect of molecular weight, pH, salt concentration, and mixing ratios of the two polyelectrolytes on the morphological, rheological, and physical properties of the phase-separated mixtures for various polymer pairs, as discussed in Chapter 1.3.3. Common polymeric systems include bio-derived natural polymers, like gelatin, plant gums, and polysaccharides with carboxyl or sulfate groups,[1,2] and synthetic polymers, like PAA, PSS, PDADMAC, PVTAC, PDMAEMA etc.[3–6] Most of the works focus on one system and provide extensive experimental investigations and analysis on the observed facts. However, there still lacks a comprehensive work that can combine the delivered results horizontally from multiple systems of different chemical structures with theoretical calculations to facilitate a comprehensive understanding of the polyelectrolyte complexation system.

To our best knowledge, there are a few attempts to compare the experimental results from different polymer systems in recent publications. Fu et al has quantitatively compared the ion binding strength among five kinds of polycations from primary amine to tertiary amine and four kinds of polyanions with carboxyl or sulfate groups by evaluating how easily the formed complexes could be dissolved by a common salt of KBr.[4] After analyzing the Gibbs free energy of different ion binding pairs collectively, they found chemical structures that can associate with a higher number of water molecules were bound more loosely. Specifically small primary amines had the strongest attraction for anions, and sulfates with styrenic structures could associate with cations closer than carboxyl groups. By the same logic, the ion diffusion coefficients was

positively correlated with water content and negatively correlated with interaction strength. This work provided readers with a general understanding of the phase behaviors along the broad spectrum of polyelectrolytes with different functionalities. Another comparative work by Sadman et al has demonstrated the hydrophobicity of the side chains could also change the rheological responses and swelling properties of the PEC materials.[7] They quaternized poly(4-vintlpyridine) with methyl, ethyl, and propyl substituents and found the salt resistance concentrations of PECs were increasing in the same order, which was discussed in Chapter 3 as well.

However, the detailed compositional map for different polymeric systems is still lacking. Besides the influence from functional groups, the effect of polymer backbone should not be ignored. With the two projects described in Chapter 2 and 3, we were in a good stance to compare the two systems and quantitatively investigate properties of the complexation induced by different chemical structures. Furthermore, we attempted to base our analysis on recently-developed theory of polyelectrolyte complexation based on random phase approximation (RPA) and scaling relationships with our collaborator Dr. Artem M. Rumyantsev for predictive capability.[8–10] Incorporation of the physical theory allowed for a clear isolation of one single parameter, which was unobtainable in experimental efforts. As mentioned in the previous two chapters, the polypeptide pair of PRE-PLK and the aliphatic pair of PAA-PAH have identical functional groups. Accordingly, the electrostatic interactions within each polyelectrolyte pairs should be the same, and the major differences of their phase behaviors should stem from polymer backbones. In order to avoid possible complications from other parameters, polymers of similar chain length of PRE-PLK and PAA-PAH were chosen. Since most of the polymers used in industrial applications of layer-by-layer membrane, ultrafiltration, and coatings have aliphatic

backbones, understanding the role of solvent quality would add another tunable dimension in controlling the performance of PEC-based materials.

4.2 Results and Discussion

4.2.1 Comparison of Binodal Phase Diagrams of PRE-PLK and PAA-PAH Systems

The polymerization degrees of PLK, PRE, sodium salt form of PAA, and chloride salt form of PAH were 105, 96, 158, and 160 respectively. We have used the experimental data from

Figure 4-1. Binodal phase diagrams of PRE-PLK and PAA-PAH systems.

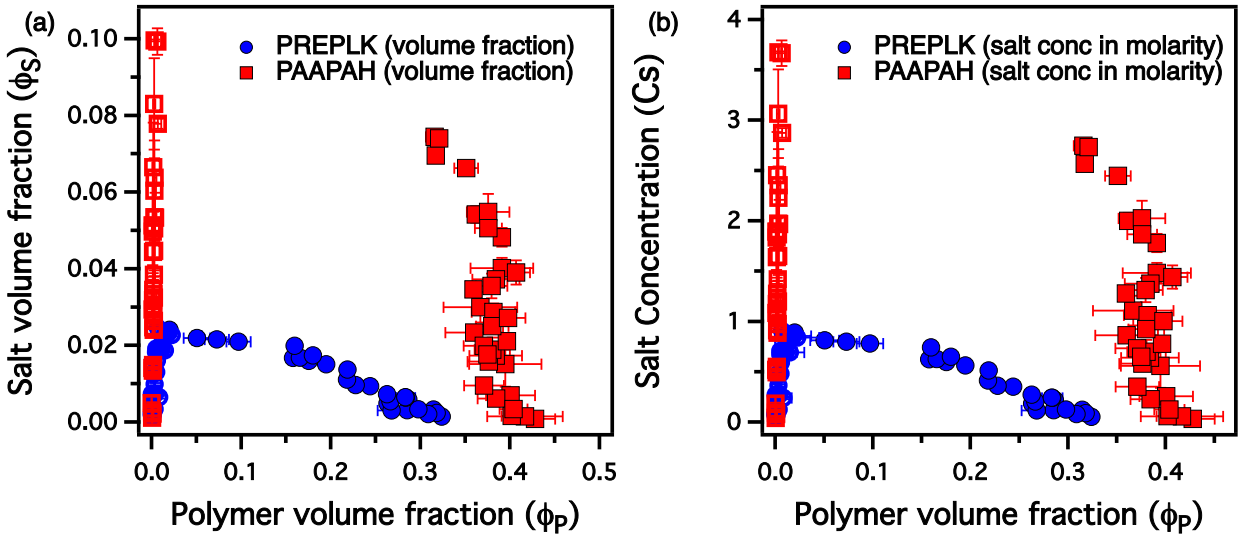

(a) The binodal composition partitioning data for PRE-PLK in volume fraction. (b) The binodal composition partitioning data for PAA-PAH in molarity conversion.

the two previous projects and plotted the binodal phase diagrams shown in **Figure 4-1**. (a) showed the polymer concentration (ϕ_P)-salt concentration (ϕ_S) map for PRE-PLK and PAA-PAH systems, and the salt volume fraction was converted to salt molarity in (b) for better comparison with theoretical calculation and easier correlation with practical experimental conditions. After putting the experimental results of PRE-PLK and PAA-PAH together, the

differences in the two systems appeared more pronounced. Above everything else, it could be observed that the polymer content in the coacervate phase of the hydrophilic polypeptide system was generally less than that of the more hydrophobic PAA-PAH system, which is understandable due to the fact that peptide linkage has higher affinity towards aqueous solvent and would interact with more water molecules than the polymers with aliphatic backbones. Furthermore, in the ϕ_P-ϕ_S plane, the two branches representing the complex phase and supernatant phase merged into one critical point for the polypeptide system, indicating formation of one homogenous phase by addition of salt. However, this behavior has not been observed for the PAA-PAH system, since the high tolerance of salt for formed precipitates prevented complete dissolution. Based on the data obtained from turbidity and microscopic measurements, the salt resistance concentration for PRE-PLK coacervates mixing at $\phi_{P,0}$=1% *wt*/*v* was 1.0M of NaCl, whereas the PAA-PAH precipitates withstood up to 4.0M of NaCl. The conversion from weight fractions to molarities was done by assuming same density of polymer and salt in bulk and solution state, wherein densities $\rho_{PRE-PLK}$ = 1.2515 g/mL, $\rho_{PAA-PAH}$= 1.3308 g/mL, ρ_{salt}= 2.16 g/mL, and ρ_{water}= 1.00 g/mL were used at 20 °C. Even though the converted value of salt molarities in the supernatant phase from measured data of weight fractions for PLK-PRE system was 0.9M and PAA-PAH was 3.7M compared with 1.0M and 4.0M of corresponding calculated values, this minor difference was acceptable due to the density difference between solid and solution states of substances and experimental measuring errors.

Lastly, the decrease of polymer content ϕ_P in the complex phase was much slower in aliphatic system with addition of salt, shown by steeper slope of the right branch on the phase diagrams. For example, at ϕ_S from 0.5M to 2M, the complex branch of the PAA-PAH system was nearly vertical, meaning little compositional change. Overall, the PRE-PLK and PAA-PAH

systems could be regarded as the two ends of the hydrophilicity versus hydrophobicity spectrum. With the same degree of electrostatic interactions, the general shapes of the binodal phase diagrams could also be remarkably different by changing the chemistries of the polymer backbones. As the next step, we would continue our study to pair PRE with PAH or PLK with

Figure 4-2. Binodals of associative phase separation in aqueous solution ($u = 1$) of oppositely charged polyelectrolytes.

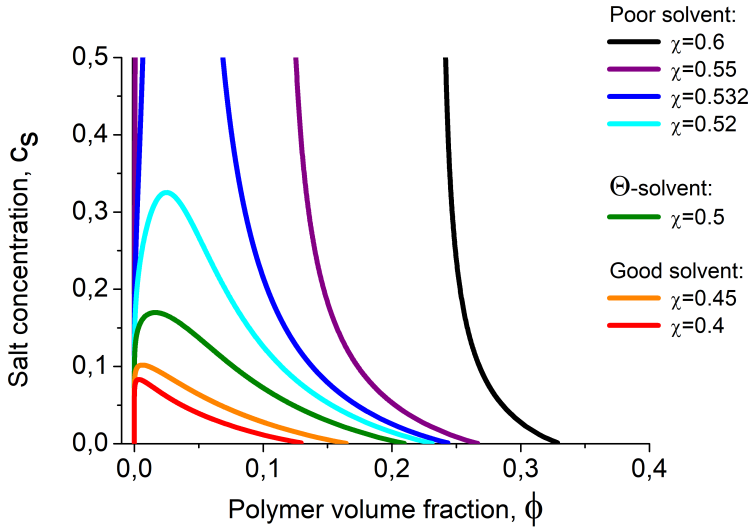

Chain length is $N = 10^3$, fraction of ionic monomers $f = 0.1$. Series of curves corresponds to the different solvent quality for polyions defined by the Flory-Huggins parameter χ.

PAA, and those two pairs were expected to lie in the middle of the hydrophilicity spectrum with their binodal phase diagrams sitting between the corresponding boundaries of the PAA-PAH and PRE-PLK systems.

4.2.2 Effect of Solvent Quality on Phase Behaviors Based on RPA-based Theory

Theoretically, the hydrophobicity of the polymer backbone could be characterized by the Flory-Huggins interaction parameter χ between polymer units and solvent molecules. Based on

the scaling theory developed by our collaborator Dr. Artem M. Rumyantsev from references 8 and 10, we varied the value of χ systematically. The dependence of the coacervate density on the

Figure 4-3. Effect of chain length on the binodal phase behaviors.

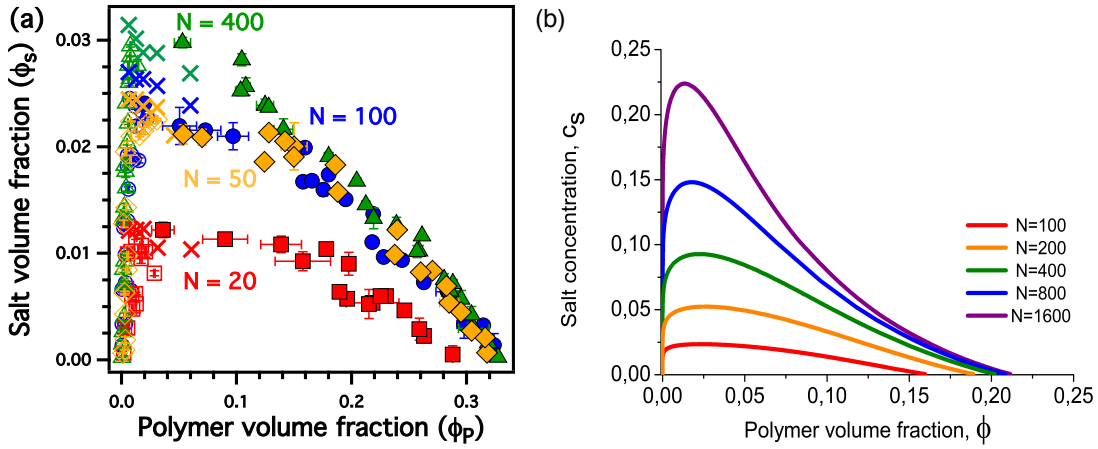

(a) Binodal phase diagrams measured by thermogravimetric analysis and turbidity experiments for PRE-PLK system with polymerization degree of 20, 50, 100, and 400. (b) Theoretical plots of binodal phase diagrams based on RPA theory for polymer of different chain lengths.

solvent quality for the polyion chains can be predicted, shown in **Figure 4-2**. The set of curves for different values of χ ranging from poor solvent to good solvent conditions were plotted, wherein polyions were assumed to have 1000 repeating units and charging density f was set to 0.1 to satisfy the limit of weakly charged systems in applying the RPA. In Θ-solvent, shown by green curve with $\chi = 0.5$, the PEC stability was provided solely by electrostatic interactions. When salt concentration was sufficiently high, Coulomb attraction was fully screened resulting in coacervate density decreasing to that of the supernatant. In good solvent, shown by red and orange curves with $\chi < 0.5$, PEC stability was dependent on electrostatic interactions which were opposed by short-range repulsion of polyions. When salt was added, electrostatic attraction was weakened. At a certain salt concentration, short-range repulsion of chains in good solvent

overcame electrostatic attraction and the complexation dissociated. However, the situation was different for hydrophobic polymers. In poor solvent, shown by curves with χ > 0.5, coacervate stability was due to both (i) electrostatic attraction of the chains and (ii) their intermolecular and intramolecular short-range hydrophobic attractions, like in a single globule/dense phase of neutral hydrophobic polymer.[8] At low salt concentrations ϕ_S, both factors contributed to the PEC stability providing high concentration of polymers in the complex phase. Addition of salt caused screening effect of electrostatics, so that at high ϕ_S coacervate stability was solely due to short-range hydrophobic attraction of the polymer chains. In this circumstance, PEC remained stable at any salt concentrations, but the polymer content in the complex phase ϕ_P would first go down and then stay constant as salt was gradually added, electrostatic attraction weakened, and finally hydrophobicity dominated. Additionally, The threshold χ value between the complex phase disintegrating upon salt addition and that remaining stable even at high salt concentrations ϕ_S was approximately equal to the critical point coordinate in the solution of neutral polymer and corresponded to weakly poor solvent by the following:

$$\chi_{cr} = \frac{1}{2}\left(1 + \frac{1}{\sqrt{N}}\right)^2 \approx \frac{1}{2} + \frac{1}{\sqrt{N}}$$

For the given parameters value of N=1000, χ_{cr} ≈0.532, shown by blue curve in **Figure 4-2**. With this relationship, when N=100~150, the critical value of χ is between 0.6~0.58. From Chapter 3, Larson and coworkers have chosen the χ value of 0.75 for PAA-PDADMAC system under acidic conditions to demonstrate the hydrophobicity of poly(acrylic acid), which is reasonable according to our calculations as well.

By comparison of the theoretical results and our experimental observations, the two agreed with each other in the following aspects. In poor solvent, polyelectrolyte complexes could

exist even at high salt concentrations, and the general shapes of binodal boundaries in poor solvent were plotted for the first time by experiments.[12] Then, the density of coacervate phase increased as solvent quality became poor, both in the absence of salt and at nonzero ϕ_S. Additionally, coacervate density gradually reduced by salt addition at low ϕ_S in poor solvent, then it saturated. On the other hand, we also had to point out two major disagreements. In our calculations, we adopted the assumption of weakly charged polyelectrolytes, $f \ll 1$. In this case, theory predicted higher salt concentration within the coacervate compared with supernatant phase, which was contrary to experimental observations on salt partitioning between supernatant and coacervates formed from fully charged polyelectrolytes, $f = 1$. Corresponding modifications can be introduced in future works, but it requires discussion on the salt behavior within the complex phase, for instance solvation effect, variation of dielectric constant, and determination of hydration layers of salt. Then, the second stage of density decrease for hydrophobic polymers at extremely high salt concentration has not been reproduced by this theory since such high ϕ_S is inaccessible by it. Notably, complexes formed among styrenic polymers, namely PSS and PDADMAC, have been shown to dissolve completely within 2M of KBr solutions, whereas PAA-PAH complexes persisted in 4M of KBr solutions shown by **Figure 3-15** in Chapter 3.[13] If we look at chemical structures alone, the styrenic polymers should be more hydrophobic compared with aliphatic ones and would be more resistant against external salt. The main reason for this unusual behavior may be caused by the fact that the charged moiety on PAH is primary amine while PDADMAC has the functional groups of quaternary ammonium. The spatial hindrance of PDADMAC makes polyanions hard to associate closely with the positively charged center, therefore enriching the formed complexes with higher content of water. Similarly, with

the sulfonate group also being bulky and hard to approach by oppositely charged molecules, the physical cross-linked network of PSS-PDADMAC is less stable and resistant against salt.[4,13]

Figure 4-4. Salt resistance concentration as a function of polymer chain length N from theory.

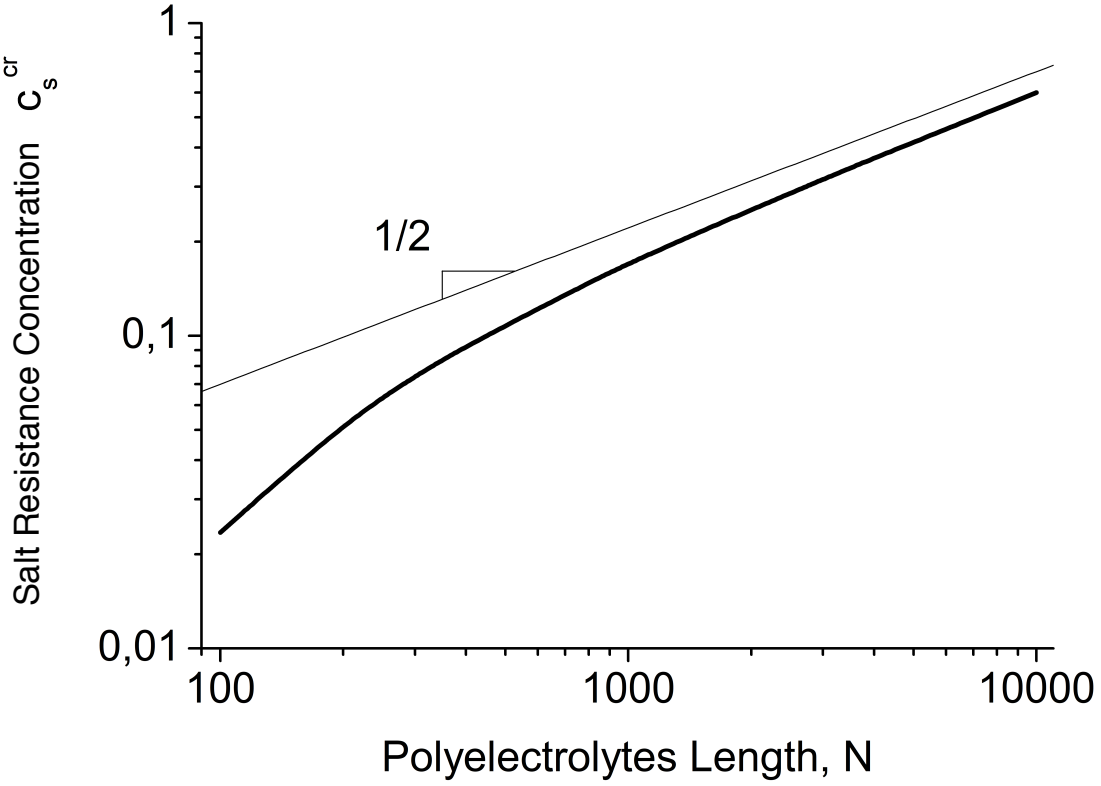

4.2.3 Effect of Chain Length on Binodal Phase Behaviors

Another noteworthy point during the investigation of the PRE-PLK system was the saturation of polymer concentration increase with chain lengths. As could be seen from **Figure 4-3(a)**, the compositional difference or coacervate density was relatively pronounced between polymers with chain length of 20 and 50. However, the phase diagrams for PRE_{50}-PLK_{50} and PRE_{100}-PLK_{100} were indistinguishable. Even for PRE_{400}-PLK_{400}, the right branch of the complex phase nearly overlapped with 50mers and 100mers in the low ϕ_S regime. Calculated curves

based on RPA theory were plotted for Θ-solvent with χ = 0.5, fraction of ionic units f=0.1 and dimensionless Bjerrum length u=1 (aqueous coacervate). **Figure 4-4** of log-log plot showed the relationship of the salt resistance concentration C_s^{cr} as a function of chain length N. In agreement with previous literature,[2,13–17] both experimental results and theoretical predictions indicated salt resistance concentration increased with chain length N. From **Figure 4-4**, for sufficiently high values of chain length (N>200 in this case), the scaling law of C_s^{cr}~$N^{1/2}$ was valid upon Θ-solvent condition. Result $c_s^{cr} \sim N^{1/2}$ accorded with the scaling expectations.[8] Indeed, in the theta solvent at high salt concentration, the blob size scales as $\xi \simeq c_s/f^2$ and the number of monomers is $g \simeq \xi^2 \simeq c_s^2/f^4$. The coacervate disintegration could be estimated from the equality between the number of monomers within the blob and in the chain (defining the k_BT gain per a globule formed from 1 polyanion and 1 polycation at coacervation), $g \simeq N$, which yields $N \sim c_s^{1/2}$. This scaling law meant the increase of the density for the complex phase saturates with N, in accordance with the experimental data. However, this relationship is limited to the case of the theory applicability, where salt concentration in the solution$\ll$ 1. **Figure 4-4** also exhibited that at short chain length c_s^{cr} grew faster than at high N.

4.3 Conclusion

In this chapter, we have systematically compared the experimental binodal phase behaviors of PRE-PLK system with hydrophilic polymer backbones and PAA-PAH pair with hydrophobic aliphatic backbones based on measured dated. This study provided insights on the effect of solvent quality when the electrostatic interactions were identical. Furthermore, the experimental findings were supported by theoretical results based on the RPA and scaling relationships. In good or theta solvent, the complexation process is mainly driven by electrostatic

attractions between charged species and entropy gain from counterion release, but hydrophobicity would play a vital role when the solvent is poor for the polyelectrolytes, leading to high salt resistances and lower water content of the resultant complexes. We acknowledge here that the limitations of low charge density and salt concentrations needs to be imposed when conducting RPA theory during the calculation, and the two experimental systems we concerned did not fit perfectly in this regime. However, the theoretical results could still shed light on understanding important physical properties in the system and help to demonstrate the importance of solvent effect on the overall phase behaviors for PEC materials.

Additionally, the saturation concerning the density of the complex phase could be quantitatively explained by the fact that in theta solvent, the salt resistances concentration is proportional to the square root of the polymer chain length. On the other hand, it could also be understood through the entropy gain concerning ideal mixing of polymer solutions as $\sum_i (\phi_i / N_i) \ln \phi_i$, with ϕ_i and N_i being the volume fraction and degree of polymerization of the each of the species present in the solution. For large values of N, the increase of entropy gain from mixing is less compared with smaller N. This work offered a unique perspective to integrate results from different systems with various chemical structures, which can be a starting point for instructive comparison for future studies since more researches on polyelectrolyte complexation are being conducted and a larger selection of polymers are being employed.

4.4 References

1. Veis, A. A review of the early development of the thermodynamics of the complex coacervation phase separation. *Adv. Colloid Interface Sci.* **167**, 2–11 (2011).

2. Arthur, V., Edward, B. & Shirley, M. Molecular weight fractionation and the self-suppression of complex coacervation. *Biopolymers* **5**, 37–59 (1967).

3. Fu, J. & Schlenoff, J. B. Driving Forces for Oppositely Charged Polyion Association in Aqueous Solutions: Enthalpic, Entropic, but Not Electrostatic. *J. Am. Chem. Soc.* **138**, 980–990 (2016).

4. Fu, J., Fares, H. M. & Schlenoff, J. B. Ion-Pairing Strength in Polyelectrolyte Complexes. *Macromolecules* (2017). doi:10.1021/acs.macromol.6b02445

5. Li, L. *et al.* Phase Behavior and Salt Partitioning in Polyelectrolyte Complex Coacervates. *Macromolecules* **51**, 2988–2995 (2018).

6. Chollakup, R., Smitthipong, W., Eisenbach, C. D. & Tirrell, M. Phase behavior and coacervation of aqueous poly(acrylic acid)-poly(allylamine) solutions. *Macromolecules* **43**, 2518–2528 (2010).

7. Sadman, K. *et al.* Influence of Hydrophobicity on Polyelectrolyte Complexation. *Macromolecules* **50**, 9417–9426 (2017).

8. Rumyantsev, A. M., Zhulina, E. B. & Borisov, O. V. Complex Coacervate of Weakly Charged Polyelectrolytes: Diagram of States. *Macromolecules* (2018). doi:10.1021/acs.macromol.8b00342

9. Rumyantsev, A. M. & Potemkin, I. I. Explicit description of complexation between oppositely charged polyelectrolytes as an advantage of the random phase approximation over the scaling approach. *Phys. Chem. Chem. Phys.* (2017). doi:10.1039/c7cp05300b

10. Rumyantsev, A. M., Kramarenko, E. Y. & Borisov, O. V. Microphase Separation in Complex Coacervate Due to Incompatibility between Polyanion and Polycation. *Macromolecules* **51**, 6587–6601 (2018).

11. Rumyantsev, A. M., Zhulina, E. B. & Borisov, O. V. Scaling Theory of Complex Coacervate Core Micelles. *ACS Macro Lett.* **7**, 811–816 (2018).

12. Lou, J., Friedowitz, S., Qin, J. & Xia, Y. Tunable Coacervation of Well-Defined Homologous Polyanions and Polycations by Local Polarity. *ACS Cent. Sci.* **5**, 549–557 (2019).

13. Wang, Q. & Schlenoff, J. B. The polyelectrolyte complex/coacervate continuum.

Macromolecules (2014). doi:10.1021/ma500500q

14. Chollakup, R., Beck, J. B., Dirnberger, K., Tirrell, M. & Eisenbach, C. D. Polyelectrolyte molecular weight and salt effects on the phase behavior and coacervation of aqueous solutions of poly(acrylic acid) sodium salt and poly(allylamine) hydrochloride hydrochloride. *Macromolecules* **46**, 2376–2390 (2013).

15. Priftis, D. & Tirrell, M. Phase behaviour and complex coacervation of aqueous polypeptide solutions. *Soft Matter* **8**, 9396–9405 (2012).

16. Spruijt, E., Westphal, A. H., Borst, J. W., Cohen Stuart, M. A. & Van Der Gucht, J. Binodal compositions of polyelectrolyte complexes. *Macromolecules* **43**, 6476–6484 (2010).

17. Meng, X., Perry, S. L. & Schiffman, J. D. Complex Coacervation: Chemically Stable Fibers Electrospun from Aqueous Polyelectrolyte Solutions. *ACS Macro Lett.* **6**, 505–511 (2017).